

LATE MIOCENE EXTENSIONAL DEFORMATION IN THE SIERRA BACHA,
COASTAL SONORA, MEXICO: IMPLICATIONS FOR THE KINEMATIC
EVOLUTION OF THE PROTO-GULF OF CALIFORNIA

by

MICHAEL HARRISON DARIN

A THESIS

Presented to the Department of Geological Sciences
and the Graduate School of the University of Oregon
in partial fulfillment of the requirements
for the degree of
Master of Science

December 2011

THESIS APPROVAL PAGE

Student: Michael Harrison Darin

Title: Late Miocene Extensional Deformation in the Sierra Bacha, Coastal Sonora, Mexico: Implications for the Kinematic Evolution of the Proto-Gulf of California

This thesis has been accepted and approved in partial fulfillment of the requirements for the Master of Science degree in the Department of Geological Sciences by:

| | |
|-----------------------|-------------|
| Dr. Rebecca J. Dorsey | Chairperson |
| Dr. Marli B. Miller | Member |
| Dr. Ray J. Weldon II | Member |

and

| | |
|-----------------------|--|
| Kimberly Andrews Espy | Vice President for Research & Innovation/Dean of the Graduate School |
|-----------------------|--|

Original approval signatures are on file with the University of Oregon Graduate School.

Degree awarded December 2011

© 2011 Michael Harrison Darin

THESIS ABSTRACT

Michael Harrison Darin

Master of Science

Department of Geological Sciences

December 2011

Title: Late Miocene Extensional Deformation in the Sierra Bacha, Coastal Sonora, Mexico: Implications for the Kinematic Evolution of the Proto-Gulf of California

The Gulf of California is an active rift basin formed by late Cenozoic dextral-oblique extension along the Pacific-North America plate boundary. Well exposed volcanic and sedimentary rocks in the Sierra Bacha, coastal Sonora, Mexico, preserve a history of proto-Gulf (late Miocene) deformation and offer insight into the structures and kinematics responsible for localization of the plate boundary and inception of the Gulf at about 6 Ma. Geologic mapping, fault kinematic analysis, and paleomagnetic data suggest that proto-Gulf deformation in the Sierra Bacha occurred primarily by ENE-WSW extension and that vertical-axis rotation related to dextral strain was minor. Lack of significant dextral shear supports an emerging model for proto-Gulf deformation in which dextral strain was not ubiquitous across Sonora but instead became localized during latest Miocene time in a narrow coastal shear zone that mechanically weakened the lithosphere and helped facilitate continental rupture.

This thesis includes the “Geologic Map of the Sierra Bacha, Coastal Sonora, Mexico” as supplemental material.

CURRICULUM VITAE

NAME OF AUTHOR: Michael Harrison Darin

GRADUATE AND UNDERGRADUATE SCHOOLS ATTENDED:

University of Oregon, Eugene
University of Colorado at Boulder

DEGREES AWARDED:

Master of Science, Geology, 2011, University of Oregon
Bachelor of Arts, Political Science, 2007, University of Colorado at Boulder

AREAS OF SPECIAL INTEREST:

Geologic mapping
Structural geology
Regional tectonics

PROFESSIONAL EXPERIENCE:

Graduate Teaching Fellow and Research Assistant, Department of Geological Sciences, University of Oregon, September 2009 to present

Field/Research Assistant, Department of Geological Sciences, University of Colorado at Boulder, June 2008 to January 2009

Seismic Site Reconnaissance Intern, USArray Earthscope project, June 2007 to August 2007

GRANTS, AWARDS, AND HONORS:

Graduate Teaching Fellowship, Department of Geological Sciences, University of Oregon, 2009-2011

Best Poster Award, Second Place, Annual AAPG/SEG Rocky Mountain Rendezvous, 2011

Graduate Student Research Grant, Geological Society of America, 2010

PUBLICATIONS:

Darin, M.H., Dorsey, R.J., Oskin, M.E., Iriondo, A., and Bennett, S.E.K., 2010, Late Miocene extensional deformation in the Sierra Bacha, Sonora, Mexico: Implications for the kinematic evolution of the proto-Gulf of California: Geological Society of America Abstracts with Programs, v. 42, no. 5, p. 318.

Bennett, S.E., Oskin, M.E., Dorsey, R.J., Skinner, L.A., Umhoefer, P.J., and Darin, M.H., 2010, Reconstructing the strain history of the northern Gulf of California-Salton Trough oblique rift: American Geophysical Union Fall Meeting, San Francisco, California, abstract #T33C-2263.

ACKNOWLEDGMENTS

First and foremost, I offer sincere gratitude to Becky Dorsey for the opportunity to develop and live out my burgeoning passion for geology. Her superlative instruction, enthusiasm, professionalism, and scrupulous attention to detail have been invaluable in my own development as a young geoscientist. I owe special thanks and appreciation to Scott Bennett and Mike Oskin for considerable assistance and guidance in the field and office. Many thanks to Marli Miller, Ray Weldon, Dave Blackwell and Joann Stock for insightful discussions and for sharing their expertise. Field work would not have been possible (or as enjoyable) without critical assistance from Carl Swanson and Eric Loes, who uttered not a single complaint regarding the heat, strenuous hikes, and countless “pokey” things in the Sonoran desert. This work also benefitted from thoughtful discussions with Leland O’Driscoll, Al Handwerker, Lucy Walsh, and Tom Peryam. Thanks also to Joe Kirschvink, Sarah Slotznick, and Steve Skinner at the Caltech Paleomagnetism Laboratory for generous assistance and use of their equipment.

This work would not have been possible without the support of the native Comcaac (Seri) tribe of western Sonora, Mexico. I offer sincere thanks to Ernesto Molina for granting access to the study area. I also thank Héctor Pérez, John Sheedy, Tom Donovan, Marlu Robledo, Abram Fleishman, Naomi Blinick, and everyone else at the Prescott College Kino Bay Center for Cultural and Ecological Studies in Bahía de Kino, Sonora, Mexico for accommodations, help and support far from home. Thanks to my wonderful family for their unconditional love, support, and confident encouragement, and to all my friends who endured innumerable hikes with me through incredible landscapes that caused my imagination (and mouth) to run wild.

This research was supported in part by a grant from the National Science Foundation (EAR-0738723) to Dr. Rebecca J. Dorsey at the University of Oregon, and by a Graduate Student Research Grant from the Geological Society of America.

TABLE OF CONTENTS

| Chapter | Page |
|--|------|
| I. INTRODUCTION | 1 |
| II. TECTONIC SETTING AND PREVIOUS WORK..... | 5 |
| Kinematic Models..... | 7 |
| Proto-Gulf Dextral Shear in the GEP..... | 9 |
| Previous Work in Coastal Sonora..... | 12 |
| Progressive Localization Hypothesis..... | 13 |
| III. METHODS | 15 |
| Geologic and Structural Mapping..... | 15 |
| Fault Kinematic Analysis..... | 15 |
| Paleomagnetic Analysis..... | 17 |
| XRF Geochemical Analysis..... | 18 |
| Geochronology..... | 19 |
| IV. GEOLOGY AND STRATIGRAPHY OF THE SIERRA BACHA..... | 20 |
| Study Area and Access | 20 |
| Stratigraphic Overview | 20 |
| Pre-Tertiary Basement | 24 |
| Paleotopography | 26 |
| Group 1: Basal Sedimentary Rocks (pre-15 Ma)..... | 26 |
| Group 2: Pre-Rift Rocks (~15-12 Ma)..... | 28 |
| Tuff of Cerro Colorado (<i>Mtcc</i>) | 33 |
| Tuff of San Ignacio (<i>Mtsi</i>) | 33 |
| Tuff of San Felipe (<i>Mtsf</i>) | 34 |
| Distinctions between <i>Mtsi</i> and <i>Mtsf</i> | 36 |
| Group 3a: Early Syn-Rift Rocks (12.5~10 Ma)..... | 38 |

| Chapter | Page |
|---|--------|
| Tuff of Desemboque (<i>Mtd</i>) | 41 |
| Group 3b: Late Syn-Rift Rocks (~10-6 Ma)..... | 41 |
| Group 4: Post-Rift Rocks (post-6 Ma)..... | 42 |
| V. STRUCTURAL GEOLOGY | 45 |
| Dominant Structural Trends..... | 45 |
| Major Structures..... | 47 |
| Fault Kinematic Analysis..... | 51 |
| VI. PALEOMAGNETISM | 56 |
| Reference Sites..... | 63 |
| Vertical-Axis Rotation..... | 65 |
| VII. DISCUSSION | 67 |
| Extensional Strain in the Sierra Bacha..... | 67 |
| Fault Orientations..... | 67 |
| Timing of Extension | 69 |
| Magnitude of Extension..... | 70 |
| Dextral Strain in the Sierra Bacha | 71 |
| Summary of Strain History | 74 |
| Implications for Regional Tectonic Models | 74 |
| VIII. CONCLUSIONS..... | 80 |
| APPENDICES | |
| A. FAULT KINEMATIC DATA | 82 |
| B. PALEOMAGNETIC DATA..... | 84 |

Chapter

Page

REFERENCES CITED..... 86

SUPPLEMENTAL FILES

PLATE 1. GEOLOGIC MAP OF THE SIERRA BACHA, COASTAL SONORA,
MEXICO (1:30,000)

LIST OF FIGURES

| Figure | Page |
|--|------|
| <p>1. Regional map of southwestern North America and the Gulf of California rift. Subduction of the Farallon plate and related microplates beneath North America ended ca. ~12.5 Ma (green), leading to a transitional phase of plate boundary reorganization from ~12-6 Ma referred to as the “Proto-Gulf of California”</p> | 2 |
| <p>2. Competing kinematic models for the timing and distribution of extensional and dextral strain related to evolution of the Gulf of California since ~12 Ma. The pre-12.5 Ma subduction boundary is dashed in green; RTJ - Rivera Triple Junction</p> | 8 |
| <p>3. Regional tectonic map of the northern Gulf of California and coastal Sonora showing onshore and offshore rift-related structures. Bennett (2009) documented a minimum of 15 km of localized dextral shear ca. 7-6 Ma in the Kino-Chueca Shear Zone (orange) based on detailed structural mapping and paleomagnetic analysis in the Cerro Kino.</p> | 11 |
| <p>4. Summary geologic map of the Sierra Bacha in coastal Sonora, Mexico. See Fig. 3 for location. Detailed, 1:30,000 scale “Geologic Map of the Sierra Bacha Coastal Sonora, Mexico” (Plate 1) is included with this thesis as supplemental material</p> | 21 |
| <p>5. Stratigraphic columns for the Sierra Bacha area (see Fig. 4 for locations and explanation), illustrating typical unit thicknesses and existing age constraints. BF - Bacha fault, NF - Noriega fault, PCF - Pozo Coyote fault.</p> | 23 |
| <p>6. Total alkali versus silica (TAS) diagram (Le Maitre et al., 1989) showing the classification of volcanic units from the Sierra Bacha. Bulk rock XRF major and trace element data are listed in Table 2. All samples (except <i>Mdf</i>) lie within the basaltic-trachyandesite to rhyolite fields and show high total alkali concentrations > 6 wt%</p> | 29 |
| <p>7. Field photographs of the 12.5 Ma tuff of San Ignacio (Mtsi). (Top-left) Lower densely welded zone showing 1 to 3 cm-long white-pink pumice fiame. (Top-right) Spherule-rich zone of vapor phase alteration; notebook is 19 x 12 cm. (Bottom) Rheomorphism in Mtsi from the Cerro Las Burras where it reaches a maximum thickness of ~350 m.</p> | 35 |

| Figure | Page |
|--|------|
| 8. Comparison of bulk rock trace element data for the 12.5 Ma tuffs of San Ignacio (Mtsi) and San Felipe (Mtsf). Mtsf in the Sierra Bacha (green) correlates strongly with other geochemical data for Mtsf from Baja California and coastal Sonora (black - Stock et al., 1999; purple - Oskin and Stock, 2003b). | 37 |
| 9. Clast count data for conglomerate units in the study area. Note substantial increase in basement clast percentage with time from ~16% in group 3a (12.5-10 Ma) conglomerates to 44% in group 4 (post-6 Ma) conglomerates, which might be related to post-10 Ma tectonic unroofing and basement exhumation during proto-Gulf rifting. | 43 |
| 10. Equal area projections of structural data from bedding (A) and faults (B) in the Sierra Bacha study area, including from left to right: planes, poles to planes with averages in blue, and rose diagram of structural strike. A) Average bedding dip for ~15-10.4 Ma units (blue) show an average orientation of 323, 42° NE (n=194) | 46 |
| 11. Structural cross sections of the Sierra Bacha (see Fig. 4 for locations). The structural dips of unexposed faults could not be measured directly, and thus, were assumed to be parallel to those nearby. High fault-to-bedding cutoff angles and shallowly dipping faults (consistent with field measurements of exposed structures) are inferred for unexposed and concealed structures. | 48 |
| 12. Fault kinematic analysis results. Plot of fault dip vs. slip vector rake (Top-left) and measured fault surfaces (great circles) and kinematic indicators (Top-right) colored red, blue, and green representing normal, oblique, and strike-slip shear senses, respectively | 52 |
| 13. Interpretation of anomalous slip vectors based on paleostress orientations responsible for average conjugate fault pair. A) Poles to fault planes (n=65) show two distinct populations which define the average fault orientation as a conjugate set of moderately dipping, NW-SE-striking normal faults; B) Fault striae (n=41) in expected and anomalous slip | 54 |
| 14. (A) Typical paleomagnetic results for the Tuff of San Ignacio (Mtsi). Example core #9 of 12 shown, including clockwise from top-left: Equal Area, Zijderveld, J/J ₀ Intensity, and site-mean ChRM plots. Lower plot shows site-mean direction (star) and α -95 confidence (red) for DS-17 | 58 |

| Figure | Page |
|---|------|
| 15. Paleomagnetic site locations and estimates of vertical-axis rotation for the Sierra Bacha (see Fig. 4 for explanation of map units). The location of drill site DS-17(Mtsi) is shown but rotation cannot be estimated due to lack of a stable reference site. The remaining sites show unresolvable rotation within standard error limits | 64 |
| 16. Speculative tectonic model for coastal Sonora during late Miocene time. According to this model, older normal faults (black) accommodated large-magnitude NE-SW extension from ~10-6 Ma. Significant dextral shear introduced at ca. 7 Ma on newly initiated and/or reactivated structures (red) transferred and progressively localized dextral strain. | 76 |

LIST OF TABLES

| Table | Page |
|---|------|
| 1. Summary of Available Geochronologic Data for Lithologic Units in the Sierra Bacha Area, Coastal Sonora, Mexico | 27 |
| 2. XRF Bulk Rock Analysis of Major and Trace Element Compositions | 30 |
| 3. Paleomagnetic Data and Rotation Calculations for Sites in the Sierra Bacha, Coastal Sonora, Mexico | 57 |

CHAPTER I

INTRODUCTION

The transition from diffuse oblique continental extension to localized rifting and the onset of seafloor spreading is one of the least understood aspects of continental breakup. Modern oblique rifts that preserve a detailed continental record of rift-related deformation offer valuable insights into the structural evolution of obliquely rifted margins and the mechanisms that lead to continental rupture. The Gulf of California is a young proto-oceanic basin that formed during late Cenozoic dextral-oblique extension along the Pacific-North America plate boundary (Fig. 1). Although the tectonic evolution of the region is relatively well known (e.g. Hausback, 1984; Stock & Hodges, 1989; Lonsdale, 1989; Gans, 1997; Atwater & Stock, 1998; Oskin & Stock, 2003c; Fletcher et al., 2007; Lizarralde et al., 2007), the conditions and processes that led to localization of the plate boundary within the North American continent remain poorly understood. This rare example of a youthful oceanic basin offers a unique opportunity to explore the kinematics of lithospheric rupture and the structural evolution of a well-exposed obliquely rifted continental margin.

The Gulf Extensional Province (GEP) is a region of extended continental crust that includes a large area from eastern Baja California to interior Mexico (Fig. 1). Significant extension in this region began after subduction west of Baja California ended at ca. 12.5 Ma (Spencer & Normark, 1979; Mammerickx & Klitgord, 1982; Stock & Hodges, 1989). Latest Miocene localization of plate boundary strain resulted in marine

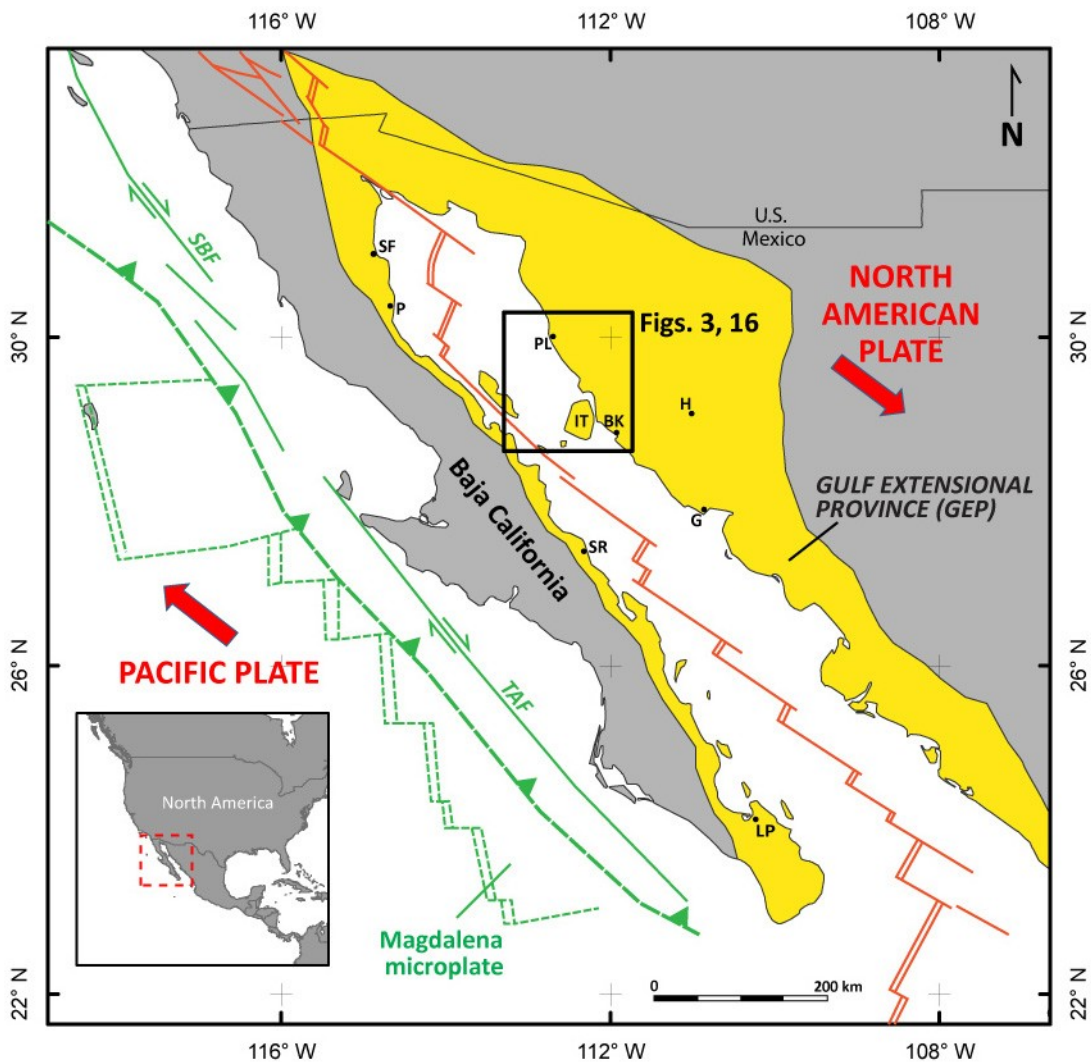


Figure 1. Regional map of southwestern North America and the Gulf of California rift. Subduction of the Farallon plate and related microplates beneath North America ended ca. ~12.5 Ma (green), leading to a transitional phase of plate boundary reorganization from ~12-6 Ma referred to as the “Proto-Gulf of California” (e.g. Karig and Jansky, 1972). The timing, magnitude, and distribution of proto-Gulf strain remain poorly understood and debated. Incipient coupling between the Pacific and North America plates during proto-Gulf time caused deformation on offshore transform faults and on the North American continent in the Gulf Extensional Province (GEP; yellow). Pacific-North America plate boundary localization within the continent ca. 6 Ma initiated the modern phase of oblique rifting and the formation of the Gulf of California (active modern plate boundary in red). Abbreviations: SF - San Felipe, P - Puertecitos, PL - Puerto Libertad, IT - Isla Tiburón, BK - Bahía Kino, H - Hermosillo, G - Guaymas, SR - Santa Rosalía, LP - La Paz, SBF - San Benito Fault, TAF - Tosco-Abrejos Fault.

incursion in the northern Gulf at ca. 6 Ma and established the modern phase of oblique spreading (Oskin & Stock, 2003a, b). The time period between 12.5 and 6 Ma, and the region known as the GEP, are collectively referred to as the “proto-Gulf of California” (e.g. Karig & Jansky, 1972; Stock & Hodges, 1989). Contrasting kinematic models (discussed in the following section) have been proposed for the style and distribution of proto-Gulf (late Miocene) deformation in western Mexico, yet neither model directly addresses the structural mechanisms responsible for the localization of plate boundary strain, which is required for successful rupture of continental lithosphere.

In addition to continental extension, oblique intracontinental rift zones are commonly affected by strike-slip deformation. Previous studies of fault mechanics and strain evolution suggest that strike-slip faults may be more effective at localizing strain in the upper crust than normal faults (e.g. Buck, 1991; Zoback, 1991; Buck et al. 1999). In regions undergoing extension, lateral variations in crustal thickness produce differential vertical stresses, leading to horizontal stress gradients that transmit strain to unthinned crust and promote widening of the rift zone (Buck, 1991). In contrast, extension-related buoyancy forces are not generated by *lateral* displacement on strike-slip faults. Thus the strike-slip component of transtension is mechanically favored to localize strain in oblique rift settings such as the Gulf of California, but this hypothesis has not been widely tested in previous studies. It is necessary to document the timing, style and distribution of crustal deformation in order to assess the role of strike-slip faulting in real examples of strain localization and lithospheric rupture.

This thesis presents the results of an integrated field, kinematic, and paleomagnetic study of late Miocene deformation in the Sierra Bacha, at the eastern rifted

margin of the Gulf of California in coastal Sonora, Mexico. The study area is located immediately northeast (inboard) of a coastal shear zone that experienced localized dextral-oblique transtensional faulting and block rotation between about 7 and 6 Ma (Bennett, 2009). Analysis of well-exposed volcanic rocks in the Sierra Bacha allow me to document the timing, distribution, and kinematics of late Miocene faulting, and compare its structural evolution to that of the coastal shear zone. The results of this study, integrated with previous studies, are used to test an emerging hypothesis for post-extensional progressive localization of dextral strain in coastal Sonora during latest Miocene time (~7-6 Ma), shortly prior to lithospheric rupture and opening of the northern Gulf. Alternatively, evidence of significant dextral shear in the Sierra Bacha between 12 and 6 Ma would discount this hypothesis and instead support the distributed transtension model of Fletcher et al. (2007).

CHAPTER II

TECTONIC SETTING & PREVIOUS WORK

Prior to the onset of extension in the GEP at ca. 12.5 Ma, western Mexico was the site of a Miocene volcanic arc related to subduction of the Farallon plate beneath North America (Fig. 1; Atwater, 1970, 1989). Calc-alkaline arc volcanism migrated west during Oligocene-Miocene time, eventually localizing along the trend of the present-day Gulf of California ca. 16-12 Ma (Gastil et al., 1979; Hausback, 1984; Sawlan, 1991; Oskin and Stock, 2003b). Most of the GEP did not undergo extension during arc volcanism (Hausback, 1984; Lee et al., 1996; Martín et al., 2000; Nagy, 2000), though extension and metamorphic core-complex formation synchronous with and immediately following arc magmatism has been documented east of the GEP in the Sierra Madre Occidental and in southern California, largely prior to the onset of large-magnitude extension in the GEP (Nourse et al., 1994; Gans, 1997; Wong and Gans, 2003).

The transition from subduction to dextral transtension between the Pacific and North America plates occurred via ridge-trench interactions and step-wise abandonment of microplates (Atwater 1970; Stock and Molnar, 1988; Atwater and Stock, 1998). By ca. 12.5 Ma, subduction had ceased and the full length of the Pacific plate was in contact with northwestern Mexico (Mammerickx and Klitgord, 1982). The coeval termination of arc volcanism and the onset of diffuse continental extension in the GEP marked the beginning of the “proto-Gulf” phase of plate boundary evolution (Karig and Jansky, 1972; Stock and Hodges, 1989).

Deformation during proto-Gulf time (12.5-6 Ma) was the result of a major tectonic reorganization of the North American margin starting ca. 12.5 Ma. A large southward jump of the Rivera triple junction led to incipient coupling between the Pacific and North American plates, resulting in shear and extensional deformation in the continental borderland that isolated Baja California as a microplate in the evolving plate boundary system (Karig and Jansky, 1972; Spencer and Normark, 1979; Hausback, 1984; Stock and Hodges 1989; Lonsdale, 1991). Exactly how extension and dextral strain were distributed throughout proto-Gulf time is a matter of current debate and is discussed in detail in the following section. Near the end of late Miocene time (ca. 6 Ma) localization of strain along the axis of the Gulf of California initiated a nascent ocean basin along the axis of the GEP (Oskin et al., 2001; and Stock, 2003b). This nascent, obliquely rifted ocean basin formed along the axis of the former Miocene volcanic arc where hot, thick crust created a zone of weakness that controlled the location of the modern plate boundary (Gastil, 1968; Hausback, 1984; Henry, 1989). While arc-related thermal weakening likely exerted an important control on the *location* of the modern plate boundary, it does not explain the prolonged time delay between subduction and localized rifting between 12.5 and 6 Ma. A central goal of this study is to investigate the role that other structural mechanisms (e.g. strike-slip faults, fault reactivation, stress reorientation) might have played in the temporal evolution of the plate boundary during proto-Gulf time.

In contrast with debates surrounding the proto-Gulf period, there is general agreement regarding the evolution of the modern Gulf of California since ca. 6 Ma. Localization of Pacific-North America plate motion in the Gulf created a narrow zone of

crustal thinning and subsidence that likely caused marine incursion into the northern Gulf region by ca. 6.3 Ma (Oskin et al., 2001; Oskin and Stock, 2003a). The initial rift axis was established in the eastern basins of the Gulf near the modern Sonoran shoreline, migrated westward ca. 3.3-2.0 Ma, and is now focused along the western margin of the Gulf of California (Stock et al., 1991; Oskin and Stock, 2003a; González-Fernández et al., 2005; Aragón-Arreola and Martín-Barajas, 2007). The modern plate boundary is an oblique transtensional rift with small spreading centers linked by an en-echelon array of right-stepping, NW-striking dextral transforms that feed into the San Andreas fault system to the north (Fig. 1; Fenby and Gastil, 1991; DeMets and Dixon, 1999).

Kinematic Models

As previously mentioned, the distribution of transtensional strain between structures west of Baja and in the GEP and the reason for the prolonged delay between the cessation of subduction ca. 12.5 Ma and the onset of localized dextral transtension in the Gulf of California at ca. 6 Ma are poorly understood (Fig. 1; Spencer and Normark, 1979; Stock and Hodges, 1989; Oskin et al., 2001). Two end-member models have been proposed to describe the structural evolution of the Gulf of California. The two-stage “strain-partitioning” model proposes that late Miocene transtensional strain was partitioned into (i) strike-slip offset on offshore transform faults west of Baja California and (ii) orthogonal NE-SW extension in the GEP (Fig. 2A). According to this model, the strain partitioned deformation pattern was followed by a discrete change to localized dextral shear and oblique rifting in the modern Gulf starting ca. 6 Ma (Fig. 2A; Karig and Jensky, 1972; Spencer & Normark, 1979; Hausback, 1984; Lonsdale, 1989; Stock & Hodges, 1989). In contrast, the “distributed transtension” model proposes that

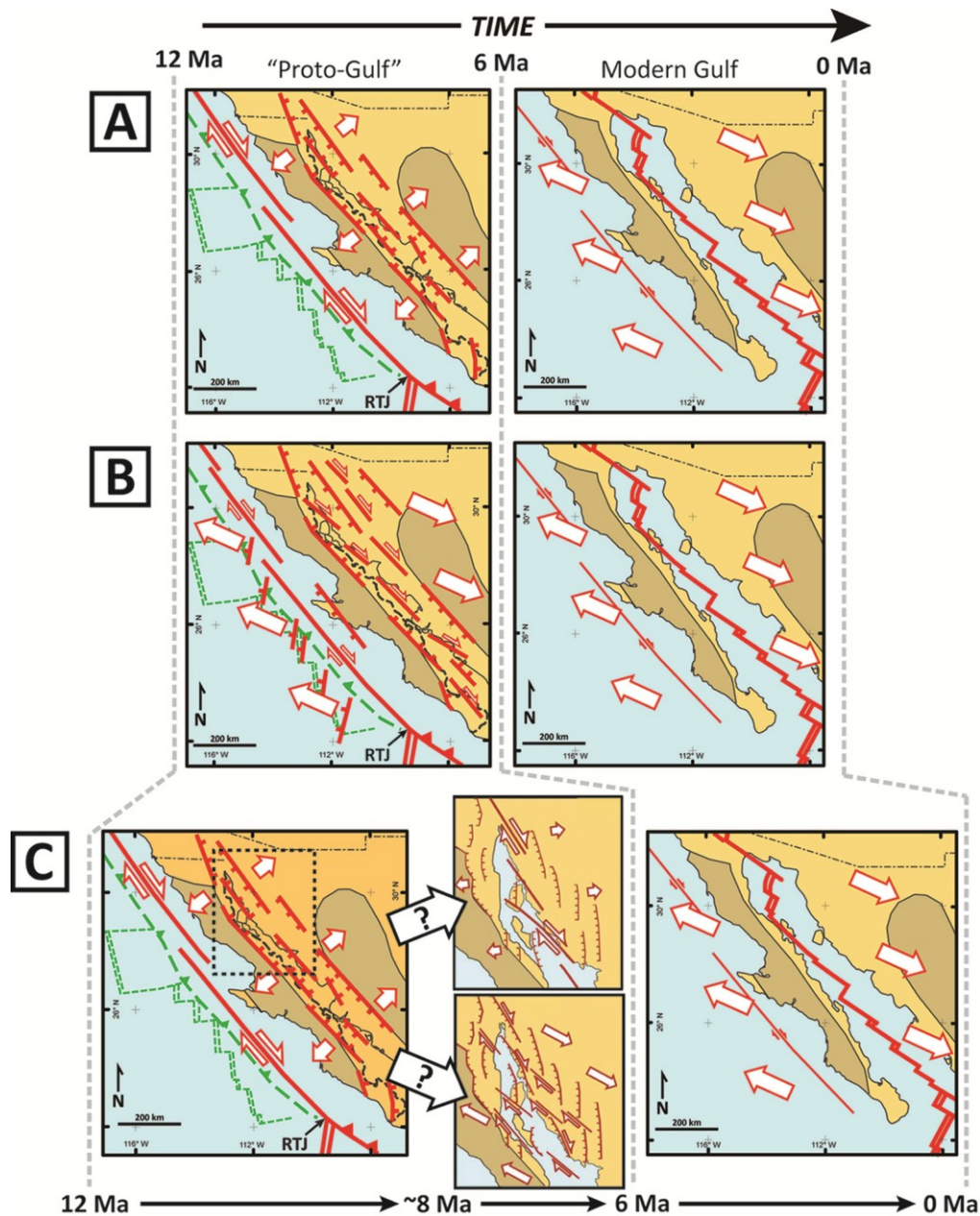


Figure 2. Competing kinematic models for the timing and distribution of extensional and dextral strain related to evolution of the Gulf of California since ~12 Ma. The pre-12.5 Ma subduction boundary is dashed in green; RTJ - Rivera Triple Junction. A) “Strain partitioning” model of Stock and Hodges (1989) in which proto-Gulf (12-6 Ma) strain was partitioned between offshore dextral shear and extension in the Gulf Extensional Province (GEP). Transtensional strain since ca. 6 Ma (right) has occurred almost entirely within the oblique modern Gulf of California rift. B) “Distributed transtension” model of Fletcher et al. (2007) which proposes a single stage of diffuse and integrated extension and dextral strain offshore west of Baja and on the North American continent within the GEP. C) “Progressive localization” model (Bennett, 2009; this study) in which early proto-Gulf strain (~12-8 Ma) was partitioned according to the strain partitioning model (A), but progressively localized into either narrow dextral shear zones (top) or a diffuse zone of transtensional strain during latest Miocene time (~8-6 Ma).

oblique-divergent plate motion has been accommodated by a single phase of diffuse, integrated transtension offshore west of Baja and onshore in the GEP from 12.5 Ma to the present (Fig. 2B; Gans, 1997; Fletcher et al., 2003; Fletcher et al., 2007; Seiler et al., 2010).

A third alternative, “hybrid” model involves the progressive localization of the plate boundary through time (Bennett, 2009). According to this model, proto-Gulf deformation started out partitioned between dextral shear on transform faults west of Baja and orthogonal extension onshore in the GEP (strain partitioning). With time, dextral strain became progressively focused into the GEP (Fig. 2C). While it is generally agreed that the GEP underwent extension during proto-Gulf time, the kinematics of extension and dextral strain are not well understood and are particularly controversial in tectonic models for proto-Gulf evolution.

Proto-Gulf Dextral Shear in the GEP

Dextral shear along the plate boundary or within the GEP during late Miocene time is required by observations from both sides of the Gulf of California. Global plate circuit models estimate a total of ~650 kilometers of dextral displacement between the Pacific and North American plates since 12.5 Ma (Atwater and Stock, 1998). An estimated 270-300 km of Pacific-North American relative plate motion has been accommodated by dextral shear in the modern Gulf since 6 Ma (DeMets, 1995; DeMets and Dixon, 1999; Oskin et al., 2001; Oskin and Stock, 2003a). Thus, the remaining ~350 km must be accounted for by some combination of offshore transform faults west of Baja and onshore dextral shear in the GEP during late Miocene (proto-Gulf) rifting (i.e. 12.5-6 Ma). Distributed dextral strain in the Sonoran Basin-and-Range and the GEP was

documented by Gans (1997), but the magnitude of strain was not determined. In northwestern Sonora, up to 40 km of dextral offset of a Tertiary conglomerate with distinctive basement clasts was inferred by Nourse et al. (2005), but the timing of offset is poorly constrained. Herman and Gans (2006) found evidence for significant clockwise vertical-axis rotations of up to 100° related to dextral shear in the Sierra el Aguaje near Guaymas (Fig. 1), all of which is thought to have occurred between 12 and 9 Ma.

The presence of distinctive limestone clasts with Permian fusulinid fossils in an Eocene-Oligocene fluvial conglomerate allowed previous workers to estimate ~300 km of northwestward lateral offset between the Sierra Seri (~7 km southeast of the Sierra Bacha; Fig. 3) and similar outcrops near San Felipe on the Baja peninsula (Fig. 1; Gastil et al., 1973; Bryant, 1986). The source area for the conglomerate is ~50-75 km northeast of Sierra Seri outcrops in coastal Sonora, but could be significantly less after restoring late Miocene extension in the GEP (Gastil et al., 1973). In addition to onshore evidence for proto-Gulf dextral shear, recent provenance studies of the offshore Magdalena fan west of Baja only attribute up to 150 km of dextral slip to the offshore Tosco-Abreojos and San Benito faults (Grove et al., 2005; Fletcher et al., 2007). This is significantly less than earlier predictions of ~300 km of offshore dextral displacement and requires a larger component of dextral strain onshore within the GEP to satisfy plate circuit models.

Altogether, observations of proto-Gulf dextral shear argue against the strain partitioning end-member model of Stock and Hodges (1989) (Fig. 2A). However, evidence of predominantly orthogonal extension on both conjugate rift margins during most of proto-Gulf time (e.g. Lewis and Stock, 1998; Mora-Alvarez and McDowell, 2000; Umhoefer et al., 2002; Bennett, 2009) indicates that distributed transtension was

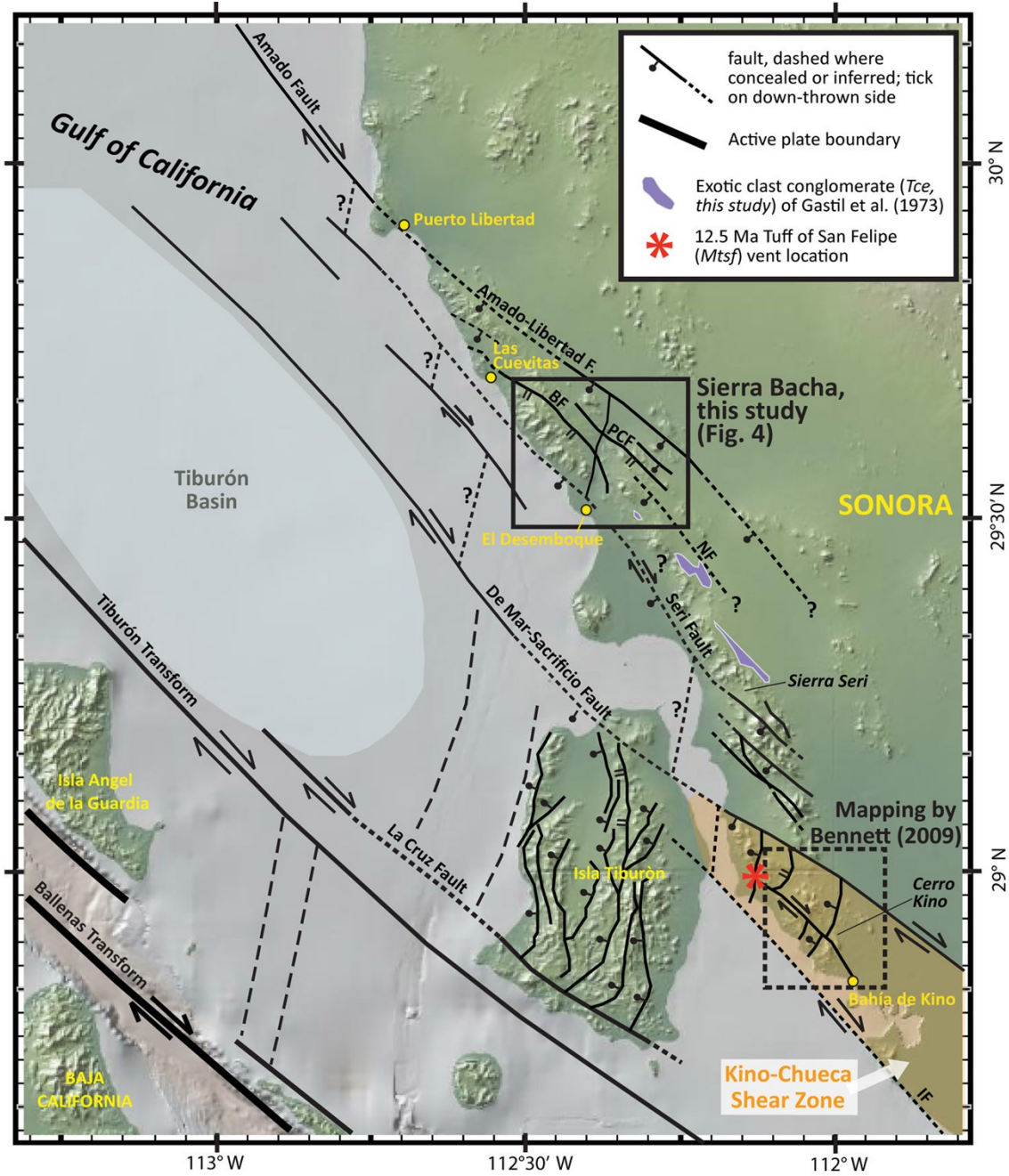


Figure 3. Regional tectonic map of the northern Gulf of California and coastal Sonora showing onshore and offshore rift-related structures. Bennett (2009) documented a minimum of 15 km of localized dextral shear ca. 7-6 Ma in the Kino-Chueca Shear Zone (orange) based on detailed structural mapping and paleomagnetic analysis in the Cerro Kino area (dashed box). The spatial and temporal distribution of similar dextral shear in adjacent areas like the Sierra Bacha (solid box, this study) is unknown. BF - Bacha fault, NF – Noriega fault, PCF - Pozo Coyote fault.

not ubiquitous throughout the GEP as suggested by the alternative end member model (Fig. 2B; Fletcher et al., 2007). These observations suggest that an intermediate model for proto-Gulf evolution might better reconcile existing geologic data. Evidence of late Miocene dextral shear in the GEP (e.g. Herman and Gans, 2006; Bennett, 2009) highlights the need for additional geologic constraints from preserved early-rift structures to assess the role that strike-slip faults played in continental breakup and the formation of the Gulf of California.

Previous Work in Coastal Sonora

Geologic studies of late Miocene volcanic and sedimentary rocks in Sonora provide a record of proto-Gulf extension and dextral shear in the GEP. Gastil and Krummenacher (1976) produced the first reconnaissance geologic map (1:150,000 scale) and substantial geochronology for rocks in coastal Sonora from Bahia de Kino north to Puerto Lobos. Gastil and Krummenacher (1977) first recognized striking similarities in the geology and deformation style between rocks in northeastern Baja California and those in coastal Sonora, and more recent geochemical and stratigraphic studies in Baja, Isla Tiburón, and Sonora confirm these observations (Mora-Alvarez and McDowell, 2000; Oskin and Stock, 2003b,c). Oskin and Stock (2003b, c) estimated ~300 km of Pacific–North America relative plate displacement between coastal Sonora and the Baja peninsula since ca. 6 Ma based on correlations of four ignimbrite markers (dated at 12.6 to 6.1 Ma) from northeastern Baja California to Isla Tiburón and coastal Sonora,.

Bennett (2009) used detailed geologic mapping (1:10,000 scale), structural analysis and paleomagnetic data in the Cerro Kino area of coastal Sonora to document a transition from extension-dominated transtension to shear-dominated transtension at ca. 7

Ma, after which the coastal “Kino-Chueca Shear Zone” (Fig. 3) hosted a minimum of 15 km of proto-Gulf dextral shear immediately prior to plate boundary localization in the Gulf at ca. 6 Ma. The Kino-Chueca shear zone, bounded on the northeast by the Sacrificio fault and on the southwest by the offshore Infernillo fault (Fig. 3), is thought to represent a narrow zone of localized dextral shear where elevated strain rates and focused transtension may have served as a catalyst for lithospheric rupture and inception of the Gulf California (Bennett, 2009).

Progressive Localization Hypothesis

Evidence from both conjugate rifted margins of the Gulf of California suggests that neither the strain partitioning (Stock and Hodges, 1989) nor the distributed transtension (Fletcher et al., 2007) end-member models sufficiently describe proto-Gulf kinematics without some modification. Bennett (2009) proposed a new hybrid model for late Miocene progressive localization of proto-Gulf strain in the northern Gulf of California. According to this model, initiation of dextral strike-slip faults in a narrow zone of focused transtension in coastal Sonora near the end of late Miocene (proto-Gulf) time resulted in acceleration of strain rate that led to lithospheric rupture and the transition from continental extension to seafloor spreading. Evidence for dextral displacement and significant clockwise vertical-axis rotation along strike to the southeast near Guaymas (Herman and Gans, 2006) lends support to this model. These results suggest a causal link between rift obliquity and the potential for lithospheric rupture, since highly oblique rifts like the Gulf of California commonly host significant shear strain on steep strike-slip and oblique-slip faults (Withjack and Jamison, 1986; Agostini et al., 2009). However, the possible presence of major strike-slip faults inboard and

northeast of the Kino-Chueca shear zone, which would support the distributed transtension model, has not been tested in previous studies. In this study, geologic mapping and structural data from well-exposed late Miocene rocks in the Sierra Bacha, adjacent to a well-documented coastal shear zone, are used to test existing kinematic models of proto-Gulf evolution and to investigate the processes that led to initial opening of the northern Gulf of California.

CHAPTER III

METHODS

Geologic and Structural Mapping

Detailed geologic and structural mapping (Plate 1) was conducted in 2010 and 2011 on SPOTImage multispectral 2.5 meter resolution imagery from Google Earth draped with a worldwide UTM grid. Topographic base maps used for reference include the 'Desemboque' and 'Arivaipa' 1:50,000-scale Carta Topografica base maps produced by the Comision de Estudios del Territorio Nacional, Mexico. Field mapping was conducted at scales of 1:10,000 and 1:30,000 and integrated with analysis of high-resolution satellite imagery to identify and correlate major structures and stratigraphic units across the study area. Since most major structures are not well exposed, their locations and geometries are commonly inferred from stratigraphic constraints such as missing or repeated intervals, fault-to-bedding cutoff angles, and structural separation observed in map view. Lithologic, petrographic, and geochemical analyses helped test and corroborate stratigraphic correlations between isolated localities.

Fault Kinematic Analysis

Fault surfaces and kinematic indicators (e.g. slickenside lineations, striations, and mullions) were measured in the field for structural analysis and reconstruction of paleostress axes that produced proto-Gulf deformation in the Sierra Bacha. A total of 65 exposed fault surfaces and 41 kinematic indicators were measured in late Miocene units deposited between ~14.5 Ma and 10.4 Ma. Each fault slip measurement included the

orientation (strike and dip) of the fault surface, rake of the fault slip indicator, and sense of shear. Together, these kinematic features represent the direction of relative motion between adjacent fault blocks. In most cases, sense of shear could not be determined in the field due to the limited preservation of fault surfaces and absence of the adjacent block. Where a reliable shear sense indicator was not observed, a shear sense direction was assigned to each measurement using two main assumptions: (1) fault striations formed under a dominantly extensional (as opposed to contractional) stress field, and (2) the overall structural style of regional-scale faults reflects the same stress conditions as microstructures, given a large enough dataset. Following these assumptions, slickenline data with a significant component of dip-slip (i.e. rake = 20 - 90° from horizontal) were assigned a normal shear sense with the appropriate strike-slip component (e.g. dextral-normal or sinistral-normal) based on the rake direction. For kinematic indicators with a low dip-slip component (rake 0-20° from horizontal), a shear sense was assigned that reflected dextral motion on W- and NW-striking faults, and sinistral motion for N- and NE-striking faults, consistent with regional-scale strain patterns. Principal paleostress orientations were determined using FaultKinWin v. 1.2.2 and FaultKin v.4.3.5 for Mac OS (Allmendinger et al., 1994), which utilizes the right dihedral geometrical method of calculating P and T stress tensors (Angelier and Mechler, 1977; Pfiffner and Burkhard, 1987). All fault kinematic data analyzed in this study are listed in Appendix A.

Kinematic analysis of fault slip data in this study is based on the general assumption that slip occurs along a fault plane in the direction of maximum resolved shear stress (Wallace, 1951; Bott, 1959). Thus, the orientations of kinematic indicators on fault surfaces provide valuable information about paleostress conditions and, given a

large population of faults, are assumed to be representative of the paleostress orientation that caused slip to occur. Inversion of fault slip datasets can then be used to reconstruct a reduced stress tensor and paleostress axes for a given fault array (Carey and Brunier, 1974; Angelier et al., 1982).

Paleomagnetic Analysis

A total of 61 randomly oriented core samples were collected from 5 drill sites in the Sierra Bacha. Between 6 and 19 cores were extracted from each site using a portable gasoline-powered drill with a 1-inch diameter water-cooled diamond bit. Each core was oriented in the field with both a magnetic compass and a sun compass to an accuracy of $\pm 1^\circ$. Samples typically were collected from an area spread over 5 to 200 meters at each site to allow within-site homogeneity of remnant magnetization to be evaluated. In the lab, specimens were cut to a length of 1 cm and subjected to demagnetization experiments. All experiments were performed by the author at the California Institute of Technology Paleomagnetism Laboratory in a Model 581 2-G SQUID (Superconducting Quantum Interference Device) rock magnetometer, housed in a magnetically shielded μ -metal room. Natural remnant magnetization (NRM) was measured for each of the specimens, followed by two identical low-temperature (LT) steps in which each specimen was cooled to 77 K in liquid nitrogen (N_2) and allowed to warm to room temperature. Magnetization was measured after each cooling-warming cycle. No other thermal demagnetization steps were performed. All 61 specimens were then subjected to 13 total AF demagnetization steps from 25 to 100 mT in increments of 25 mT, high-AF demagnetization from 100 to 300 mT in increments of 50 mT, and 300 to 800 mT in steps of 100 mT.

Raw paleomagnetic data were obtained using Paleomagnetic Magnetometer Control System, 2010, v 2.4.0 (Kirschvink et al., 2008). All data were analyzed in PaleoMag v 3.1b2 (Jones, 2002) using the principal component analysis of Kirschvink (1980) for calculating the best fit for a linear vector of magnetic remanence using selected demagnetization steps for each specimen. The NRM of a rock is generally composed of at least two components: a primary NRM component inherited during rock formation and a secondary NRM component acquired during exposure to subsequent geomagnetic fields. Partial demagnetization experiments allow the identification and removal of low-stability NRM components which are inferred to be secondary NRM components (Butler, 1992). Progressive alternating-field (AF) demagnetization steps isolate the high-stability components which, in most cases, are inferred to be a primary NRM that represents the geomagnetic field at the time of rock formation. The high-stability component, however, is not necessarily the primary NRM as multiple overprinting magnetization components may have been inherited by the rock. For this reason, the high-stability component of NRM is generally referred to as the characteristic remnant magnetization (ChRM). Vertical-axis rotations were calculated using the methods of Beck (1980) and Demarest (1983).

XRF Geochemical Analysis

Ten samples from the Sierra Bacha were sent to the XRF (x-ray fluorescence) Lab at Michigan State University to obtain geochemical data for igneous rock classification and correlation of regionally extensive ignimbrites. All geochemical analyses were performed using a Bruker S4 PIONEER 4 kW wavelength dispersive x-ray fluorescence spectrometer. Bulk rock analysis involved high-temperature fusion of powdered samples

into homogenous glass disks by dilution with a lithium-tetraborate flux. Each sample was analyzed for major elements, and the trace elements Rb, Sr, and Zr. Data reduction was performed with SPECTRAplus software using fundamental parameters.

Geochronology

The ages of volcanic rocks reported in Table 1 from this study were determined by our colleague Alex Iriondo at UNAM-Juriquilla using U-Pb and Ar/Ar methods. All geochronologic data and descriptions of the analytical methods will be included in a future publication summarizing the results of this work.

CHAPTER IV

GEOLOGY AND STRATIGRAPHY OF THE SIERRA BACHA

Study Area and Access

The Sierra Bacha (Figs. 3, 4) is a coastal mountain range in northwestern Sonora, Mexico, located 160 kilometers WNW of Hermosillo and 100 kilometers NNW of Bahía de Kino. On most topographic maps of this region, the name “Sierra Bacha” refers only to the range adjacent to the coast in the northwesternmost study area, and in some cases the name “Sierra Tordilla” is used interchangeably. For the purpose of this study, all references to the “Sierra Bacha” hereafter refer to the coastal range as well as adjacent areas to the east and southeast. The 500 square kilometer study area is bounded to the west by the eastern margin of the Gulf of California, and to the east by the extensive alluvial floodplain of the Rio San Ignacio ~25 km inboard of the coast. The study area lies almost entirely within territory claimed by the indigenous Comcáac nation (Seri tribe) of western Sonora; permission and access were personally granted by tribal elders. Sonora Highway 003, located in the northeastern map area, is the only paved road in the region and provides the most reliable access to the area. High clearance vehicles and caution are recommended when navigating the dirt roads and dry arroyos.

Stratigraphic Overview

Geologic mapping, lithologic and petrographic analysis, Ar/Ar and U-Pb geochronology, XRF bulk rock analysis, and clast counts reveal 44 distinctive Neogene units in the Sierra Bacha study area (Plate 1, see supplemental file). For simplicity and

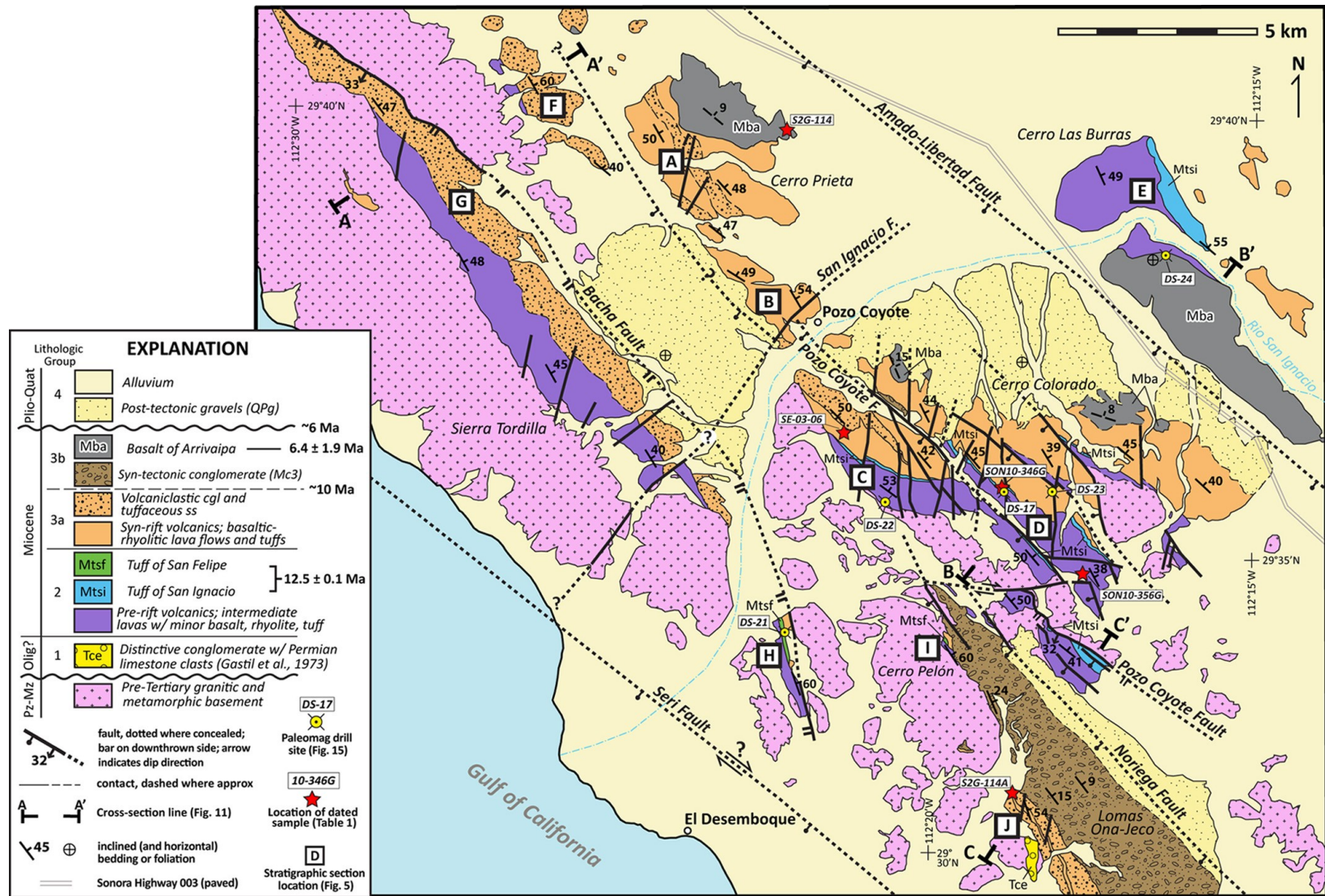


Figure 4. Summary geologic map of the Sierra Bacha in coastal Sonora, Mexico. See Fig. 3 for location. Detailed, 1:30,000 scale “Geologic Map of the Sierra Bacha, Coastal Sonora, Mexico” (Plate 1) is included with this thesis as supplemental material.

consistency with previous and ongoing studies, this study uses the established regional stratigraphic framework for coastal Sonora of Oskin & Stock (2003c) and Bennett (2009). Within this framework, stratigraphic units overlying basement rocks are divided into five tectono-volcanic groups as depicted on the summary geologic map of the Sierra Bacha (Fig. 4) and in the local stratigraphic sections (Fig. 5). Basement rocks in the study area include granitic rocks of the late Cretaceous coastal Sonora batholith as well as their associated Mesozoic-Paleozoic(?) metamorphic protoliths (Gastil and Krummenacher, 1976, 1977; Ramos-Velázquez et al., 2008).

The mostly volcanic section above the basement nonconformity has a composite thickness of up to 2,500 meters and consists predominantly of intermediate lava flows with interbedded basalts, rhyolites, welded tuffs, and nonmarine sedimentary rocks. Stratigraphic groups 1 and 2 comprise units that were deposited prior to rifting in the GEP. The only group 1 unit present in the Sierra Bacha is an Oligocene to middle Miocene fluvial conglomerate with distinctive Permian fusulinid-bearing clasts first described by Gastil et al. (1973). Rocks of group 2 consist of peraluminous basalt, andesite, and rhyolite lava flows, ash flow tuffs, and minor volcanoclastics deposited during subduction-related arc-volcanism in coastal Sonora (Hausback, 1984; Oskin & Stock, 2003b). The youngest units in group 2 are a pair of 12.5 Ma ignimbrites: the tuff of San Felipe ('*Mtsf*'; Stock et al., 1999; Oskin et al., 2001; Oskin and Stock, 2003b) and the tuff of San Ignacio ('*Mtsi*'; this study). These units are laterally extensive markers that permit correlation of discontinuous lava flows and domes across the map area and mark the boundary between groups 2 and 3. Group 3 units were deposited after the cessation of subduction and during early rifting in the Gulf of California (Oskin & Stock,

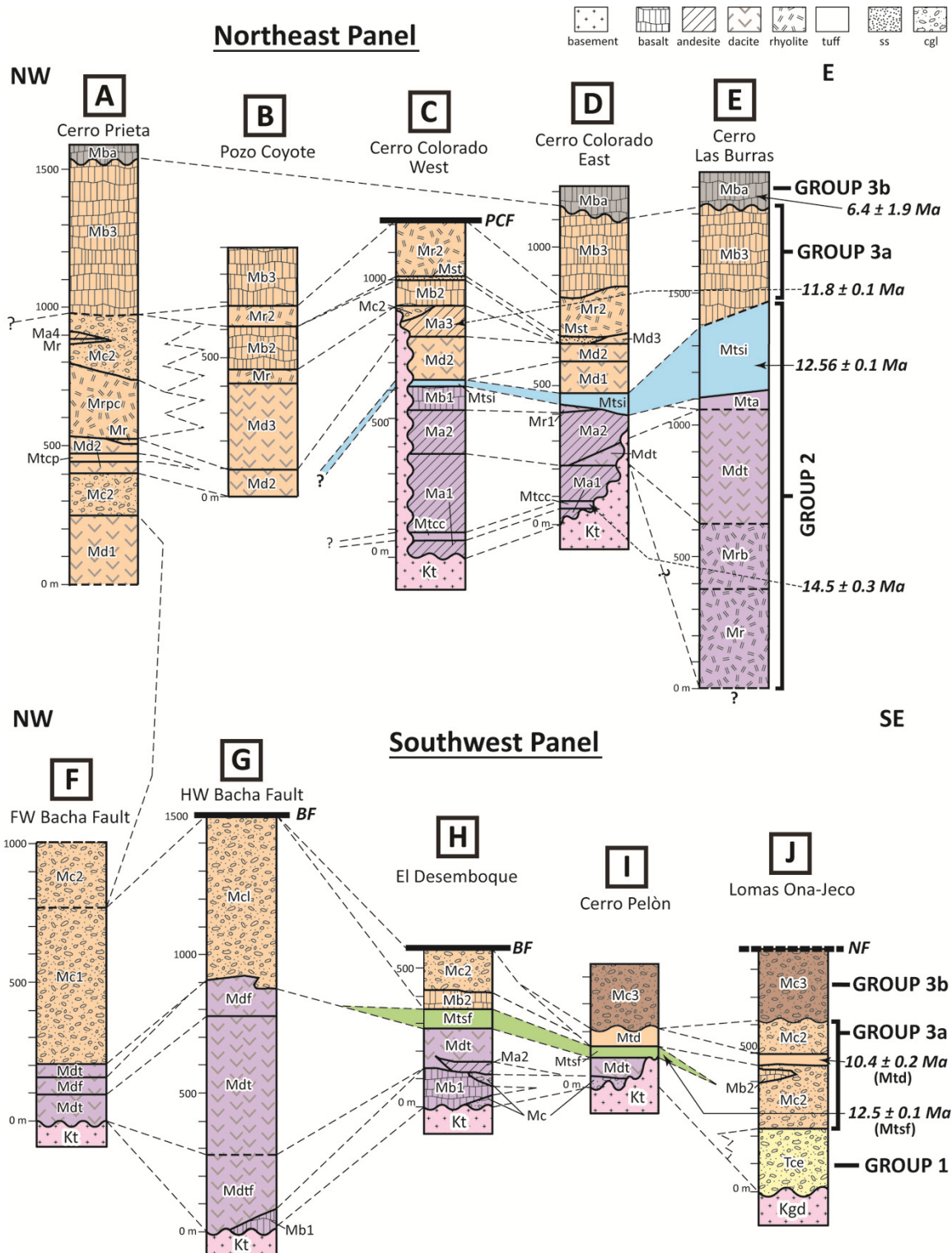


Figure 5. Stratigraphic columns for the Sierra Bacha area (see Fig. 4 for locations and explanation), illustrating typical unit thicknesses and existing age constraints. BF - Bacha fault, NF - Noriega fault, PCF - Pozo Coyote fault.

2003b). In this study, group 3 is subdivided into early syn-rift (groups 3a) and late syn-rift (group 3b) deposits. Group 3a units were deposited between 12.5 and ~10 Ma and range from basaltic to rhyolitic lava flows, with interfingering pyroclastic and volcanoclastic deposits. Importantly, all group 3a strata have similar moderate dips to the northeast with no discernible up-section change. In contrast, group 3b contains nonmarine conglomerates, basalt flows, and rare thin ash beds deposited between ~10 and 6 Ma that reveal an up-section decrease in bedding dip (fanning-dips) that record syn-depositional tilting during rifting in the GEP. Group 4 contains widespread, undeformed nonmarine, post-6 Ma sedimentary rocks.

Pre-Tertiary Basement

Pre-Tertiary basement in the Sierra Bacha consists of Mesozoic-Paleozoic-age metamorphic rocks and intrusive late Cretaceous granitoids of the coastal Sonora batholith (Anderson and Silver, 1969; Gastil et al., 1974; Gastil and Krummenacher, 1977; Gastil, 1993; Ramos-Velázquez et al., 2008). Metamorphic rocks include mostly low-grade, hornfels-facies metasediments with abundant primary quartz and secondary muscovite (*ms*), along with minor meta-volcanics (*mv*), meta-carbonate (*mcb*), and quartzite (*Pzq*) (Plate 1). Very fine-grained quartzite, which is only exposed in one locality just southwest of Pozo Coyote, is not observed elsewhere in Mesozoic strata of Sonora, leading some to interpret it as an unusual facies of Paleozoic strata west of the miogeoclinal margin (Gastil and Krummenacher, 1977; Stewart, 1988). Meta-carbonates are also inferred to be late Precambrian to Mesozoic in age and include mostly meta-limestone with 5-25 cm-thick planar lamellae and calcite-cemented sandstone. Unidentified fragmentary silicified fossils(?) 1-3 cm in length show both cylindrical and

4-6-sided prismatic/angular forms, and are abundant in very rare but densely-packed ~10 cm-thick horizons (29.52353° N, 112.31983° W).

Granitic basement rocks are exposed throughout the map area except in the northeastern region, and consist primarily of medium to coarse-grained tonalite (*Kt*) with plagioclase > quartz > biotite >> alkali feldspar, and granodiorite (*Kgd*) with plagioclase > quartz > alkali feldspar ≈ biotite. In some places, *Kt* contains locally abundant metasedimentary enclaves that are typical of S-type granites formed from metasedimentary protoliths. Granite (*Kg*) containing microcline megacrysts up to 3 cm in length and quartz > alkali feldspar >> biotite ≈ plagioclase is present in the central study area as 10-30 meter-thick dikes and a single concentric pluton that forms a prominent peak in the Cerro Pelón. Cross-cutting relationships and the presence of tonalite xenoliths within the granite indicate that virtually all *Kg* intrusions postdate emplacement of *Kt*. A single fine to medium-grained quartz diorite (*Kd*) intrusion is located in the northwestern map area which contains plagioclase > amphibole ≈ biotite > quartz ± orthopyroxene.

Although no isotopic ages were determined for crystalline basement rocks in the study area, reliable relative age constraints exist from coastal intrusions immediately adjacent to the Sierra Bacha, collectively referred to as the coastal Sonoran batholith (Ramos-Velázquez et al., 2008). U-Pb and Ar⁴⁰/Ar³⁹ ages of granitic intrusions from coastal Sonora reportedly range from ca. 100-69 Ma (Anderson and Silver, 1969; Gastil and Krummenacher, 1977; Ramos-Velázquez et al., 2008; Bennett, 2009). Ramos-Velázquez et al. (2008) report a cooling age of 69.4 ± 1.2 Ma [U-Pb] for the Tepopa tonalite located 15 kilometers south of the southern edge of the map area. A similar age

of 71.7 ± 1.4 Ma [K-Ar] was reported by Gastil and Krummenacher (1977) for a granodiorite located 4 kilometers west of the northwestern edge of the map area near Las Cuevitas (Fig. 3; Table 1).

Paleotopography

Mapping for this study revealed significant onlap of Group 2 and 3 volcanic and sedimentary strata onto basement rocks in the Cerro Colorado and near Pozo Coyote. The buttress unconformity generally has shallow ($< 10^\circ$) onlap angles, except one locality in the western Cerro Colorado where the onlap angle approaches $\sim 40^\circ$. These relationships provide evidence for significant paleotopography that was produced by exhumation and erosion after late Cretaceous intrusion of granitic basement rocks. The presence of low to moderate paleo-topographic relief (up to ~ 500 m) in the Sierra Bacha introduces some uncertainty to structural interpretations in the following sections.

Group 1: Basal Sedimentary Rocks (pre-15 Ma)

Group 1 strata consist of basal sedimentary units that nonconformably overlie the granitic and metamorphic basement complex, representing the oldest Neogene deposits in the GEP (Oskin & Stock, 2003b). The only unit in the Sierra Bacha area that undeniably belongs to stratigraphic group 1 is a distinctive fluvial conglomerate with an exotic clast assemblage (*Tce*) (Gastil et al., 1973; Bryant, 1986). In the study area, *Tce* is a mostly clast-supported pebble-cobble conglomerate with sparse boulders up to 60 cm in diameter and a white to red granular, grussy matrix. Clasts are well to very well rounded and include quartzite, tonalite, meta-basement, chert, limestone, and less abundant volcanics. *Tce* in the Sierra Bacha is herein correlated with the exotic clast conglomerate of Gastil et al. (1973) based on the following criteria: 1) limestone clasts containing fusulinid(?) and

Table 1. Summary of Available Geochronologic Data for Lithologic Units in the Sierra Bacha Area, Coastal Sonora, Mexico

| Lithologic Group | Sample number | Lithologic Unit | Map symbol (this study) | Rock type | Long. (°W) or Easting* (m) | Lat. (°N) or Northing* (m) | Age (Ma) | Isotopic technique | Mineral | Reference |
|------------------|---------------|------------------------|-------------------------|-------------------|----------------------------|----------------------------|--------------|--------------------|--------------|-------------------------------|
| <u>Group 3b</u> | S2G-114 | Basalt of Arivaipa | Mba | basalt | 112.376733° | 29.663879° | 6.4 ± 1.9 | K-Ar | whole rock | Gastil & Krummenacher (1977) |
| <u>Group 3a</u> | S2G-114A | Tuff of Desemboque | Mtd | ash-flow tuff | 112.311228° | 29.513669° | 10.4 ± 0.2 | K-Ar | feldspar | Gastil & Krummenacher (1977) |
| | SE-03-06 | volcanic | Ma3 | basaltic-andesite | 368797 | 3274621 | 11.76 ± 0.08 | Ar/Ar | glass matrix | A. Iriondo (unpubl. data) |
| <u>Group 2</u> | PC-98-18** | Tuff of San Felipe | Mtsf | ash-flow tuff | 394475 | 3208720 | 12.50 ± 0.08 | Ar/Ar | anorthoclase | Bennett et al. (2007) |
| | SON10-346G | Tuff of San Ignacio | Mtsi | ash-flow tuff | 372427 | 3273392 | 12.56 ± 0.09 | U-Pb | zircon | A. Iriondo (unpubl. data) |
| | SON10-356G | Tuff of Cerro Colorado | Mtcc | ash-flow tuff | 374730 | 3271014 | 14.5 ± 0.3 | U-Pb | zircon | A. Iriondo (unpubl. data) |
| <u>Basement</u> | KI-12-46** | Tepopa Tonalite | Kt | tonalite | 365796 | 3247634 | 69.4 ± 1.2 | U-Pb | zircon | Ramos-Velázquez et al. (2008) |
| | S0H-281** | batholithic basement | Kgd | granodiorite | 112.558826° | 29.69698° | 71.7 ± 1.4 | K-Ar | biotite | Gastil & Krummenacher (1977) |

* UTM coordinates from zone 12R, WGS 84 Datum

** Sample collected from outside of the study area; location not shown in Fig. 4

gastropod(?) fossils, 2) similar extra-regional clast assemblage, and 3) proximity to previously mapped outcrops along strike to the southeast in the Sierra Seri (Fig. 3).

The age of *Tce* is weakly constrained by geologic and stratigraphic data from Baja California and coastal Sonora. The oldest conformable unit overlying group 1 strata in Baja California is the 12.5 Ma Tuff of San Felipe (Stock et al., 1999). Upper group 1 strata in Baja are intercalated with volcanic flows as old as ca. 20-21 Ma (Lewis, 1994; Stock, 1989). In the Sierra Bacha, group 1 strata are overlain by the 14.5 Ma Tuff of Cerro Colorado (*Mtcc*), middle to late Miocene conglomerates (*Mc2*), and the 10.4 ± 0.2 Ma Tuff of Desemboque (*Mtd*). These data, along with additional stratigraphic constraints on Baja (e.g. Dorsey & Burns, 1994; Oskin & Stock, 2003c) suggest an Oligocene to middle Miocene age for group 1 strata, possibly as young as ~15 Ma.

Group 2: Pre-Rift Rocks (~15-12 Ma)

Rocks of stratigraphic group 2 consist of basaltic-rhyolitic lava flows and interbedded pyroclastics that, according to previous workers (Gastil et al., 1979; Sawlan, 1991), were deposited during active subduction and Miocene arc volcanism (Figs. 4, 5). Calc-alkaline to alkaline volcanic units predominantly consist of peraluminous basaltic-trachyandesite, trachyandesite, and dacite flows (Fig. 6) and are best exposed in the Cerro Colorado and in the coastal Sierra Tordilla. Group 2 units have an average composite thickness of ~500-700 meters and attain a maximum thickness of ~1100 meters in the Cerro Las Burras (Fig. 5). Basal units nonconformably overlie crystalline and metamorphic basement and in some areas conformably overlie thin deposits of group 1 strata. All geochemical data are listed in Table 2.

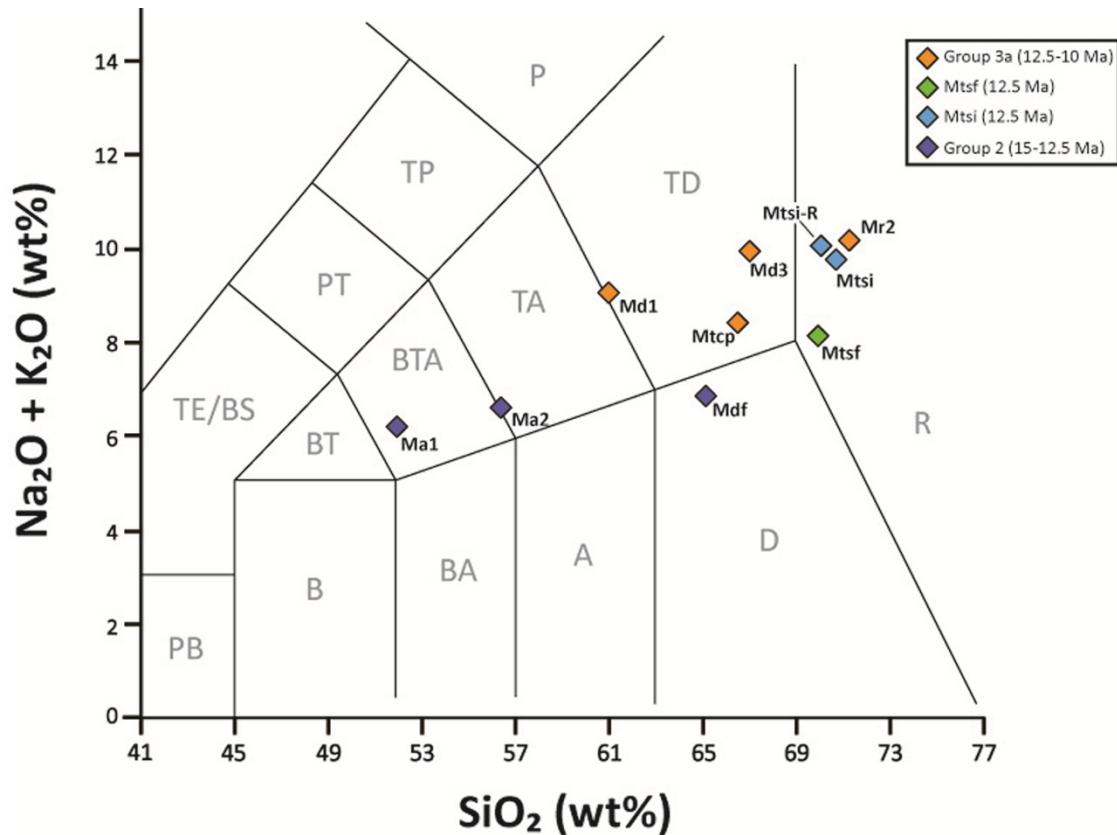


Figure 6. Total alkali versus silica (TAS) diagram (Le Maitre et al., 1989) showing the classification of volcanic units from the Sierra Bacha. Bulk rock XRF major- and trace-element data are listed in Table 2. All samples (except *Mdf*) lie within the basaltic-trachyandesite to rhyolite fields and show high total alkali concentrations > 6 wt%. Abbreviations: PB = picro-basalt, B = basalt, BA = basaltic-andesite, A = andesite, D = dacite, R = rhyolite, TB = trachy-basalt, BTA = basaltic trachy-andesite, TA = trachy-andesite, TD = trachyte/trachy-dacite, TE/BS = tephrite/basanite, PT = phono-tephrite, TP = tephri-phonolite, P = phonolite.

Lava flows range in composition from trachybasalt to rhyolite, although the most voluminous units are basaltic-andesite and andesite. *Ma1* is a suite of 2-4 gray-purple, plagioclase-phyric, basaltic-trachyandesite lava flows with locally abundant vesicles filled with secondary zeolite minerals. Exposures are typically weathered and rubbly, and total thickness is ~ 200 -400 meters. The age of *Ma1* is constrained by the interbedded Tuff of Cerro Colorado (*Mtcc*), which has a U-Pb zircon age of 14.5 ± 0.3 Ma (Table 1).

Table 2. XRF Bulk Rock Analysis of Major and Trace Element Compositions

| Lithologic Unit | Ma1 | Ma2 | Mdf | Mtsi* | Mtsi | Mtsf | Md1 | Md3 | Mr2 | Mtcp |
|------------------------------------|-----------|-----------|-----------|-----------|------------|-----------|-----------|-----------|----------|-----------|
| Group | 2 | 2 | 2 | 2 | 2 | 2 | 3a | 3a | 3a | 3a |
| Sample ID | SON10-358 | SON10-46 | SON11-46M | SON11-83a | SON10-346G | SON11-73B | SON10-127 | SON10-273 | SON11-99 | SON11-124 |
| Age (Ma) | ~14.5 | 14.5-12.5 | > 12.5 | 12.5 | 12.5 | 12.5 | 12.5-11.8 | < 11.8 | < 11.8 | < 12.5 |
| wt % | | | | | | | | | | |
| SiO₂ | 51.78 | 55.94 | 65.01 | 69.93 | 70.56 | 69.8 | 60.75 | 66.88 | 71.14 | 66.36 |
| TiO₂ | 2.29 | 1.43 | 0.54 | 0.2 | 0.21 | 0.14 | 0.98 | 0.28 | 0.24 | 0.35 |
| Al₂O₃ | 16.16 | 17.18 | 15.63 | 13.6 | 13.58 | 11.86 | 16.11 | 14.75 | 12.97 | 15.32 |
| Fe₂O₃ | 10.98 | 7.67 | 3.91 | 2.24 | 2.53 | 1.86 | 6.49 | 3.93 | 3.78 | 2.89 |
| MnO | 0.17 | 0.11 | 0.06 | 0.03 | 0.06 | 0.05 | 0.11 | 0.12 | 0.07 | 0.06 |
| MgO | 3.95 | 3.02 | 1.39 | 0.17 | 0.37 | 0.32 | 1.71 | 0.26 | 0.01 | 0.93 |
| CaO | 6.63 | 5.91 | 3.71 | 0.88 | 0.94 | 3.97 | 2.86 | 1.7 | 0.37 | 2.73 |
| Na₂O | 4.68 | 4.75 | 4.33 | 1.41 | 4.06 | 3.53 | 5.85 | 5.95 | 5.27 | 4.79 |
| K₂O | 1.54 | 1.83 | 2.54 | 8.65 | 5.71 | 4.61 | 3.19 | 4 | 4.89 | 3.65 |
| P₂O₅ | 0.43 | 0.34 | 0.3 | 0.06 | 0.08 | 0.05 | 0.41 | 0.08 | 0.04 | 0.11 |
| Totals | 98.61 | 98.18 | 97.42 | 97.17 | 98.1 | 96.19 | 98.46 | 97.95 | 98.78 | 97.19 |
| LOI (%) | 1.22 | 1.61 | 2.32 | 2.66 | 1.78 | 3.7 | 1.35 | 1.75 | 1.06 | 2.58 |
| ppm | | | | | | | | | | |
| Rb | 23 | 40 | 61 | 326 | 220 | 180 | 68 | 93 | 135 | 97 |
| Sr | 501 | 673 | 599 | 96 | 44 | 44 | 328 | 144 | 16 | 471 |
| Zr | 285 | 249 | 309 | 242 | 447 | 410 | 468 | 513 | 980 | 333 |

* Rheomorphic *Mtsi* labeled "Mtsi-R" in Figure 6

Mss consists of epiclastic sandstone and grus typically 1- to 3-meters-thick (up to 15 m), with massive to well-laminated beds of immature, fine to medium-grained sandstone (quartz >> alkali \approx biotite). Its composition resembles that of the underlying granitic basement complex and deposits are commonly found resting directly on weathered tonalitic basement rocks and also intercalated with undifferentiated yellow lithic tuffs (*Mtu*) and andesite flows (*Ma1*) in the Cerro Colorado (Plate 1).

Ma2 is a 400 meter thick stack of purple, aphyric trachyandesite in the southwestern Cerro Colorado that is cut by multiple feeder dikes and agglomeritic breccia zones characteristic of an andesite dome proximal facies. More distal facies have 1- to 2-meter-thick red (oxidized) breccias at their bases and show an average combined thickness of ~200-300 meters that thins considerably to the north and northeast. A similar aphyric andesite flow is also observed just west of the Cerro Pelón in footwall strata of the Bacha fault. Petrographic analysis reveals ~1-2% microlitic plagioclase and pyroxene(?) in an aphanitic groundmass. *Mr1* is a densely foliated rhyolite lava flow found only in the Cerro Colorado. This unit contains up to 5% phenocrysts (quartz \approx sanidine > feldspar) in a pink-purple groundmass and reaches a maximum thickness of ~50 meters. A thick sequence of gray-purple, quartz-feldspar-phyric rhyodacite flows (*Mr*) and compositionally similar rhyolitic breccias (*Mrb*) are found only in the Cerro Las Burras. Because the ages of these units are unknown and constrained only by their stratigraphic positions below the 12.5 Ma tuff of San Ignacio (*Mtsi*), they might instead belong in stratigraphic group 1 (pre-15 Ma).

A distinctly different local stratigraphy, observed in the western study area, is dominated by a proximal to medial stratovolcano facies consisting of dacite lava flows

and mono-lithologic tuffs and breccias. Dacite lava flows (*Mdf*) are porphyritic with ~15% phenocrysts of plagioclase >> biotite > quartz. *Mdt* predominantly consists of lithic-rich tuffs with subordinate tuff breccias and lava flows. Tuffs and breccias have a nearly homogeneous composition of porphyritic *Mdf* clasts that makes *Mdt* a key stratigraphic marker. The ages of these units in the northwestern map area are not constrained by dated stratigraphy, but are inferred to be coeval with other group 2 strata to the east and southeast. Northeast of Desemboque, the 12.5 Ma tuff of San Felipe (*Mtsf*) is in concordant contact with *Mdt* below (Plate 1). In addition, similar group 2 units on Baja California, described as plagioclase- and biotite-rich porphyritic dacites with related tuffs and breccias, have ages ranging from 15.5 to 16.7 Ma (e.g. the Tombstone Dacite of Nagy et al., 1999). The basaltic facies of group 2 (*Mbl*) consists of thin discontinuous exposures of indurated, glassy basalt flows that rarely reach thicknesses greater than 20 meters. Some flows are aphanitic while others show up to 10% altered olivine and pyroxene(?) phenocrysts.

The Tuff of Arivaipa (*Mta*) is deep maroon-red, partially welded, crystal- and lithic-rich rhyolite tuff ~50-80 meters-thick and only exposed in the Cerro Las Burras in the northeastern map area (Plate 1). A 1- to 4-meter-thick white-red brecciated base grades into the partially welded lithic-rich section containing 15% brown, red, purple, black, subangular volcanic lithics with rare tonalite xenoliths. Phenocrystic quartz and plagioclase (up to 5%) and undeformed yellow, ashy pumice are diagnostic of this tuff. The upper 2-3 meters of *Mta* are nonwelded and contain abundant yellow and white pumice clasts with no phenocrysts. A discontinuous white, ashy, quartz-rich tuff layer is observed ~30 meters down from the top of the unit, which is up to 10 meters-thick and

difficult to follow along strike. The age of *Mta* is unknown and constrained only by the overlying 12.5 Ma tuff of San Ignacio (*Mtsi*).

Tuff of Cerro Colorado (Mtcc)

The Tuff of Cerro Colorado (*Mtcc*) is a 10-40 m thick yellow-red crystal-lithic rhyolite tuff. U-Pb zircon data reveals a maximum eruption age of 14.5 ± 0.3 Ma for *Mtcc* (Table 1). This tuff overlies the basement nonconformity or *Ma1* throughout most of the Cerro Colorado, marking the base of the volcanic section in the Cerro Colorado and most of the study area. The base of *Mtcc* is a 2-8 m thick, yellow-orange, nonwelded member with yellow-red-purple tephra and subangular volcanic lithics, grading upward into a brick red, partially-welded crystal-lithic tuff with yellow and grey pumice (up to 5%) and ~10% phenocrysts (quartz > feldspar). In some places *Mtcc* contains multiple cooling units several meters thick and occasionally displays a purple, densely welded upper unit with significantly less pumice and smaller lithic fragments. The uppermost welded members form resistant ridges flanked by colorful talus slopes on both sides.

Tuff of San Ignacio (Mtsi)

The Tuff of San Ignacio (*Mtsi*) is a widespread, pink-white-orange, densely welded, spherulitic rhyolite ash-flow tuff with an average thickness of 20-40 meters (up to 350 m) that was not recognized prior to this study (Plate 1; Figs. 4, 5). A high precision U-Pb age of 12.56 ± 0.09 Ma was calculated for *Mtsi* (Table1), nearly identical to the age of the well studied tuff of San Felipe (e.g. Stock et al., 1999; Oskin and Stock, 2003b).

Mtsi is an ashy, bubble-gum pink to white, crystal-poor tuff with unique subrounded to angular, plagioclase-phyric, vesicular andesite lithics up to 5 cm in

diameter (average ~1 cm) and rare centimeter-scale white to pink fiamme (Fig. 7). Abundant 0.5-3 cm-diameter quartz-filled spherules and lithophysae in a pink-white, ashy groundmass are especially diagnostic of this tuff and pervasive throughout the vapor-phase alteration zone. Petrographic examination reveals very rare small pumice fragments, partially dissolved potassium feldspar, quartz, and biotite in an ash-rich groundmass. Very rare quartz and biotite phenocrysts are also observed in hand sample. The base of *Mtsi* is commonly a ~1-5 m-thick, dense black-brown vitrophyre with rare feldspar micro-phenocrysts. A 0.5-1.5 m-thick, orange-brown, laminated basal surge deposit in the central and southern Cerro Colorado locally contains abundant tonalite pebbles and cobbles. The basal unit is overlain by a 5-8 meter-thick salmon-orange, crystal and lithic-rich welded zone with minor phenocrysts including quartz >> feldspar > biotite. The welded zone grades upward into a partially welded, spherulitic vapor-phase alteration zone which ranges from 10 to 30 m-thick in most exposures.

Internal rheomorphic flow deformation in the form of severely folded and recrystallized pumice fiamme is characteristic of *Mtsi* in the Cerro Las Burras where it reaches a maximum thickness of ~350 meters. Flow-banding is densely-spaced (< 1 cm) and rheomorphism is irregularly distributed with pumice lineations showing varying degrees of deformation, some stretched out up to 30 cm-long (1:50 aspect ratio).

Tuff of San Felipe (Mtsf)

The Tuff of San Felipe (*Mtsf*) is a well-documented regionally extensive rhyolite ignimbrite that serves as an important marker horizon for reconstructions of the Gulf Extensional Province (Stock et al., 1999; Oskin et al., 2001; Oskin and Stock, 2003b). Bennett et al. (2007) report a high-precision $\text{Ar}^{40}/\text{Ar}^{39}$ age of 12.50 ± 0.08 Ma for *Mtsf*

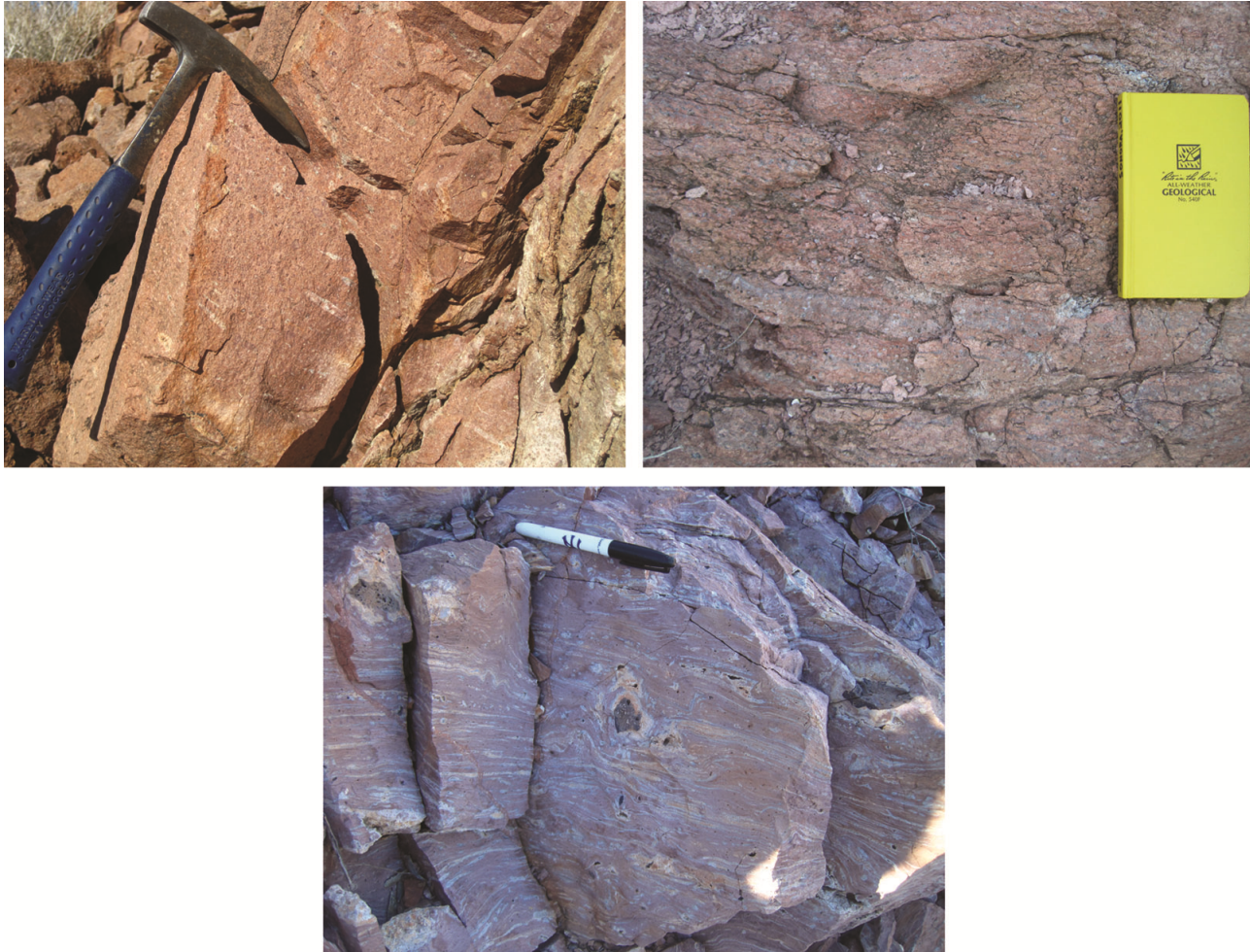


Figure 7. Field photographs of the 12.5 Ma tuff of San Ignacio (*Mtsi*). (Top-left) Lower densely welded zone showing 1 to 3 cm-long, white-pink flattened pumice flake. (Top-right) Spherule-rich zone of vapor phase alteration; notebook is 19 x 12 cm. (Bottom) Rheomorphism in *Mtsi* from the Cerro Las Burras where it reaches a maximum thickness of ~350 m. Pumice are completely replaced by secondary quartz and irregularly folded and stretched up to 40 cm in length. Dark vesicular trachyandesite inclusions (3 total in photo) are up to 4 cm in diameter.

(Table 1). Vent-proximal facies are found east of the Sierra San Felipe in northeastern Baja and west of the Cerro Kino in coastal Sonora (Fig.3), and the entire tuff sheet is estimated to cover an area $> 4000 \text{ km}^2$ on both margins of the Gulf (Oskin and Stock, 2003b). *Mtsf* is a maroon-orange densely welded tuff with multiple cooling units that contain abundant yellow-white pumice and 10-15% anorthoclase phenocrysts, rare zoned pyroxene, and absolutely no phenocrystic quartz. Abundant flattened pumice fiamme reach lengths of up to 25 cm that form a well-defined eutaxitic foliation in *Mtsf*. Trachyte-rhyolite inclusions are a common diagnostic feature of this ignimbrite, most of which contain abundant alkali feldspar in a dark glassy groundmass.

Mtsf is only exposed at two localities in the study area (Plate 1; Fig. 4). These locations represent the northernmost identified outcrops of *Mtsf* on the eastern rifted margin of the Gulf of California. Northeast of El Desemboque, *Mtsf* is ~25-70 m-thick with a thin (< 1 meter) discontinuous black vitrophyre. The lower densely welded, fiamme-rich member (20-40 m-thick) grades upward into a non-welded zone with intact, undeformed pumice (5-30 m-thick).

Distinctions between Mtsi and Mtsf

Mtsi and *Mtsf* share the same age within standard error, a similar unique paleomagnetic remanence direction, and both contain similarly distinct dark volcanic inclusions. However, geochemical and mineralogical differences indicate that *Mtsi* and *Mtsf* are different tuffs. *Mtsf* completely lacks quartz and biotite phenocrysts, which are rare but present in *Mtsi*. Comparison of Rb, Sr, and Zr trace element data for *Mtsi* and *Mtsf* from this and previous studies (Stock et al., 1999; Oskin and Stock, 2003b) shows subtle chemical difference between the two tuffs (Fig. 8). Additionally, *Mtsi* deposits

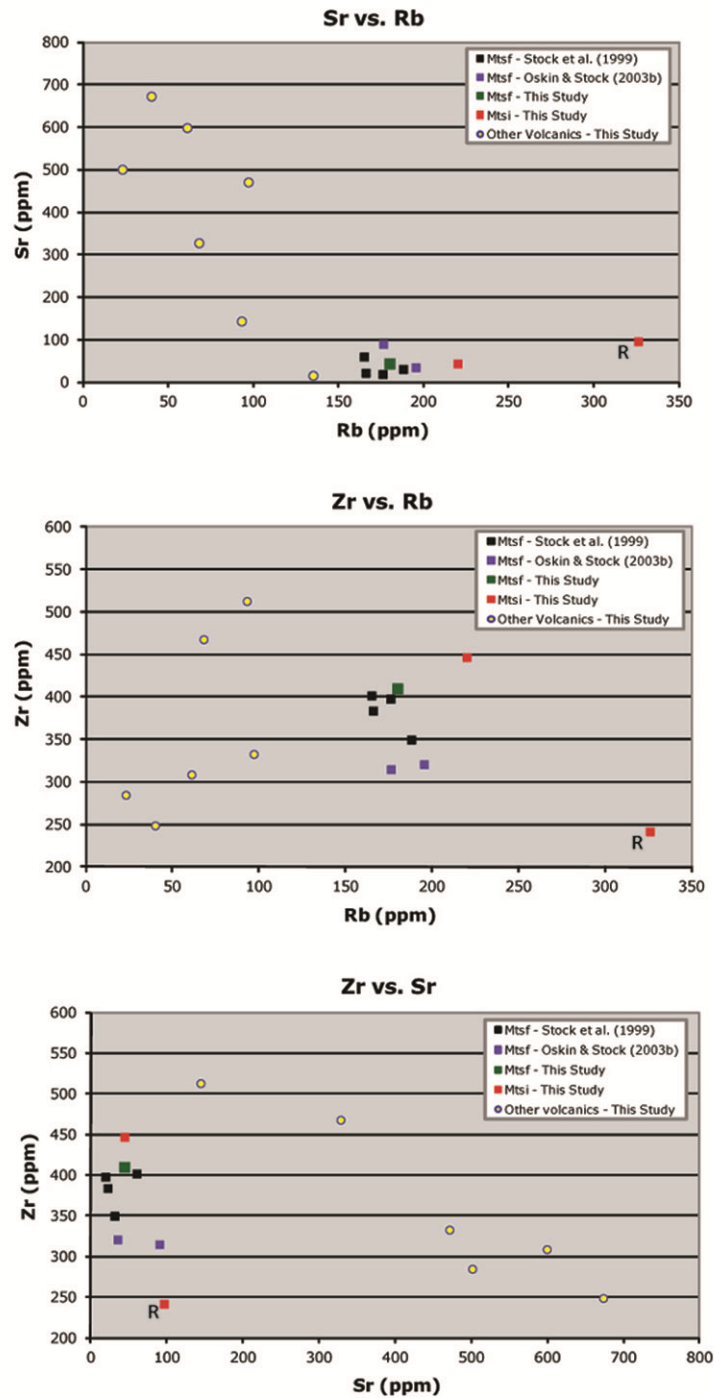


Figure 8. Comparison of bulk rock trace element data for the 12.5 Ma tuffs of San Ignacio (*Mtsi*) and San Felipe (*Mtsf*). *Mtsf* in the Sierra Bacha (green) correlates strongly with other geochemical data for *Mtsf* from Baja California and coastal Sonora (black - Stock et al., 1999; purple - Oskin and Stock, 2003b). *Mtsi* (red) samples do not correlate well with *Mtsf*, suggesting that they represent different tuff units. Alteration associated with rheomorphic flow deformation in the *Mtsi* sample marked “R” may explain its decorrelation with the other *Mtsi* sample.

thicken dramatically to the northeast in the Sierra Bacha, representing a proposed vent located northeast of the study area. In contrast, the vent for *Mtsf* is located ~70 km south of the study area in the Cerro Kino area (Fig. 3). The fact that the tuffs erupted nearly simultaneously yet are not found in stratigraphic contact with one another in the Sierra Bacha is rather conspicuous (Fig. 5). This could be due to (i) very limited exposure of *Mtsf* in the study area, or (ii) coincidental confluence of the most distal facies of both tuffs in the Sierra Bacha region. In summary, the available geologic evidence indicates that *Mtsi* and *Mtsf* are different lithologic units erupted nearly synchronously ca. 12.5 Ma. The distribution and vent location of *Mtsi* and its genetic relationship with *Mtsf* remain incompletely understood and would require additional work in coastal Sonora and possibly Baja California to understand the nature of the relationship between these unique and widespread pyroclastic flows.

Group 3a: Early Syn-Rift Rocks (12.5~10 Ma)

Group 3 rocks were deposited after subduction and during early rifting in the proto-Gulf of California ca 12.5-10 Ma (Oskin & Stock, 2003b). The sequence has an average composite thickness of ~600-1000 meters, reaching a maximum exposed thickness of 1550 meters in the Cerro Prieta area (Plate 1; Figs. 4, 5). Rock types include peraluminous basaltic to rhyolitic lava flows, nonmarine volcanoclastic conglomerate and sandstone, and minor pyroclastic flows.

In the Cerro Colorado, *Md1* and *Md2* are stony, purple-grey, aphanitic trachydacite flows with < 2% altered sanidine phenocrysts in a microlitic plagioclase groundmass with minor pyroxene. Both units contain multiple ~20-60 m-thick flows with 1-4 m-thick reddish (oxidized) basal flow breccias. 2-3 m-thick yellow-green

pyroclastics are present between individual flows in the northern Cerro Colorado. The only difference between *Md1* and *Md2* is that *Md2* commonly displays a well-defined 1-4 cm-spaced flow foliation, and up to 5% blocky sanidine and plagioclase phenocrysts. Exposures of *Md3* are rare and discontinuous in the central and eastern study area and consist of 20-40 m-thick grey, alkali-enriched trachydacite flows containing 10-15% altered phenocrysts (plagioclase > alkali feldspar \approx amphibole >> apatite).

Ma3 is a black basaltic-andesite flow with a plagioclase- and altered pyroxene-rich microlitic groundmass and no olivine. It is best exposed ~3 kilometers south of Pozo Coyote where it is ~100 m-thick and intercalated with 2-3 m-thick red tuffaceous sandstones and pyroclastic breccias (Plate 1). Rare lath-shaped plagioclase phenocrysts are up to 2 mm-long and vesicles are commonly filled with secondary white-yellow zeolite minerals. An $^{40}\text{Ar}/^{39}\text{Ar}$ isochron age of 11.76 ± 0.08 Ma was determined for this unit (A. Iriondo, unpubl. data). *Mst* is up to 25 m-thick and consists of well-laminated lithic tuffs and tuffaceous sandstone with yellow-white-light green pumice and dark volcanic lithics in an ashy yellow matrix. Individual beds are 30-100 cm-thick and show normal grading of pumice and lithics. *Mr2* is an aphanitic grey-light purple, resistant rhyolite flow with a well-defined flow foliation defined by glassy lens and frothy grey lineations with pervasive secondary quartz precipitation in some localities. This unit consists of one or two 60-90 m-thick flows with a unique pink-red-white airfall ash at the base and a discontinuous green-black 1-3 m-thick vitrophyre. *Mb2* is a sequence of 10-20 m-thick glassy, black, plagioclase-phyric basalt flows with up to 10% phenocrysts (plagioclase > orthopyroxene >> amphibole) and cindery pyroclastic breccias up to 5 m-thick. A thicker sequence of basalt flows (*Mb3*) represents the youngest stratigraphic unit

in group 3a. These deposits are mostly dark purple-black, aphanitic vesicular basalt with ~1% plagioclase phenocrysts in a glassy groundmass and reach up to ~400 m-thick where there is good structural control. *Ma4* is a local vesicular basaltic-andesite flow in the Cerro Prieta with abundant (10-20%) altered red pyroxene. The tuff of Cerro Prieta (*Mtcp*) is a pink, densely welded rhyodacite tuff with a 1-2 m-thick basal vitrophyre, eutaxitic foliation defined by flat recrystallized pumice frame, and 10-15% phenocrysts (sanidine > biotite > quartz). *Mtcp* bears a slight resemblance to *Mtsi* in both mineralogy and the abundance of spherules in the vapor phase alteration zones. However, *Mtcp* is not correlated with *Mtsi* based on (1) its stratigraphic position above *Md1* and *Mtsi*, (2) higher abundance of phenocrystic quartz and biotite, and (3) dissimilar geochemical signature (Fig. 6). A thick sequence of similar pink, porphyritic rhyodacite flows (*Mrcp*) containing ~15% phenocrysts (feldspar > quartz ≈ biotite) and an irregular flow foliation overlies nonmarine conglomerates and *Mtcp* in the Cerro Prieta. A 1-10 m-thick yellow airfall ash is present at base of each lava flow, usually below a 1-3 m-thick basal vitrophyre.

Mc1 consists of monolithologic volcanoclastic conglomerate and breccia in the northwestern map area that overlies similar composition dacite flows and tuffs (*Mdf*, *Mdt*, and *Mdtf*). The 750 m-thick unit is a massive, poorly-sorted, pebble-cobble conglomerate with a grey ashy matrix. Compositional homogeneity consisting of porphyritic *Mdf* clasts is diagnostic of *Mc1*. In contrast, *Mc2* consists of polymictic pebbly sandstone to sandy pebble conglomerate with interbedded pebble-cobble conglomerate. In the western Cerro Colorado, this unit shows locally well-developed planar stratification, mixed matrix and clast support in 5-15 cm-thick beds defined by grain segregation, and mostly subangular

to subrounded intermediate volcanic clasts with less common basement clasts and outsized boulders up to 35 cm in diameter. In the Lomas Ona-Jeco (southern area), *Mc2* is mostly massive with local planar lamination of ~20-50 cm-thick bedsets defined by grain-size variations.

Tuff of Desemboque (Mtd)

A K-Ar age of 10.4 ± 0.2 Ma was reported by Gastil and Krummenacher (1977) for an unnamed rhyolite tuff in the southern map area that is named the tuff of Desemboque (*Mtd*) by this study (Plate 1; Table 1). *Mtd* is a 40-50 m-thick rhyolite ash flow tuff with a thin (0.5-1 m), discontinuous, porphyritic black vitrophyre with euhedral plagioclase > quartz > biotite > alkali feldspar. Immediately above the base is a 5 m-thick pink, ashy, crystal-rich layer that grades into a 10-15 m-thick moderately-densely welded zone with abundant 4-12 cm-long yellow pumice fiame and 10-15% phenocrysts (feldspar > biotite \approx quartz). The upper 30 meters show extensive vapor phase alteration and abundant quartz-filled spherules in a pink groundmass (similar to *Mtsi*); spherules decrease in abundance up section to the grey-white, nonwelded top of the unit. *Mtd* is an interbed within *Mc2* conglomerate and continues along strike to the SE outside of the study area.

Group 3b: Late Syn-Rift Rocks (~10-6 Ma)

Rocks of stratigraphic group 3b unconformably overlie group 3a strata and consist of shallowly-dipping, nonmarine, syn-tectonic conglomerate (*Mc3*) and basalt flows (*Mba*) that accumulated during proto-Gulf extension in the Sierra Bacha. *Mc3* consists of massive to moderately sorted volcanoclastic matrix-rich pebble-cobble conglomerate that displays mixed matrix and clast support and rare boulders up to 50 cm in diameter, and

interbedded pebbly sandstone beds. The clast assemblage is polymictic with angular to subrounded volcanic and basement clasts in a grussy, red sand matrix. *Mc3* is very similar in composition to *Mc2* of group 3a, with two important features that distinguish it from *Mc2*: (1) *Mc3* contains a significantly higher percentage of tonalite, metasedimentary, and meta-volcanic basement clasts (Fig. 9), and (2) *Mc3* displays bedding dips that decrease systematically up-section from about 39° to horizontal in the hanging wall of the concealed Noriega fault in the southern map area (Fig. 11C). The age of this unit is constrained by its stratigraphic position above the 10.4 Ma tuff of Desemboque (*Mtd*) and below the Basalt of Arivaipa (*Mba*).

The Basalt of Arivaipa (*Mba*) is an unnamed sequence of horizontal to sub-horizontal, 10-15 m-thick basalt flows dated by Gastil and Krummenacher (1977) at 6.4 ± 1.9 Ma [K-Ar]. *Mba* unconformably overlies pre- and syn-rift strata (groups 2, 3a, 3b) in the northern, central, and eastern study area (Plate 1; Fig. 4). The best exposures of *Mba* cap high topography in the Cerro Prieta and Cerro Las Burras, where individual flows show 1-3 m-thick red-black basal flow breccias, vesicular upper and lower contacts, and well-defined ~0.5 m-spaced vertical joints. *Mba* is aphanitic with micro-phenocrysts of plagioclase. The fine-grained groundmass contains plagioclase >> olivine \approx pyroxene \approx magnetite. Small exposures of nearly flat-lying basalt in the Cerro Las Burras and NW of the Cerro Prieta contain abundant olivine phenocrysts and are correlated with *Mba*, although their position structurally below capping *Mba* are difficult to explain.

Group 4: Post-Rift Rocks (post-6 Ma)

Group 4 rocks include untilted, post-rift nonmarine sedimentary units deposited after ~6 Ma (Oskin and Stock, 2003b). These units unconformably overlie all older units

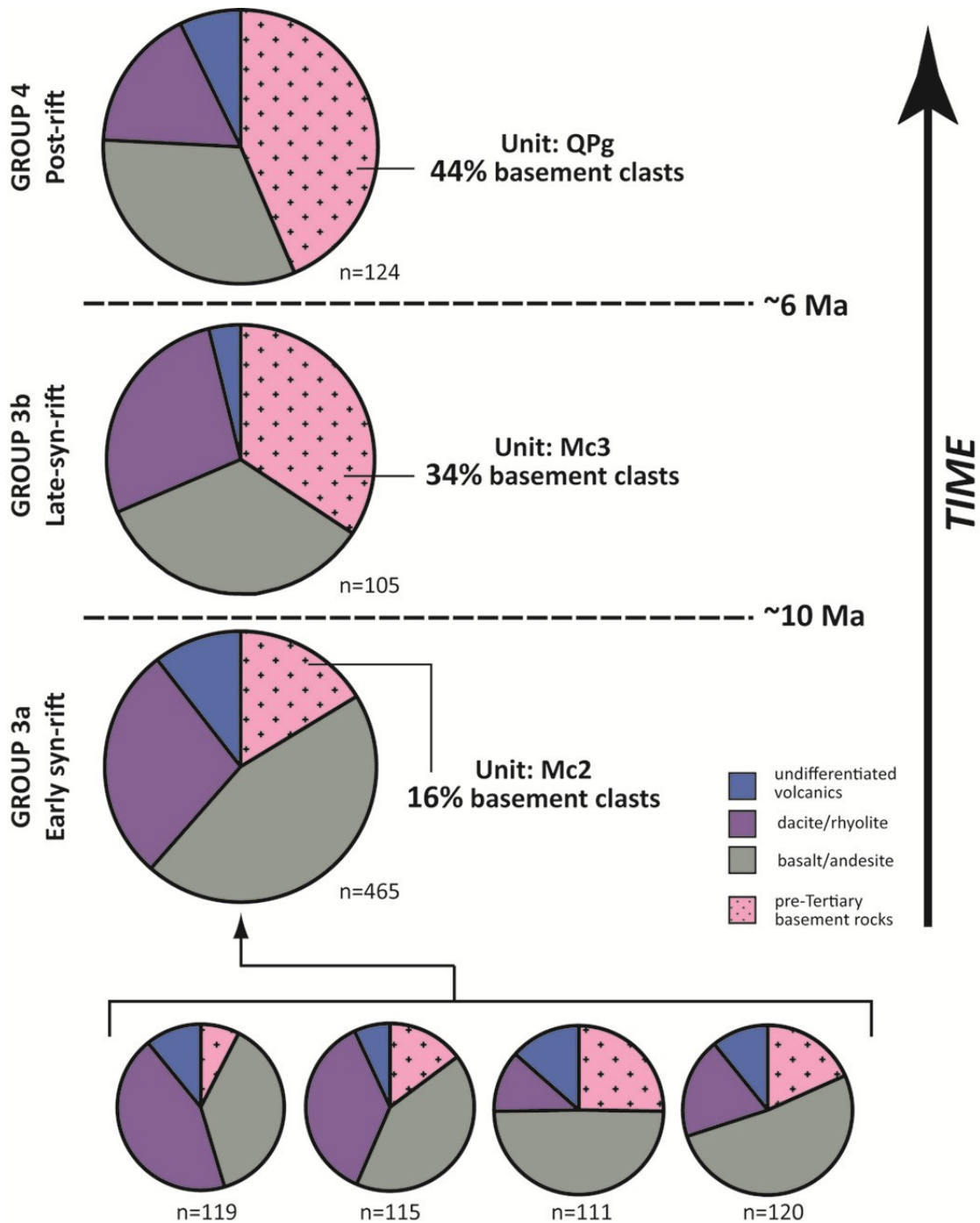


Figure 9. Clast count data for conglomerate units in the study area. Note substantial increase in basement clast percentage with time from ~16% in group 3a (12.5-10 Ma) conglomerates to 44% in group 4 (post-6 Ma) conglomerates, which might be related to post-10 Ma tectonic unroofing and basement exhumation during proto-Gulf rifting and/or variable proximity of depocenters to pre-rift basement exposures.

in the study area and include sandy alluvium (*Qal*), fluvial cross-bedded sandstone of the Rio San Ignacio (*Qrs*), volcanoclastic colluvium (*Qco*), and Plio-Quaternary volcanoclastic gravels (*QPg*) (Plate 1).

QPg consists of flat-lying pebbly sandstone and clast-supported sandy pebble conglomerate with horizontal stratification and a local primary dip up to 4° in the eastern Sierra Tordilla. Clasts are subangular to rounded and consist primarily of pebbles with sparse cobbles and rare boulders up to 90 cm-diameter. 7-35 cm-thick bedsets are well-defined by clast-supported pebble-rich beds and mostly massive with no sedimentary structures, except for rare channel scour and upper plane-bed stratification. *QPg* has a polymictic clast assemblage consisting of ~56% volcanic clasts (basalt-rhyolite) and 44% basement granitoids and metamorphic clasts (Fig. 9). These gravels are interpreted as widespread, locally-derived debris flows and alluvium that cover and obscure older pre- and syn-rift strata.

CHAPTER V

STRUCTURAL GEOLOGY

Dominant Structural Trends

The Sierra Bacha is cut by normal, sinistral, normal-oblique, and dextral faults that formed during proto-Gulf (late Miocene) deformation (Plate 1; Figs. 3, 4). The major structures are the Amado-Libertad and Bacha faults in the north, and the Pozo Coyote and Noriega faults in the central and southern parts of the study area. Most deformation took place by slip on normal faults and northeast tilting on these NW-trending, SW-dipping normal faults. A subsidiary set of NNE-SSW-trending sinistral and oblique faults display minor sinistral-normal separation (up to 250 m) and link larger normal faults. The structural framework can be broadly classified as a series of domino-style fault blocks that tilt all group 1, 2, and 3a rocks uniformly to the NE $\sim 30\text{-}60^\circ$ and form asymmetric half-grabens that are locally filled with syn-tectonic (group 3b) strata (southern study area). Bedding and eutaxitic foliations in pre- and syn-rift rocks strike NW-SE and have an average dip of 43° down to the NE (Fig. 10A). The average strike of measured fault surfaces ($n=65$) is NW-SE, sub-parallel to strike ridges of tilted strata throughout the entire field area (Fig. 10B).

Uniformly NE-tilted fault blocks, exposures of shallow to moderately dipping faults, and high fault-to-bedding cutoff angles in hanging wall strata all suggest that most normal faults did not slip at low angles, but instead were rotated to shallower ($\sim 30\text{-}40^\circ$) southwest dips. Possible mechanisms for fault rotation include a SW-dipping low-angle

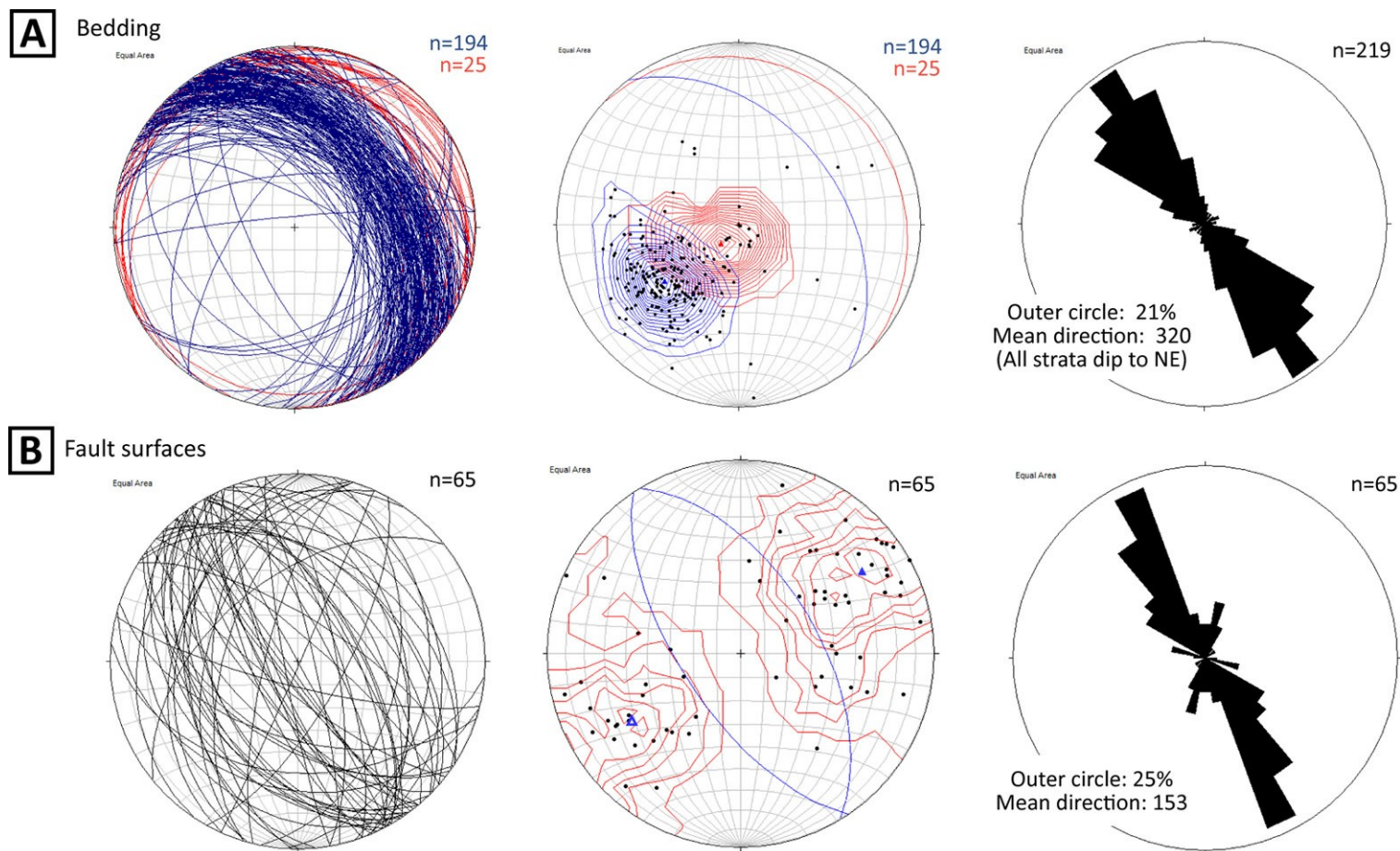


Figure 10. Equal area projections of structural data from bedding (A) and faults (B) in the Sierra Bacha study area, including from left to right: planes, poles to planes with average planes, and rose diagram of structural strike. A) Average bedding orientation for ~15-10.4 Ma units (blue) is 323, 42° NE (n=194), whereas post-10 Ma units (red) display an average orientation of 313, 11° NE (n=25). B) Poles to fault surfaces (n=65) display a bimodal distribution defining conjugate NW-SE-striking normal faults that dip moderately to the SW (filled triangle) and NE (unfilled triangle). The strikes of all measured bedding and fault surfaces are subparallel and nearly uniform.

detachment surface at depth or higher-angle second-generation faults that cross-cut and tilt earlier first-generation structures. No inferences were made in structural cross sections (Fig. 11) regarding the locations or geometries of these causative structures responsible for fault rotation, which are most likely exposed outside the study area to the northeast or concealed beneath alluvium within the Sierra Bacha.

Most fault surfaces are poorly exposed and traces of larger structures are consistently obscured by vegetation and/or Quaternary alluvium. Thus, significant uncertainties remain regarding the attitude of most major structures in the study area. The location, occurrence, and geometry of most faults are inferred from stratigraphic constraints, fault-to-bedding cutoff angles, and structural separation in map view. In structural cross sections, the orientations of unexposed faults lacking geometric constraints are assumed to be parallel to nearby faults. With the exception of the previously identified Amado-Libertad and Seri faults, this study assigns new names to rift-related structures that accommodate significant strain in the Sierra Bacha area.

Major Structures

Gastil and Krummenacher (1976, 1977) first identified the Libertad fault based on a NW-SE alluvium-covered lineament observed in air photos, and proposed that it may link northwest to the offshore Amado transform fault in the Gulf of California (Fig. 3). Total displacement and geometry of this fault are difficult to assess because the fault is everywhere covered by alluvium. Most hanging wall rocks are concealed beneath the alluvial floodplain of the Rio San Ignacio, raising the possibility of additional concealed normal faults. In order to avoid obtuse cutoff angles in the hanging wall, a dip of $\sim 35^\circ$ SW is inferred for the Amado-Libertad fault, consistent with similarly oriented large-

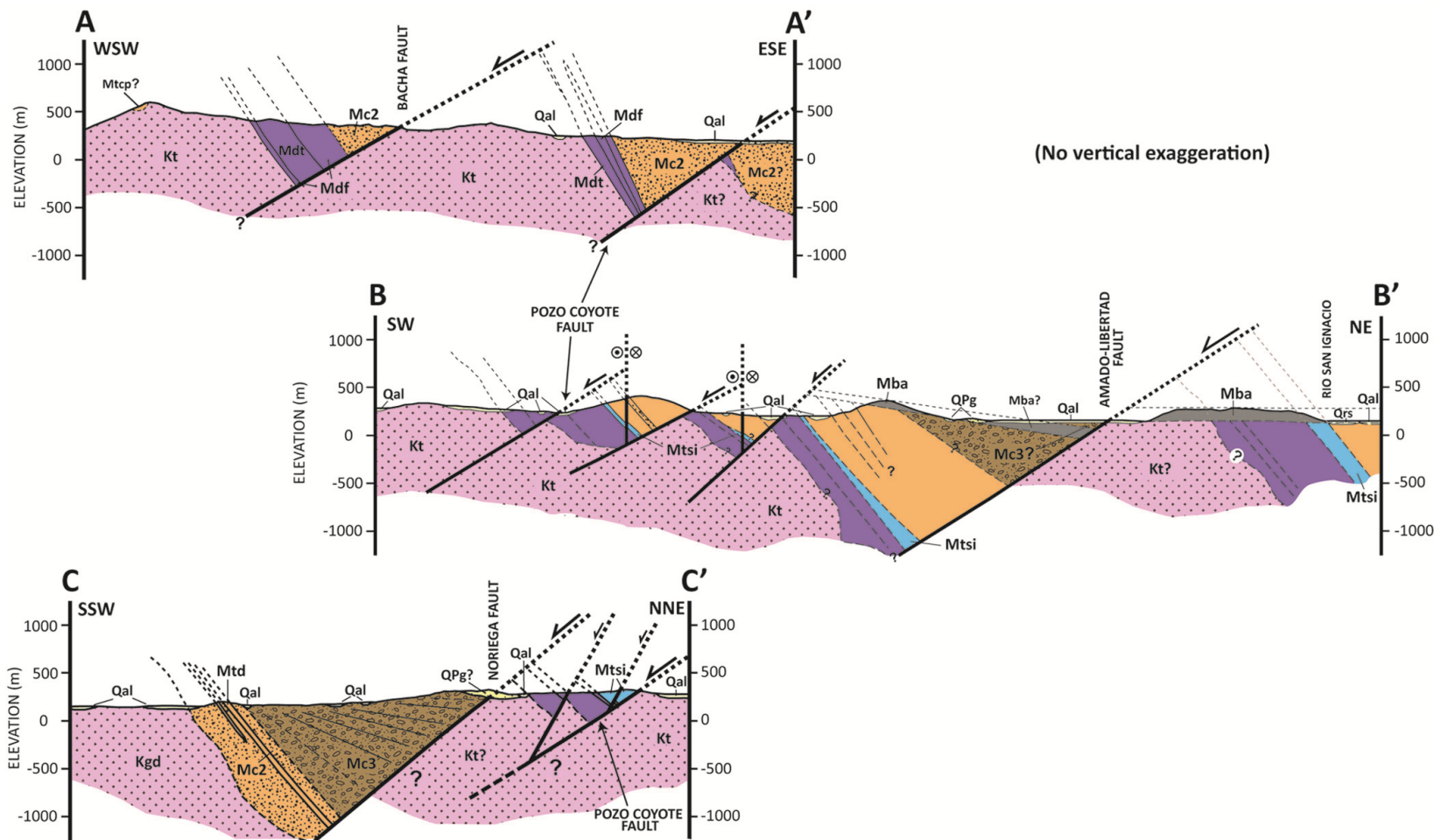


Figure 11. Structural cross sections of the Sierra Bacha (see Fig. 4 for locations). The structural dips of unexposed faults could not be measured directly, and thus, were assumed to be parallel to those nearby. High fault-to-bedding cutoff angles and shallowly dipping faults (consistent with field measurements of exposed structures) are inferred for unexposed and concealed structures. Group 2 (purple) and group 3a (orange) strata deposited between 15 and 10 Ma dip moderately and uniformly to the NE. In contrast, group 3b units (brown and gray) dip shallowly to the NE and display a fanning dip interval from 28-0° NE in section C-C', suggesting that significant extension began after ~10 Ma.

displacement normal faults elsewhere in the study area (e.g. Bacha fault) and similar to the geometry of the offshore Amado fault (Aragón-Arreola and Martín-Barajas, 2007). Based on these inferences and location of *Mtsi*, total normal offset on the Amado-Libertad fault is estimated to be ~4.1 km (Fig. 11).

The Bacha fault is a 24-km-long, NW- striking normal fault that dips gently to the SW ~33° (Plate 1; Fig. 4). Hanging-wall strata dip 45-50° to the NE, creating a high cutoff angle (~80°) that suggests the fault was initiated at a high angle and subsequently rotated to its present low dip (Fig. 11A). This fault is best exposed in the northwest part of the study area (Fig. 4) where it displays a 4-8 meter-thick tonalite breccia in the immediate footwall. The homogeneous fault breccia is pervasively fractured and contains a matrix of deep red, clay-sized gouge. Reconstructions of offset and correlatable units across the Bacha fault in the NW (*Mc2*) and along strike to the SE (*Mtsf*) show that normal offset ranges from 2.6 to 3.4 km (Fig. 11A). The presence of two small outcrop belts of *Mtsf* directly NE and SW from each other, in the hanging wall and footwall of the Bacha fault (Fig. 4), shows that there is no significant strike-slip offset on this fault. Near the south end of the Bacha fault, the strike of the fault and hanging-wall strata deviates from the typical NW-SE orientation to a more N-S trend (Fig. 4).

The Pozo Coyote fault is an 18- to 22-km-long, NW-striking normal fault in the central map area with a measured dip of 32° SW (Plate 1; Fig. 4, 11B, 11C). This fault was first identified by Gastil and Krummenacher (1976) as an unnamed fault that repeats an interval of undifferentiated volcanic strata. Where unexposed, its trace is inferred from a repeated stratigraphic interval of *Ma2* and the Tuff of San Ignacio (*Mtsi*), a key marker horizon. The Pozo Coyote fault is a relatively minor structure with ~0.5 km of

normal displacement along most of its trace (Fig. 11B). Normal offset on the fault increases southeast of where it is cut by an E-W-trending dextral transfer fault, with displacement increasing to about 1.2 km (Fig. 11C). The best exposures of this fault are located south of the dextral transfer fault in the southeastern Cerro Colorado (29.551707° N, 112.302443° W), where a 10-20 meter-thick tonalitic fault breccia is observed in the footwall. In the northwest, the Pozo Coyote fault is inferred to continue beneath alluvium southwest of Cerro Prieta (Fig. 4), but its presence is uncertain in that area. Alternatively, the Pozo Coyote fault may die out to the northwest, possibly losing displacement where it is cut by the NE-striking San Ignacio fault near Pozo Coyote (Fig. 4).

The Noriega fault is a completely covered fault in the southern map area (Plate 1; Fig. 4) that is inferred from map relationships and named for Arroyo de Noriega just south of the study area. Normal offset of up to ~2.5 km on this fault juxtaposes Miocene volcanic rocks against crystalline basement (Fig. 11C). This fault is inferred from: (1) a fanning-dip sequence in alluvial conglomerates of *Mc3* (group 3b) in which bedding dip decreases up section from ~28° NE to horizontal (Fig. 11C); and (2) presence of a regional-scale normal fault east of the Sierra Seri, directly along strike southeast of the Noriega fault (Fig. 3; Gastil and Krummenacher, 1976). The Noriega fault likely merges with this regional fault to the southeast, and it terminates to the northwest in the Sierra Bacha beneath syn- and post-tectonic (group 3b and group 4) strata.

The Seri fault is located near the coast in the southwestern map area and is completely covered by Quaternary alluvium (Plate 1; Fig. 4). Gastil and Krummenacher (1976, 1977) first identified this fault as a major range-bounding normal fault with possible dextral shear. Along strike to the southeast, the Seri fault links to a domain of

NW-striking normal faults in the Sierra Seri that record SW-NE extension and suggest little or no dextral shear (Fig. 3; Oskin and Stock, 2003c). To the northwest, it continues offshore into a basin-bounding transform fault and forms the western boundary of the coastal Sierra Tordilla (Fig. 4). Because the Seri fault is not exposed in the Sierra Bacha, no inferences have been made regarding the orientation, total displacement, and sense of slip on the Seri fault.

The San Ignacio fault is a NE-striking sinistral fault in the central map area (Plate 1; Fig. 4) first inferred (but not named) by Gastil and Krummenacher (1976). Sinistral displacement of ~1 km on this fault is constrained by offset markers in the southern Sierra Tordilla and near Pozo Coyote. The fault is poorly exposed and mostly concealed beneath younger alluvium, except in the southern Sierra Tordilla where group 2 strata are juxtaposed against crystalline basement (Fig. 4). Significant uncertainties exist regarding the timing and cross-cutting relationships between the SW-striking San Ignacio fault and the SE-striking Bacha and Pozo Coyote faults. The San Ignacio fault is shown as a continuous NE-SW-trending sinistral fault that cross-cuts the Bacha and Pozo Coyote faults (Fig. 4), but it may have been contemporaneous with the Bacha and Pozo Coyote faults and thus may link into, rather than cross-cut, the main extensional structures in the Sierra Bacha.

Fault Kinematic Analysis

Fault kinematic indicators in 15-10 Ma rocks record dominant ENE-WSW extension with a weak dextral component (Fig. 12). The stress tensor shows a horizontal maximum tensional strain axis (T-axis) oriented at azimuth 067°, and a sub-vertical axis of maximum compressional strain (P-axis). This result is consistent with the map pattern

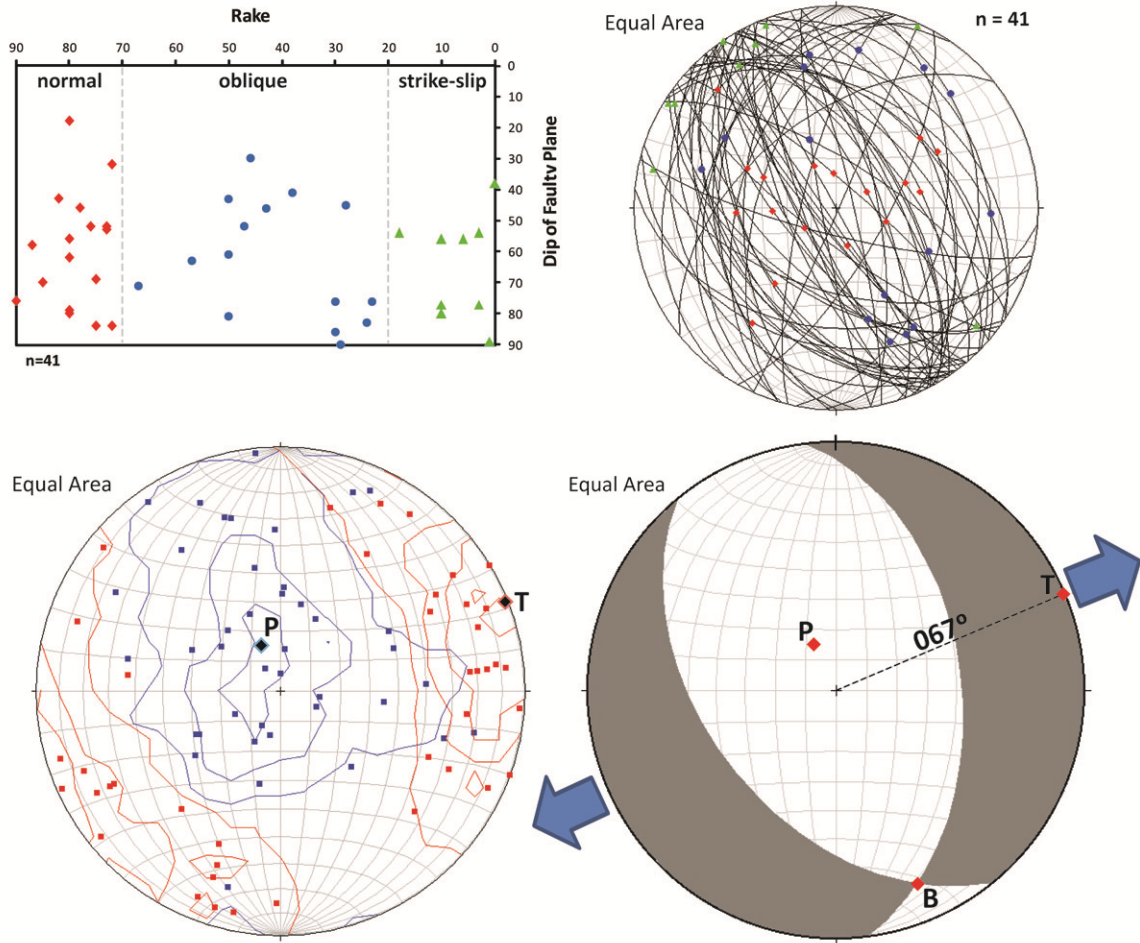


Figure 12. Fault kinematic analysis results. Plot of fault dip vs. slip vector rake (top-left) and measured fault surfaces (great circles) and kinematic indicators (top-right) colored red, blue, and green representing normal-, oblique-, and strike-slip, respectively. (bottom-left) P-axes (red) and T-axes (blue) for individual fault measurements and Kamb contour of axes (2σ confidence level); compared to the tight clustering of the poles to fault planes (Fig. 10B), the heterogeneous distribution of P and T axes indicates exposure to multiple stress states as opposed to a single uniform stress field since late Miocene time. The fault plane solution (bottom-right) displays a sub-vertical compressional axis (P-axis) and maximum tensional strain axis (T-axis) for the entire dataset oriented at azimuth 067° , indicating ENE-WSW-directed extension since ~ 15 Ma in the Sierra Bacha (blue arrows).

indicating NE-SW extension on NW-striking normal faults and, although the dataset is relatively small ($n=41$), provides a first approximation of the paleostress orientations responsible for late Miocene (and possibly later) deformation in the Sierra Bacha.

The average orientation of faults in the study area shows two clusters that define a conjugate set of moderately dipping NW-striking faults (Fig. 13A). In contrast, the scattered distribution of individual P and T axes for each fault slip datum (Fig. 12) indicates that deformation in the Sierra Bacha was almost certainly influenced by *multiple* stress states, as opposed to a single uniform stress field, since late Miocene time. The orientations of the average conjugate normal faults correspond to a vertical σ_1 and horizontal σ_3 trending NE-SW, which predicts slip vectors (striae) to have steep rakes ($> 70^\circ$) on the average fault pair (Fig. 13B). However, only a subset of measured slip vectors fall in this predicted field, while the remaining vectors define two loose clusters indicating oblique slip kinematics that could not have formed under the same paleostress conditions responsible for initiating the NW-striking normal faults (Fig. 13B, top). A practical explanation is that the oblique-slip kinematic indicators were caused by oblique fault reactivation in response to a reorientation of the paleostress field. Excluding striae with steep rakes that fall within the expected slip vector field (based on average fault orientation and its predicted paleostress orientations), two clusters are observed in the NW and SE quadrants representing the anomalous slip vector fields that indicate oblique-slip kinematics (Fig. 13B, bottom). This same result has been observed in analog block models of fault reactivation in strike-slip mode, in which oblique-slip kinematics overprint pre-existing dip-slip structures after a reorientation of the regional stress field (e.g. Withjack & Jamison, 1986; Richard & Krantz, 1991). It should be noted, however, that mean slip vectors for the anomalous populations have low concentration factors (κ) of 9.8 and 21.2 due to the small size of the data set and lack of coherent clustering.

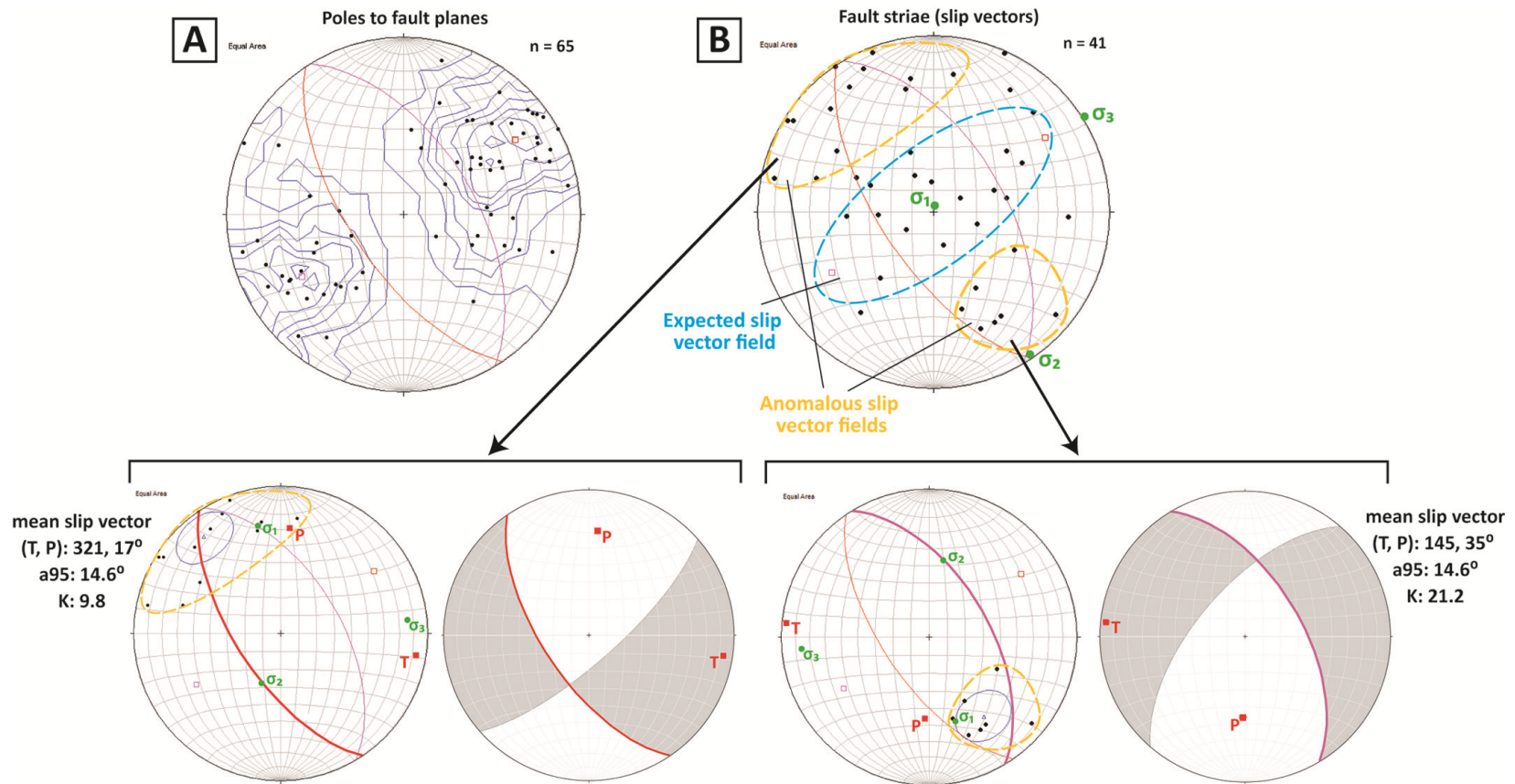


Figure 13. Interpretation of anomalous slip vectors based on paleostress orientations responsible for average conjugate fault pair. A) Poles to fault planes ($n=65$) show two distinct populations which define the average fault orientation as a conjugate set of moderately dipping, NW-SE-striking normal faults; B) Fault striae ($n=41$) in expected and anomalous slip vector fields predicted by principal stresses (green) responsible for the average conjugate fault pair. Mean vectors for the NW and SE anomalous groups lie within the average principal (red) and conjugate (pink) average faults, respectively. The stress fields that correspond to the anomalous slip vectors (below) are dramatically different than the stress state responsible for the average fault orientations (left). A plausible explanation for this is that anomalous slip vectors are related to reactivation of NW-SE-striking normal faults in oblique slip mode.

A robust test of this hypothesis would require more field measurements and kinematic data that would ideally define more convincing populations of slip vectors. These shortfalls aside, the notable difference between the high confidence in the average fault orientations and the scattered distribution of individual P and T axes conclusively demonstrates that the rocks in the Sierra Bacha were exposed to multiple stress states as opposed to a single resolvable stress field (Figs. 12, 13A). Thus, the inconsistency between predicted slip vector fields and the orientations of measured striae are interpreted to represent reactivation of pre-existing NW-SE normal faults in oblique-slip mode which was not intense or prolonged enough to initiate new structures representing the secondary transtensional stress field.

CHAPTER VI

PALEOMAGNETISM

Five volcanic units, including three pyroclastic units (*Mtcc*, *Mtsf*, and *Mtsi*) and two lava flows (*Mr2*, *Mba*) were sampled in the Sierra Bacha for paleomagnetic analysis (Fig. 4). All paleomagnetic data are reported in Table 3. Based on the geomagnetic polarity timescale of Ogg and Smith (2004), the isotopic ages for *Mtsf* (12.5 ± 0.08 Ma) and *Mtsi* (12.56 ± 0.09 Ma) indicate that these tuffs likely were erupted during reversed polarity subchron C5Ar.1r (12.415 - 12.730 Ma). *Mtcc* (14.5 ± 0.3 Ma) was deposited during normal subchron C5ADn (14.194 – 14.581 Ma). Both *Mba* (6.4 ± 1.9 Ma) and *Mr2* (relative age: 11.8 – 6.4 Ma) show normal polarity remnant magnetization, but insufficient age constraints prohibit placement into a specific geomagnetic polarity interval. Characteristic remnant magnetization (ChRM) directions for the five sites drilled in the Sierra Bacha cluster well ($\alpha\text{-95} < 10^\circ$) indicating that they are almost certainly primary NRM components.

In general, NRM, LT, and low-AF steps showed anomalous low-stability directions that were excluded from ChRM vector analysis since they most likely represent secondary NRM components acquired after deposition. Directions were typically resolved at higher AF steps (e.g. 200–800 mT) which showed higher stability and tended to isolate a distinct (likely primary) ChRM vector. These vectors were combined for each locality to obtain Fisher and Bingham statistics for the site-mean ChRM (Fig. 14, A-E).

Table 3. Paleomagnetic Data and Rotation Calculations for Sites in the Sierra Bacha, Coastal Sonora, Mexico

| Drill Site/Unit* | Age (Ma) | Bedding [†] | | | | | | Tilt-Corrected Fisher Statistics [‡] | | | | Rotation and Flattening | | | |
|------------------|----------|----------------------|-----------|--------|-----|------------------|---------------------------|---|------|------|--------|-------------------------|-----------------|----------------|-----------------|
| | | Lat (°N) | Long (°W) | Strike | Dip | N/N ₀ | Corr. Factor [#] | Dec | Inc | α95 | K | R [°] | ΔR ^ψ | F [°] | ΔF ^ψ |
| DS-17, Mtsi | 12.5 | 29.58266 | 112.31615 | 308 | 40 | 12/12 | 0.79 | 228.3 | -1.3 | 1.48 | 907.82 | ND | ND | ND | ND |
| DS-21, Mtsf | 12.5 | 29.548521 | 112.37158 | 359 | 55 | 19/19 | 0.79 | 235.5 | 4.7 | 2.6 | 181.34 | 25.4 | 2.4 | -7.7 | 2.4 |
| DS-22, Mtcc | 14.5 | 29.581697 | 112.34819 | 312 | 48 | 11/12 | 0.79 | 358.9 | 22.4 | 9.25 | 29.88 | -3.1 | 11.1 | 26.6 | 10.7 |
| DS-23, Mr2 | 12-10 | 29.580733 | 112.30192 | 295 | 52 | 5/6 | 0.77 | 355 | 20.7 | 4.5 | 229.46 | -7 | 8.5 | 28.3 | 8.3 |
| DS-24, Mba | 6.4 | 29.635678 | 112.27431 | 221 | 1 | 12/12 | 0.79 | 3.5 | 39.4 | 4.3 | 125.42 | 1.5 | 9.0 | 9.6 | 8.5 |

* See text or Plate 1 for unit names

[†] Bedding orientation used for structural correction; dip direction is 90° clockwise from strike according to the right-hand rule

N/N₀ - number of samples used to determine site-mean direction/number of samples collected

[#] Correction factor based on value of N used in calculation of ΔR, ΔF (Demarest, 1983)

[‡] Geographic (uncorrected) Fisher statistics and all Bingham statistics are listed in Appendix B

Dec - Declination in degrees; Inc - Inclination in degrees

α95 - cone of 95% confidence about site-mean direction; κ - precision parameter (Fisher, 1953)

[°] R - Rotation in degrees (clockwise = positive). DS-21 (*Mtsf*) calculated relative to Tuff of San Felipe reference site in Baja California (Bennett and Oskin, 2008); 2.3° is added to R for this site to account for finite rotation of reference site due to Pacific-North America plate motion. All other sites (DS-22, DS-23, DS-24) calculated relative to average Miocene reference pole estimated in this study (see text for details).

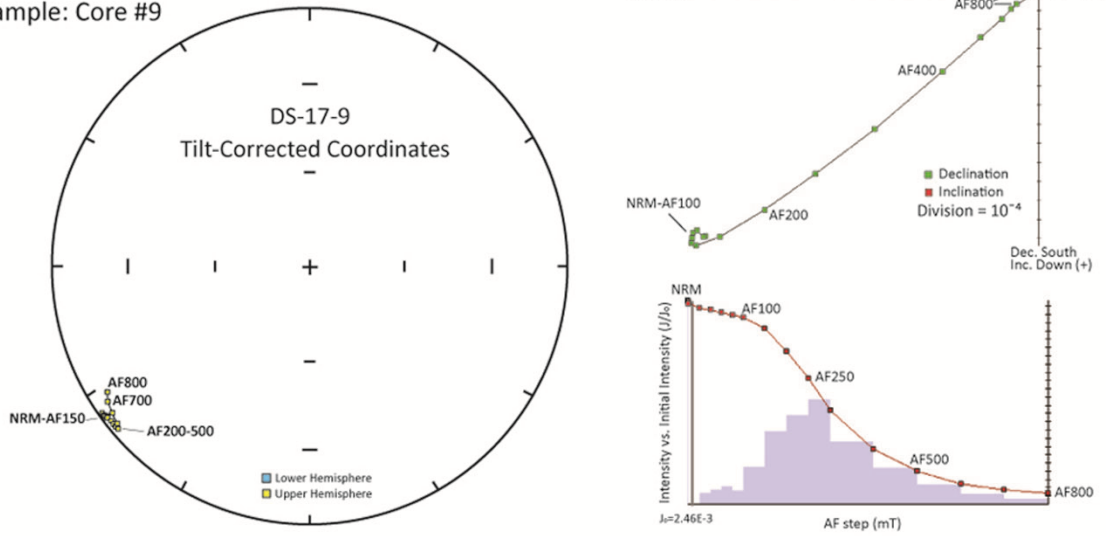
[°] F - Flattening in degrees (down from horizontal = positive). DS-21 (*Mtsf*) calculated relative to Tuff of San Felipe reference site in Baja California (Bennett and Oskin, 2008). All other sites (DS-22, DS-23, and DS-24) calculated relative to average Miocene reference pole estimated in this study (see text for details).

^ψ ΔR - 95% confidence limits on rotation; ΔF - 95% confidence limits on flattening. Both calculated according to Beck (1980) and Demarest (1983)

ND - No data; Finite rotation cannot be determined since no stable reference site exists for this unit.

A DS-17, Tuff of San Ignacio (*Mtsi*)

Example: Core #9



Site-Mean ChRM

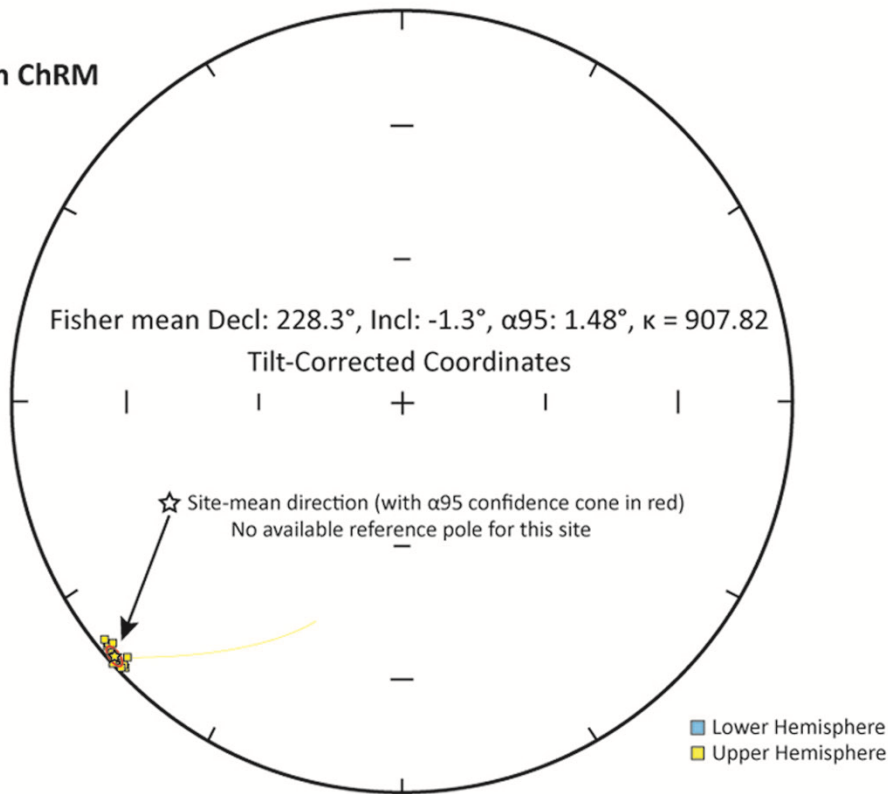
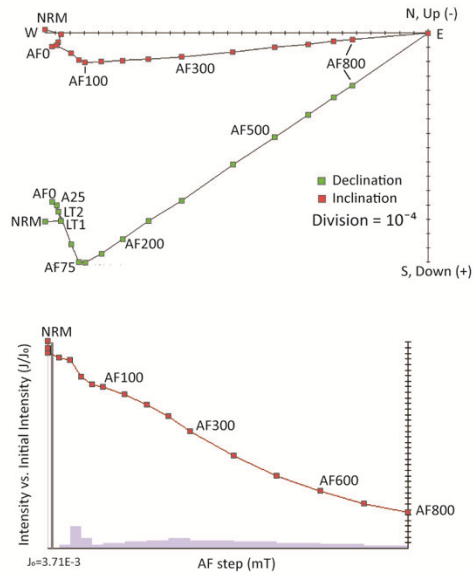
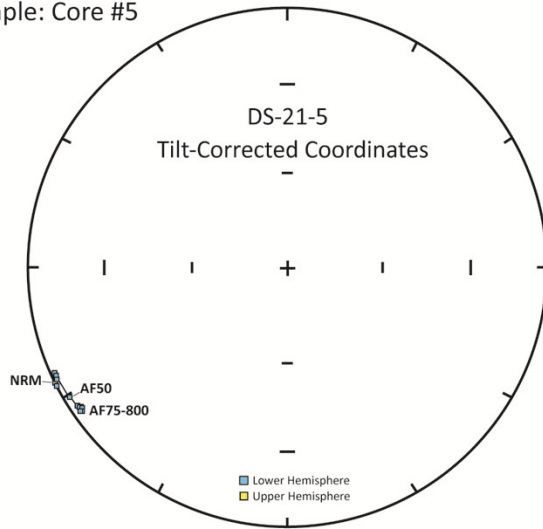


Figure 14. A) Typical paleomagnetic results for the Tuff of San Ignacio (*Mtsi*). Example core #9 of 12 shown, including clockwise from top-left: Equal Area, Zijderveld, J/J_0 Intensity, and site-mean ChRM plots. Lower plot shows site-mean direction (star) and α -95 confidence (red) for DS-17. Rotation cannot be estimated since there is no appropriate reference pole for *Mtsi*.

B DS-21, Tuff of San Felipe (*Mtsf*)

Example: Core #5



Site-Mean ChRM

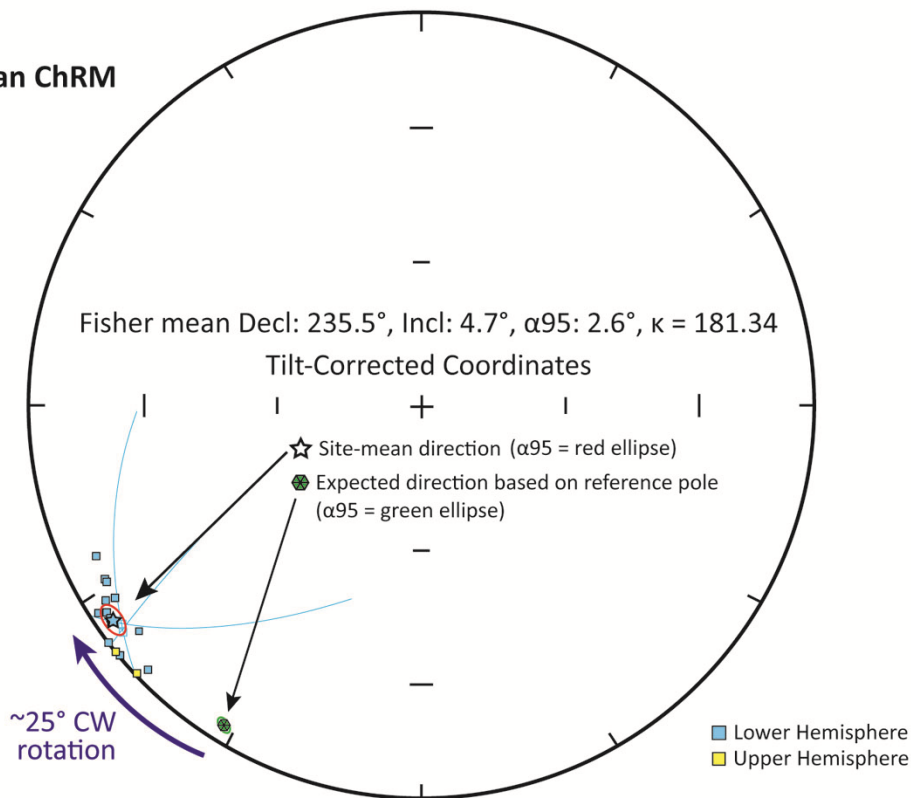


Figure 14 (continued). B) Typical paleomagnetic results for the Tuff of San Felipe (*Mtsf*). Example core #5 of 21 shown, including clockwise from top-left: Equal Area, Zijderveld, J/J_0 Intensity, and site-mean ChRM plots. Lower plot shows site-mean direction (star) and α_{95} confidence (red) for DS-21. Deviation of the site-mean direction from the expected direction (green) based on the high-precision stable *Mtsf* reference site (Bennett and Oskin, 2008) indicates $25.4^\circ \pm 2.4^\circ$ of clockwise vertical-axis rotation at this site (see Figs. 4, 15 for location).

C DS-22, Tuff of Cerro Colorado (*Mtcc*)

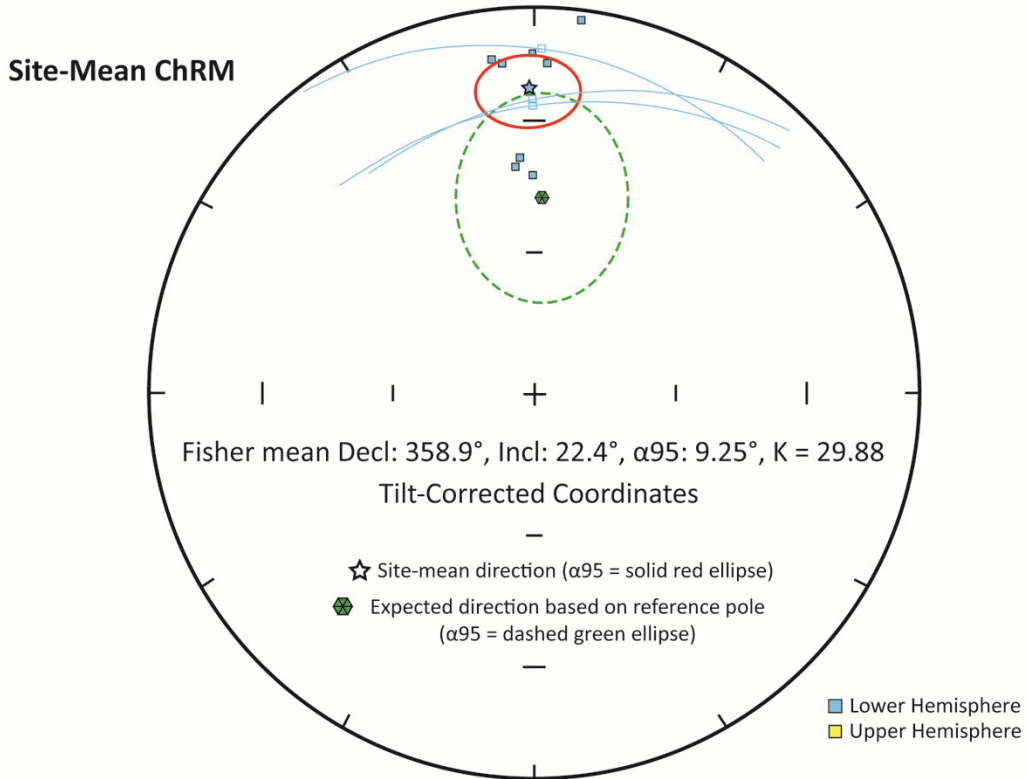
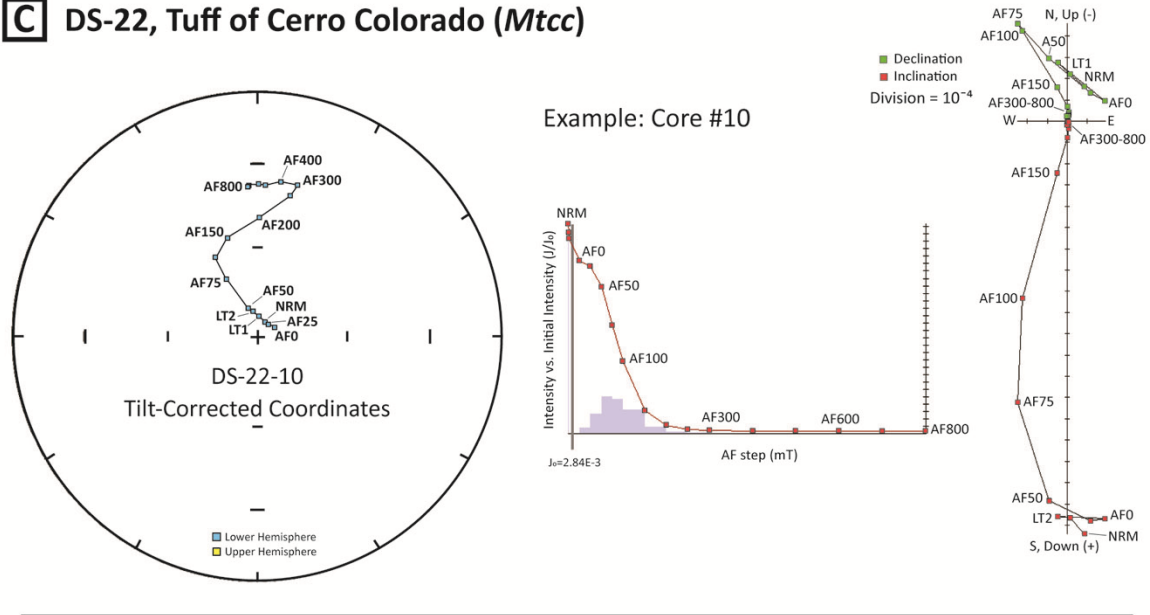


Figure 14 (continued). C) Typical paleomagnetic results for the tuff of Cerro Colorado (*Mtcc*). Example core #10 of 12 shown, including clockwise from top-left: Equal Area, J/J_0 Intensity, Zijderveld, and site-mean ChRM plots. Lower plot shows site-mean direction (star) and α_{95} confidence (red) for DS-22. The site-mean direction does not appear to be rotated significantly from the expected direction (green), however the large difference in inclination suggests some flattening of the magnetization vector (see Figs. 4, 15 for location).

D DS-23, Rhyolite #2 (*Mr2*)

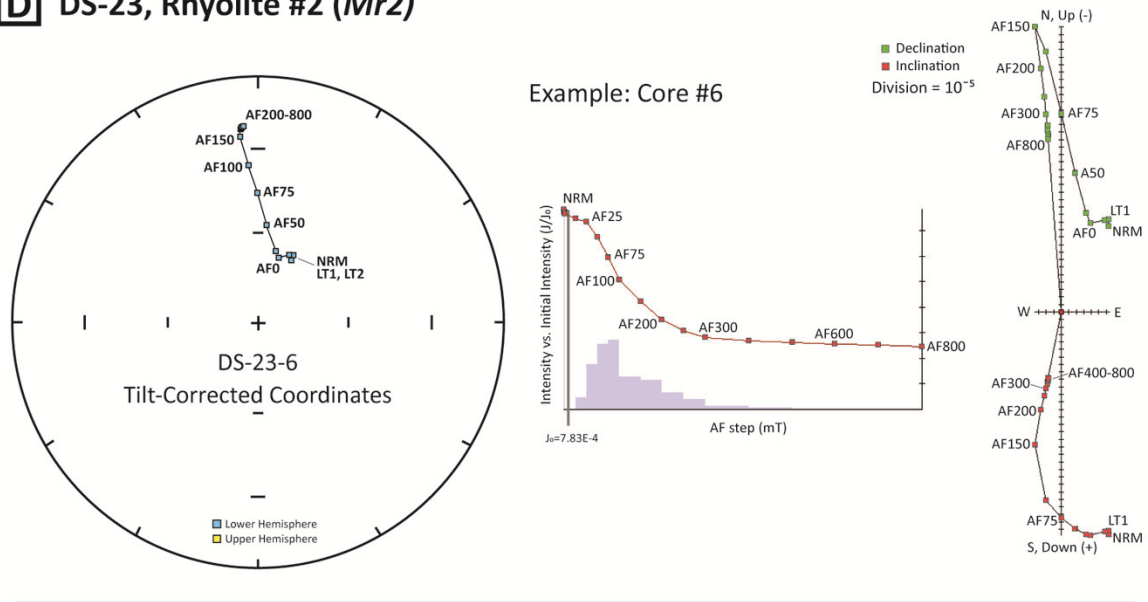
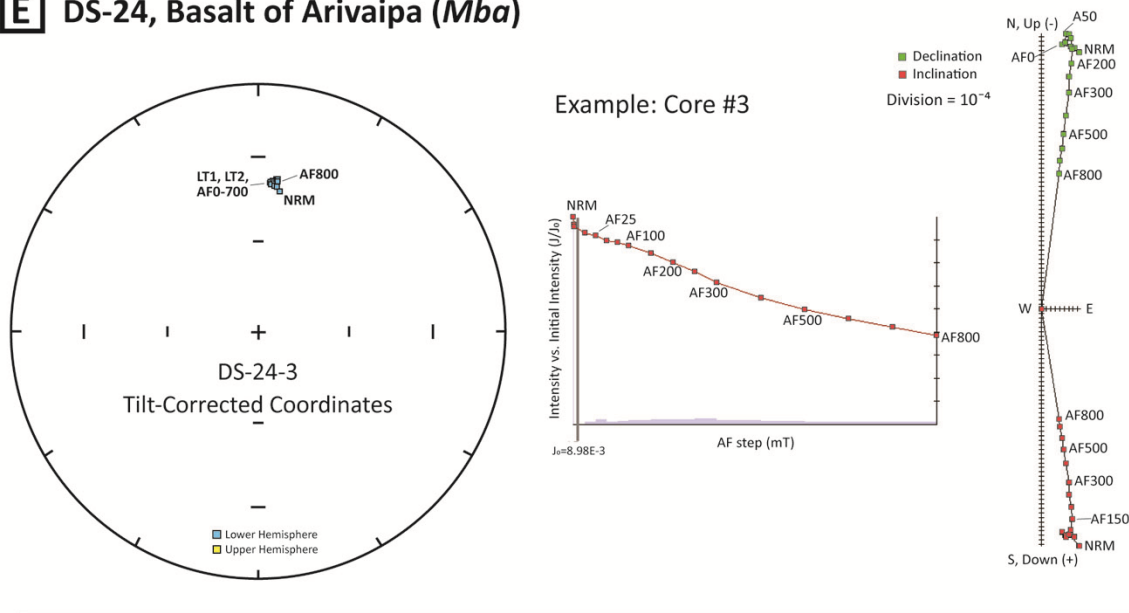


Figure 14 (continued). D) Typical paleomagnetic results for Rhyolite #2 (*Mr2*). Example core #6 of 6 shown, including clockwise from top-left: Equal Area, J/J_0 Intensity, and Zijderveld, and site-mean ChRM plots. Lower plot shows site-mean direction (star) and α -95 confidence (red) for DS-23. The site-mean direction does not appear to be rotated significantly from the expected direction (green), however the large difference in inclination suggests some flattening of the magnetization vector (see Figs. 4, 15 for location).

E DS-24, Basalt of Arivaipa (*Mba*)



Site-Mean ChRM

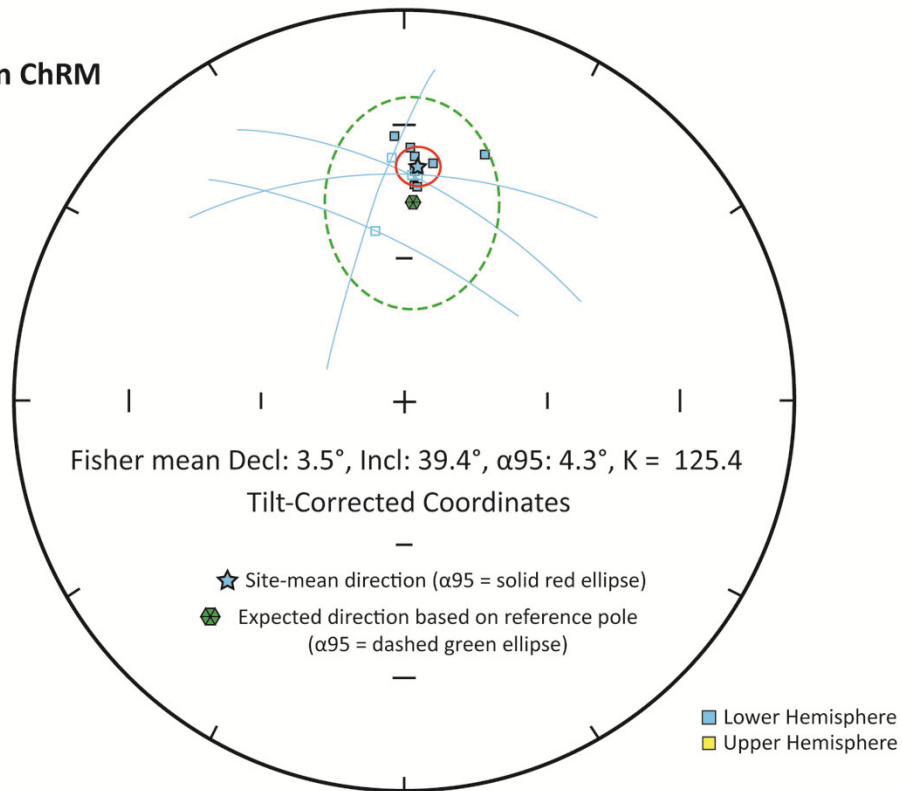


Figure 14 (continued). (E) Typical paleomagnetic results for the Basalt of Arivaipa (*Mba*). Example core #3 of 12 shown, including clockwise from top-left: Equal Area, J/J₀ Intensity, Zijderveld, and site-mean ChRM plots. Lower plot shows site-mean direction (star) and α₉₅ confidence (red) for DS-24. The site-mean direction does not appear to be significantly rotated from the expected direction (green). See Figs. 4, 15 for location.

Reference Sites

Two different paleomagnetic reference poles are compared with site-mean ChRM vectors from 4 of the 5 sites in the Sierra Bacha, to quantify vertical-axis rotations (Fig. 15). Bennett and Oskin (2008) calculated a high-precision paleomagnetic reference vector for the Tuff of San Felipe (*Mtsf*) from a tectonically stable location in Baja California. The unique magnetic direction of *Mtsf* in Baja California ($D = 212.4^\circ$, $I = -3.0^\circ$, $\alpha-95 = 1.33^\circ$) is well off the expected Miocene paleopole direction and appears to record a transitional field or geomagnetic excursion (Stock et al., 1999). This pole direction is used for calculating rotation of the *Mtsf* site (DS-21).

Mtcc (DS-22), *Mr2* (DS-23) and *Mba* (DS-24) do not have stable reference sites with which to compare site-mean ChRM directions. To estimate rotation at thesis sites, a Miocene geomagnetic pole was calculated from two stable North American paleopoles (Besse and Courtillot, 1991) and an average paleomagnetic pole for Miocene volcanic rocks on Baja California (Hagstrum et al., 1987). A 2.3° clockwise correction was added to this direction to account for post-6 Ma divergence between Baja California and Sonora (e.g. Oskin and Stock, 2003b). These three paleopoles were then averaged to account for secular variation of the Earth's magnetic field during Miocene time, resulting in an estimated mean Miocene paleomagnetic pole position (87.2° N, 182.6° E, $\alpha-95 = 8.6^\circ$). Using this reference paleopole location and spherical trigonometry of Butler (1992, p. 122), I calculate an expected magnetization direction of $D = 2^\circ$, $I = 49^\circ$ at the geographic location of the study area during Miocene time. The 2σ confidence limits for paleosecular variation around this geomagnetic pole direction were estimated from the volcanic database of Quidelleur and Courtillot (1996), a study of apparent and true polar

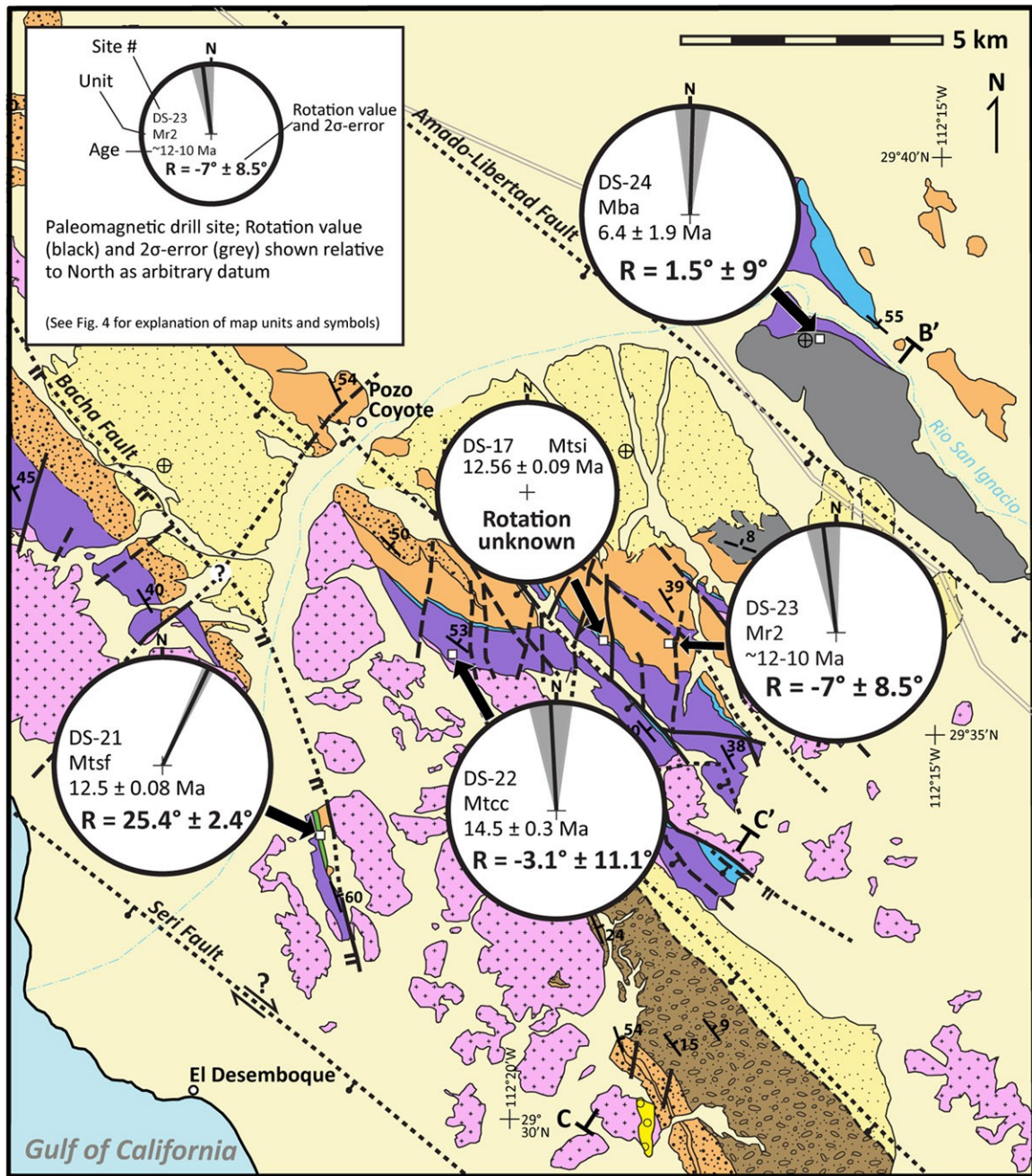


Figure 15. Paleomagnetic site locations and estimates of vertical-axis rotation for the Sierra Bacha (see Fig. 4 for explanation of map units). The location of drill site DS-17(Mtsi) is shown but rotation cannot be estimated due to lack of a stable reference site. The remaining sites show unresolvable rotation within standard error limits, except for DS-21 which shows up to 28° of clockwise vertical-axis rotation in the SW near El Desemboque. These results indicate that the Sierra Bacha area did not experience significant dextral strain during proto-Gulf time (12.5-6 Ma) except in the southwest where a relatively minor component of dextral strain is documented.

wander. Their work suggests that the approximate standard deviations of declination (σ_D) and inclination (σ_I) at latitude 30° N are 15° and 13° , respectively, which results in 2σ confidence limits (α -95[decl], α -95[incl]) of (19.7° , 26°) via: α -95(decl) = $2(\sigma_D)\cos(I)$, and α -95(decl) = $2(\sigma_I)$ (dashed circles in Fig. 14C-E). The inherently large error in the expected Miocene direction due to secular variation introduces substantial uncertainties for rotation estimates reported below. Thus, vertical-axis rotation for sites without a stable reference locality (DS-22, DS-23, and DS-24) should be considered as minimum estimates that could potentially vary by up to $\sim 40^\circ$.

No stable reference site exists for *Mtsi* (DS-17). The site-mean ChRM for this site ($D = 228.2^\circ$, $I = -1.3^\circ$, α -95 = 1.48) is similar to the unique low-inclination, southwesterly magnetization direction of the Tuff of San Felipe (Fig. 14A, B). This is consistent with the fact that the Tuff of San Felipe (12.50 ± 0.08 Ma) and the Tuff of San Ignacio (12.56 ± 0.09 Ma) have the same isotopic age within standard error. Although nearly identical in age and magnetization, geochemical and mineralogical disparities show that *Mtsi* and *Mtsf* are distinctly different tuffs that likely were erupted during the same transitional field or geomagnetic excursion during reversed polarity subchron C5Ar.1r. Transitional fields and excursions of the geocentric dipole are characterized by large-scale secular variation and their stability is not well understood (Verosub, 1982). Thus, there is no appropriate reference pole with which to estimate rotation for DS-17.

Vertical-Axis Rotation

In this study, positive rotation values (R) imply clockwise (CW) rotation related to slip on dextral faults, whereas negative values imply counter-clockwise (CCW) rotation due to slip on sinistral faults. Independent analysis of each site reveals rotation

values, including errors, ranging from -15.5° to 27.8° (Figure 15). Results for sites DS-22, DS-23, and DS-24 show no discernible vertical-axis rotation within standard error limits (Fig. 15). Site DS-22 (*Mtcc*) shows $-3.1^{\circ} \pm 11.1^{\circ}$ of rotation (Fig. 14C). Six of the twelve cores collected at this site were extracted from a slightly less welded horizon in the tuff, explaining the bimodal distribution of ChRM and the higher than average site-mean α -95 confidence limit of 9.25° . Less welded samples have inclinations $\sim 25^{\circ}$ higher than the welded samples, but declinations vary by only $\sim 3^{\circ}$ between the two ChRM populations. Site DS-23 (*Mr2*) displays $-7^{\circ} \pm 8.5^{\circ}$ of CCW rotation based on 5 cores (Fig. 14D). DS-24 (*Mba*) displays $1.5^{\circ} \pm 9^{\circ}$ of CW rotation (Fig. 14E). Because ChRM directions for these sites are within or near expected limits of paleosecular variation, they do not contain significant evidence of block rotation, although up to $\sim 20^{\circ}$ of vertical-axis rotation is permissible given paleosecular variation and the large uncertainties regarding the position of the Miocene paleopole. Site DS-21 (*Mtsf*) displays clockwise vertical-axis rotation of $25.4^{\circ} \pm 2.4^{\circ}$ in the southwestern part of the study area (Fig. 14B).

The motivation for this paleomagnetic investigation was to see if this limited dataset could reveal a discernible history of rotation in the study area. Although the resolution is rather low for a pilot study, the results provide no evidence of significant vertical-axis rotation northeast of the Bacha fault since ca. 14.5 Ma (Fig. 15). In contrast, $\sim 25^{\circ}$ of clockwise vertical-axis rotation is recorded with a high level of confidence at site DS-21, southwest and in the hanging wall of the Bacha fault. CW rotation at this site corresponds with local deviation of bedding strike from NW to NNW, suggesting that CW rotation is restricted to the area where bedding strike deviates from the normal NW trend in the southwestern study area (Figs. 4, 15).

CHAPTER VII

DISCUSSION

The data presented above suggest that proto-Gulf deformation in the Sierra Bacha was dominated by large-magnitude ENE-WSW extension between about 10 and 6 Ma. Extensional structures appear to have been overprinted by minor dextral shear related to transtensional strain within the modern (post-6 Ma) Pacific-North America plate boundary. A comparison of these results with previous studies in the Gulf Extensional Province reveals significant similarities as well as spatial and temporal variations in the strain history of the northern Gulf of California. The implications of these results for regional tectonic models and continental rapture mechanics are discussed below.

Extensional Strain in the Sierra Bacha

Evidence from geologic mapping and fault kinematic analysis provide useful constraints on the timing and magnitude of extensional strain in the Sierra Bacha since ca.15 Ma. Due to limited exposures of most faults in the study area, a number of assumptions regarding the geometry and mechanics of faulting are required before a quantitative estimate of extension can be made. These assumptions, uncertainties, and existing geologic constraints are considered below and used to calculate post-15 Ma extension in the Sierra Bacha.

Fault Orientations

Large-magnitude extension commonly involves rotation of initially high- to moderately-dipping normal faults to shallower dips (Buck, 1988; Buck and Choi 2010).

Since both the faults and the strata they cut are involved in tilting, inferences about fault orientation at depth can be made from the geometrical properties of fault-to-bedding cutoff angles (the acute angle between hanging wall rocks and the fault plane). Since the steepest plausible normal fault orientation is 90° , cutoff angles must be $\leq 90^\circ$ if hanging wall strata were horizontal prior to extension. Thus, cutoff angles $> 90^\circ$ are impossible to restore in cross sections with only a single generation of normal faults, and may imply a more complex history of faulting related to multiple generations of normal faults (e.g., Proffett, 1977; Buck and Choi, 2010). A multi-phase model of extension implies that faults are initiated at moderate to high angles and are subsequently rotated to shallower angles during extension. As tilting of early faults to shallower dips makes them less mechanically favorable for slip, steeper second-generation faults are initiated and accommodate additional extensional strain (Anderson, 1951; Proffett, 1977; Buck, 1993; Buck and Choi, 2010). This model is supported by studies of mechanical failure in rocks with normal static friction coefficients (~ 0.75), which show that normal slip failure typically does not occur on faults that dip less than $\sim 37^\circ$ (Sibson, 1985).

In the Sierra Bacha, pre-extension hanging wall units (groups 2 and 3b) dip ~ 40 - 60° to the NE (Fig. 10A). In order to avoid cutoff angles $> 90^\circ$, their bounding faults must dip *less than* 30 - 50° to the SW. The Bacha and Pozo Coyote faults have measured dips of 33° and 32° SW, corresponding to typical cutoff angles of 78° and 70° , respectively. The dips of other large normal faults are inferred by applying these cutoff angles to structural blocks where bedding dips are well constrained but the bounding faults are covered (Fig. 11). Small-offset faults between and parallel to major faults are

interpreted to be higher-angle second-generation faults that accommodated extension after tilting of the early faults to shallower dips (e.g. Fig. 11C).

Timing of Extension

The difference in dip between pre-10 Ma (groups 2 and 3a) and post-10 Ma (groups 3b and 4) rocks provides stratigraphic constraints on the timing of extension and tilting. Groups 2 and 3a units (~15-10 Ma) dip moderately to the northeast an average of 42° (n=194) and show no obvious change from the oldest to youngest units within these groups (Fig. 10A). In contrast, groups 3b and 4 (post-10 Ma) unconformably overlie older units and display an average bedding dip of 11° to the northeast (n=25). This disparity suggests that significant extensional strain in the Sierra Bacha began during or prior to deposition of group 3b at ~10 Ma. This is also supported by evidence from clast counts in conglomerate units in the Sierra Bacha that reveal an up-section increase of basement clast input from 16% in pre-10 Ma (group 2) conglomerates to 34% and 44% in 10-6 Ma and post-6 Ma conglomerates, respectively (Fig. 9). This considerable up-section change might be related to extensional unroofing and basement exhumation beginning after ~10 Ma. East of the Cerro Pelón, a 20-30 cm-thick green-gray, laminated airfall tuff with abundant quartz and small biotite phenocrysts in lower *Mc3* was not dated but may provide a critical age constraint for the oldest syn-tectonic (group 3b) strata, and thus, the onset of significant extension within the study area.

The end of major extension and tilting in the Sierra Bacha is constrained by the 6.4 ± 1.9 Ma Basalt of Arivaipa (*Mba*), which is nearly flat-lying in the footwall of the Amado-Libertad fault and dips up to 9° NE in the hanging wall (Fig. 11B). This structural discontinuity may record the waning stages of tilting during deposition of *Mba*,

in which tilting NE of the Amado-Libertad fault was finished by ca. 6.4 Ma and continued for a short while later to the SW in the Sierra Bacha.

The above fault kinematic analysis, which characterized proto-Gulf deformation as largely ENE-WSW-directed extension, is based on kinematic indicators measured in 15- to 10.4-Ma units (Fig. 12). Data collected from group 2 (15-12.5 Ma) may reflect multiple episodes of deformation related to the former subduction zone (e.g. back-arc extension or contraction), thus introducing uncertainty to conclusions about the proto-Gulf paleostress direction. No fault data were collected from group 3b strata (~10 - 6 Ma) due to insufficient exposure. Because no fault slip data were collected in rocks younger than 10.4 Ma, it is impossible to directly test for a temporal change between proto-Gulf (12.5 - 6 Ma) and modern-Gulf (6 - 0 Ma) kinematics. Existing geologic constraints imply that the majority of extensional strain in the study area took place between ~10.4 and 6.4 Ma, although a small amount of post-6.4 Ma deformation is required to produce up to 9° of tilting of *Mba* in the hanging wall of the Amado-Libertad fault (Fig. 11B). This is similar to other studies that documented major ENE-WSW extension in the GEP between 12 and 6 Ma (Gastil et al., 1975; Dokka and Merriam, 1982; Henry, 1989; Stock and Hodges, 1989; Lee et al., 1996) and post-10-Ma onset of extension elsewhere in Sonora (Mora-Alvarez and McDowell, 2000).

Magnitude of Extension

The magnitude of extension in the study area was calculated from restorations of cross sections A-A' and B-B' (Fig. 11). The major faults (and dip-slip offsets) are the Bacha fault (3.0 km), Pozo Coyote fault (0.4 km), Amado-Libertad fault (4.1 km), and two unnamed normal faults in the central Cerro Colorado (1.3 km combined). The

percent extension is calculated from a palinspastic reconstruction of individual fault blocks using paleohorizontal markers (e.g. regionally extensive ignimbrites, nonconformable basement paleosurface). The structural cross sections (Fig. 11) cumulatively record 6.4 to 6.8 km of horizontal extension. For a present map width of 18 km, the total fault offsets thus represent ~55-60% extension in the study area during late Miocene time. The restorations of cross sections A-A' and B-B' do not include extension related to slip on the concealed Seri fault in the southwest or on structures beyond the study area, and thus, may only represent a minimum estimate of extension within the Sierra Bacha. The fact that units in the footwall of the Amado-Libertad fault are tilted up to 53° to the NE suggests another concealed rift structure at depth northeast of the study area. Likewise, the Seri fault may represent the next regional rift structure southwest of the Bacha fault (Fig. 4).

Dextral Strain in the Sierra Bacha

Stratigraphic and structural data from geologic mapping, with support from the fault kinematic analysis and paleomagnetic data presented above, provide evidence for little to no dextral shear in the Sierra Bacha since ~12.5 Ma. In contrast, strong dextral shear between 7 and 6 Ma was recently documented in the Cerro Kino area just southeast and adjacent to the Sierra Bacha (Fig. 3; Bennett, 2009), suggesting a complex history of late Miocene deformation. This section summarizes existing constraints on the timing, magnitude, and distribution of dextral strain in the Sierra Bacha.

Seismic reflection profiles and maps in the northern Gulf support the possibility that the offshore Amado transform fault may project onshore to the Libertad fault (Fig. 3). The Amado transform dips moderately to the southwest (~35-50°) and forms the

northeastern boundary of the inactive Adair-Tepoca basin offshore in coastal Sonora (Aragón-Arreola and Martín-Barajas, 2007). While it has been suggested that the Amado fault accommodated significant dextral shear during late Miocene-Pliocene time, there is no geologic evidence to support significant dextral slip on the continental Amado-Libertad fault in the study area (this study). Outcrops of both *Mtsi* (12.5 Ma) and *Mba* (6.4 Ma) on both sides of the Amado-Libertad fault are located directly across strike from each other and show no evidence for lateral offset. Furthermore, restoring any significant dextral offset on the Amado-Libertad fault would translate the thickest *Mtsi* deposits in the Cerro Las Burras (up to 350 m-thick) NW across strike from the Cerro Prieta where *Mtsi* is absent. These volcanic units are, however, laterally extensive and do not serve as discrete piercing points. Thus, minor (< 5 km) dextral displacement of *Mtsi* is permissible but unlikely.

Fault-kinematic analysis shows that proto-Gulf deformation in the Sierra Bacha was dominated by large magnitude ENE-WSW extension with a minor oblique strain component (Fig. 12). Kinematic indicators that record, normal-, oblique-, and strike-slip displacement on moderately-dipping faults are inferred to represent minor reactivation of normal faults in oblique slip mode (Fig. 13). Analog models of oblique rift kinematics (e.g. Withjack and Jamison, 1986; Richard and Krantz, 1991; Agostini et al., 2009) consistently document normal fault reactivation, leading some to propose that reactivation of NW-striking normal faults in oblique slip mode played a significant role in the structural evolution of the Gulf of California (Merriam, 1965; Angelier, et al., 1981; Colletta et al., 1981; Withjack and Jamison, 1986). Small offset N- to NNE-striking sinistral-normal faults in the Sierra Bacha link into larger NW-trending normal

faults and possibly support minor dextral or oblique strain on predominantly NW-SE striking normal faults (Plate 1; Fig. 4). The San Ignacio fault in the west-central area shows ~1 km of sinistral displacement and may be related to reorientation of the stress field from orthogonal NE-SW extension to oblique transtension.

The paleomagnetic analysis also supports a weak component of dextral shear in the Sierra Bacha during *or after* late Miocene time. Structural blocks show no discernible vertical-axis rotation since ca. 14.5 Ma, except in the southwest near El Desemboque where paleomagnetic evidence and structural strikes indicate ~25° of clockwise rotation in the hanging wall of the southern Bacha fault (Fig. 15, 'DS-21'). Clockwise vertical-axis rotation recorded at DS-21 could be related to dextral shear on the nearby, unexposed Seri fault. This interpretation would imply the presence of faults concealed beneath Quaternary alluvium that caused this small part of the study area to undergo local rotation. Dextral slip on the Seri fault is unknown but plausible due to its proximity to the offshore De Mar-Sacrificio transform, which forms the NE boundary of the Kino-Chueca shear zone (Fig. 3), a narrow zone of significant localized dextral strain ca. 7-6 Ma (Bennett, 2009).

The timing of dextral shear is constrained by *Mtcc* (14.5 ± 0.3 Ma; DS-22) and *Mba* (6.4 ± 1.9 Ma; DS-24) which record the same negligible rotation (Fig. 15). This indicates that dextral shear within the area, however minor, likely occurred *after* deposition of *Mba*. Unfortunately, the low degree of confidence regarding the age of *Mba* suggests that dextral strain in the Sierra Bacha post-dates ca. 8 Ma.

Summary of Strain History

The timing, magnitude and style of deformation recorded by 14.5- to 6-Ma rocks in the Sierra Bacha suggests a two-stage tectonic model for the structural evolution of the northern Gulf of California: (1) 10-6.4 Ma orthogonal ENE-directed extension, and (2) post-6.4 Ma weak fault reactivation and minor dextral transtension. Large-magnitude extension (55-60%) on NW-striking normal faults produced domino-style faulting and tilting of pre-10 Ma strata up to 60° to the NE, and was waning by deposition of the 6.4 Ma Basalt of Arivaipa (*Mba*). Other than the small area north of Desemboque, there is no evidence for CW block rotation or strike-slip fault offsets related to dextral shear on NW-SE-striking faults in the Sierra Bacha. Structural data suggest that the normal faults were overprinted by younger and relatively minor dextral-oblique strain.

Implications for Regional Tectonic Models

Lack of significant dextral shear in the Sierra Bacha has considerable implications for proposed kinematic models of proto-Gulf evolution. The results of this study combined with other recent studies in the region (e.g. Bennett, 2009) show that dextral shear was not distributed throughout a broad zone of distributed transtension during late Miocene time, but instead became localized in a narrow zone southwest of the Sierra Bacha in coastal Sonora during latest proto-Gulf time. The well-documented occurrence of dextral strain within the GEP rules out the end-member “strain partitioning” model of Stock and Hodges (1989), which proposes that late Miocene (12-6 Ma) strain within the GEP was purely extensional (Fig. 2A). Likewise, the delayed inception of a dextral component of plate boundary transtensional strain rules out the end-member “distributed transtension” model for proto-Gulf evolution (Fig. 2B).

Instead, the transfer of plate-boundary strain from offshore transform faults west of Baja California into the continental interior and the GEP seems to have occurred gradually (Fig. 2C). Evidence from coastal Sonora suggests that strain was extension-dominated, as predicted by the strain-partitioning model, but that strain evolved into a more shear-dominated transtensional style at ca. 7 Ma (Bennett, 2009). Progressive localization of strain into discrete dextral shear zones caused an increase in strain rates that mechanically weakened the crust and served as a catalyst for lithospheric rupture. The Kino-Chueca Shear Zone south of the Sierra Bacha accommodated a minimum of ~15 km of dextral shear between ca. 7 and 6 Ma, yet a significant portion of proto-Gulf dextral shear is still unaccounted for (Oskin and Stock, 2003b; Bennett, 2009). This suggests that the Kino-Chueca Shear Zone probably was not unique and that coeval localized shear was probably occurring elsewhere in the northern Gulf immediately prior to plate boundary localization ca. 6 Ma.

The above result raises a fundamental question regarding linkages between offshore transforms that were active in the early Gulf of California (ca. 6-3 Ma) and their onshore projections along strike as largely extensional structures (Fig. 16). For example, the offshore Amado fault was a significant early rift structure in coastal Sonora that hosted considerable normal and strike-slip strain after inception of the Gulf ca. 6 Ma (Aragón-Arreola and Martín-Barajas, 2007), and has been proposed to merge with the continental Libertad fault in the Sierra Bacha (Gastil and Krummenacher, 1977). However, the results of this study show little or no dextral displacement along the Libertad fault. These regional fault relationships present an interesting and poorly

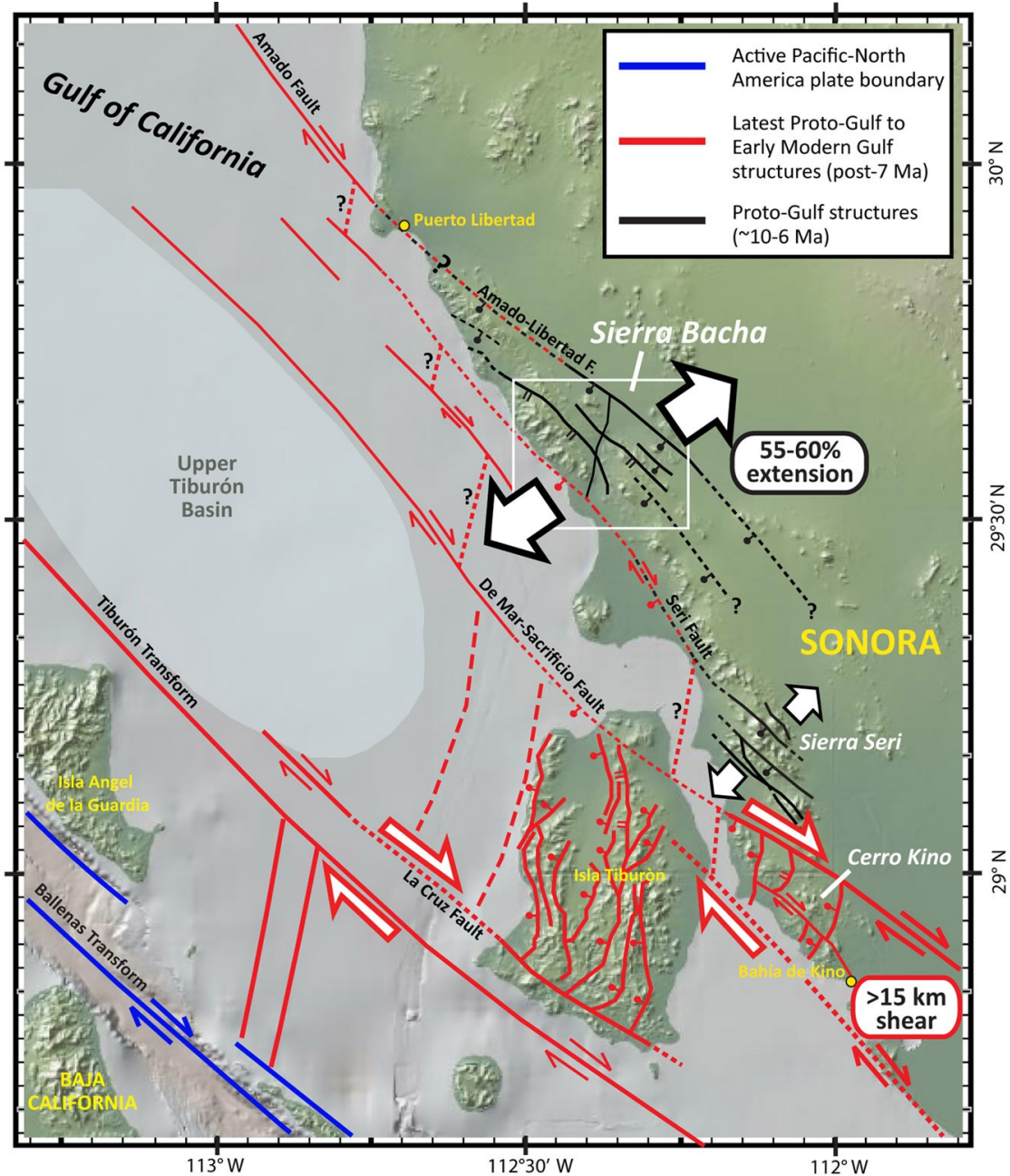


Figure 16. Speculative tectonic model for coastal Sonora during late Miocene time. According to this model, older normal faults (black) accommodated large-magnitude NE-SW extension from ~10-6 Ma. Significant dextral shear introduced at ca. 7 Ma on newly initiated and/or reactivated structures (red) transferred and progressively localized dextral strain to the southwest along a series of en-echelon, right-stepping transforms. This transition from extension-dominated transension to shear-dominated transension between 7 and 6 Ma likely played an important role in plate boundary localization and inception of the Gulf of California at ~6 Ma.

understood aspect of fault mechanics theory regarding along-strike strain gradients in the transition from oceanic to continental transform faults.

The dynamic interplay and linkage between these fault systems are difficult to evaluate given the current state of knowledge on early rift structures in the northern Gulf. However, a prospective kinematic model for late Miocene strain in coastal Sonora proposed here suggests that incipient NW-striking transform faults in the nascent Gulf of California (ca. 7-6 Ma) were linked by N- to NE-striking normal faults that transferred dextral strain to the southwest across a series of en-echelon, right-stepping dextral shear zones including the Amado and Seri faults, the Kino-Chueca Shear Zone, and potentially the La Cruz and Tiburón transforms (Fig. 16). An offshore normal-fault linkage between the Amado fault and the Seri fault could explain (1) the lack of significant dextral offset on the onshore Amado-Libertad fault in the Sierra Bacha, and (2) significant dextral shear on the Seri fault, which might have been responsible for $\sim 25^\circ$ of clockwise vertical-axis rotation in the southwestern Sierra Bacha (Fig. 15). The transfer and progressive localization of dextral strain along incipient proto-Gulf transforms and into the Kino-Chueca Shear Zone ca. 7-6 Ma (Bennett, 2009) may also explain the decrease of dextral strain inboard in the Sierra Bacha area where vertical-axis rotation is negligible (Fig. 15). According to this model, NE-SW extension in coastal Sonora from 10-6 Ma evolved into more localized, shear-dominated transtension that dramatically reduced extensional strain rates in the Sierra Bacha starting ca. 7 Ma and continuing into early modern Gulf time ($\sim 6-5$ Ma). Insufficient age constraints on the timing of extension and dextral strain make it difficult to evaluate the uncertainties regarding this speculative tectonic model.

Existing constraints on the distribution, magnitude, and timing of strain in the northern Gulf offer an opportunity to consider possible mechanisms responsible for the ~2-5 million year delay between the end of subduction west of Baja California and the onset of strong dextral shear and seafloor spreading in the GEP. Global plate circuit reconstructions reveal a significant change in relative Pacific-North America plate motion across the northern Gulf of California at ca. 8 Ma from N60W to N37W (Atwater and Stock, 1998). With the rift axis oriented ~N27W, the change in plate motion corresponds to a change in α (the acute angle between the orientation of the rift axis and the direction of relative plate motion) from 33° to 10°. Analog models of oblique rifting consistently show reactivation and reconfiguration of fault networks and a dramatic change in kinematics when rift obliquity is reduced from ~30-15° (Withjack and Jamison, 1986; Clifton et al., 2000; Agostini et al., 2009).

The well-documented change in relative plate motion and rift obliquity at 8 Ma might explain the multi-phase kinematic history proposed by the progressive localization model (Fig. 2C). Evidence throughout the GEP corroborates the possibility of a causal link between rift obliquity and strain localization. The onset of strong extension and subsidence in fault-bounded basins in the western Salton Trough at ~ 8 Ma (Dorsey et al., 2011), and contemporaneous marine incursion into the southern Gulf of California (Helenes and Carreño, 1999) might indicate the localization and acceleration of regional dextral shear into the North American continent. Additional evidence from conjugate rifted margins of the Gulf suggests that major transtensional strain in the northern GEP initiated sometime between 9 and 7 Ma (Bennett, 2009; Seiler et al., 2011).

Alternatively, the prolonged time lag between the end of subduction and onset of rift-related deformation could be related to thermal processes in the upper mantle and crust. Thermal weakening and/or erosion of a tear in the subducted slab may have delayed the arrival of hot asthenosphere beneath the GEP that ultimately weakened the lower crust and initiated localized deformation (Fletcher et al., 2007; Seiler et al., 2011). Developing an appropriate mechanical model for proto-Gulf evolution will require improved constraints on the timing and distribution of transtensional strain in the GEP from both continental and offshore marine basins.

CHAPTER VIII

CONCLUSIONS

Integrated geologic mapping, fault kinematic analysis, and paleomagnetic analysis show that the Sierra Bacha experienced ENE-WSW-directed, orthogonal extension (55-60%) between ~10 and 6 Ma. Structural data strongly support a multi-phase stress history involving dextral-oblique reactivation of primary normal faults. Available paleomagnetic data, however, provide no evidence of significant vertical-axis rotation related to dextral shear in the study area, except for ~25° of clockwise rotation in the southwest near the concealed Seri fault. The timing, magnitude and style of deformation recorded in the Sierra Bacha and in the nearby Cerro Kino indicate that dextral shear was not distributed throughout the entire Gulf Extensional Province during proto-Gulf time (12-6 Ma). Instead, dextral shear became localized into narrow zones like the Kino-Chueca Shear Zone during latest Miocene time (Bennett, 2009).

These results support a two-stage tectonic model for proto-Gulf strain in coastal Sonora, in which deformation evolved from NE-SW extension between 10 and 7 Ma to shear-dominated transtension ca. 7-6 Ma. A previously documented change in Pacific-North America relative plate motion at ~8 Ma, and inferred consequential reduction of the rift angle from ~30-15°, may have played a role in localizing a significant dextral component of transtensional strain on older NW-striking normal faults in the GEP. Localization of dextral shear during latest Miocene time elevated strain rates and

sufficiently weakened the crust, facilitating continental rapture and opening of the northern Gulf of California ca. 6 Ma.

APPENDIX A
FAULT KINEMATIC DATA

TABLE A1. FAULT DATA USED IN KINEMATIC ANALYSIS

| Fault datum | Easting* (m) | Northing* (m) | Fault Surface | | Slip Vector | | | Assigned Sense of Slip [®] |
|-------------|--------------|---------------|---------------|------------------|-------------------|-------|--------|-------------------------------------|
| | | | Strike | Dip [†] | Rake [‡] | Trend | Plunge | |
| 1 | 373854 | 3271563 | 140 | 81 | 50 | 151 | 49 | NL |
| 2 | 374137 | 3271795 | 160 | 77 | 177 | 339 | 3 | NR |
| 3 | 374137 | 3271795 | 147 | 43 | 130 | 286 | 31 | NR |
| 4 | 374727 | 3270858 | 315 | 54 | 18 | 326 | 15 | NL |
| 5 | 374801 | 3270916 | 143 | 84 | 75 | 164 | 74 | NL |
| 6 | 374860 | 3270855 | 126 | 56 | 174 | 303 | 5 | NR |
| 7 | 374984 | 3270784 | 140 | 42 | -- | -- | -- | -- |
| 8 | 374984 | 3270784 | 136 | 35 | -- | -- | -- | -- |
| 9 | 374984 | 3270784 | 175 | 39 | -- | -- | -- | -- |
| 10 | 374984 | 3270784 | 144 | 24 | -- | -- | -- | -- |
| 11 | 374984 | 3270784 | 350 | 73 | -- | -- | -- | -- |
| 12 | 375000 | 3270760 | 124 | 54 | 177 | 302 | 2 | NR |
| 13 | 375009 | 3270719 | 182 | 52 | -- | -- | -- | -- |
| 14 | 375271 | 3270669 | 333 | 66 | -- | -- | -- | -- |
| 15 | 375160 | 3270352 | 302 | 71 | 67 | 339 | 60 | NL |
| 16 | 375103 | 3270320 | 197 | 50 | -- | -- | -- | -- |
| 17 | 375574 | 3271170 | 128 | 77 | 10 | 130 | 10 | TR |
| 18 | 375585 | 3271172 | 24 | 89 | 24 | 24 | 1 | NL |
| 19 | 375293 | 3271417 | 311 | 45 | -- | -- | -- | -- |
| 20 | 374381 | 3271466 | 134 | 61 | 50 | 164 | 42 | NL |
| 21 | 374381 | 3271466 | 180 | 41 | -- | -- | -- | -- |
| 22 | 372992 | 3270108 | 196 | 36 | -- | -- | -- | -- |
| 23 | 372992 | 3270108 | 204 | 35 | -- | -- | -- | -- |
| 24 | 372865 | 3273134 | 146 | 38 | 0 | 326 | 0 | R |
| 25 | 372881 | 3272781 | 150 | 76 | 30 | 158 | 29 | NL |
| 26 | 372881 | 3272781 | 151 | 90 | 29 | 151 | 29 | NL |
| 27 | 372881 | 3272790 | 157 | 70 | -- | -- | -- | -- |
| 28 | 373220 | 3272826 | 142 | 82 | -- | -- | -- | -- |
| 29 | 373552 | 3273143 | 108 | 56 | 170 | 282 | 8 | NR |
| 30 | 372427 | 3273392 | 194 | 76 | 157 | 8 | 22 | TL |
| 31 | 372909 | 3265638 | 155 | 52 | 133 | 302 | 35 | NR |
| 32 | 374694 | 3271066 | 347 | 83 | 24 | 350 | 24 | NL |
| 33 | 371515 | 3273989 | 231 | 53 | 73 | 294 | 50 | NL |
| 34 | 373648 | 3269786 | 104 | 79 | 100 | 237 | 75 | NR |
| 35 | 373816 | 3269820 | 105 | 32 | 108 | 216 | 30 | NR |

TABLE A1. FAULT DATA USED IN KINEMATIC ANALYSIS (continued)

| Fault datum | Easting* (m) | Northing* (m) | Fault Surface | | Slip Vector | | | Assigned Sense of Slip [¶] |
|-------------|--------------|---------------|---------------|------------------|-------------------|-------|--------|-------------------------------------|
| | | | Strike | Dip [†] | Rake [‡] | Trend | Plunge | |
| 36 | 373816 | 3269825 | 095 | 40 | -- | -- | -- | -- |
| 37 | 357676 | 3281914 | 340 | 72 | -- | -- | -- | -- |
| 38 | 356854 | 3283601 | 338 | 26 | -- | -- | -- | -- |
| 39 | 356846 | 3283599 | 326 | 68 | -- | -- | -- | -- |
| 40 | 356846 | 3283599 | 330 | 64 | -- | -- | -- | -- |
| 41 | 356846 | 3283599 | 319 | 62 | 100 | 70 | 60 | NR |
| 42 | 356846 | 3283599 | 146 | 71 | -- | -- | -- | -- |
| 43 | 356846 | 3283599 | 152 | 75 | -- | -- | -- | -- |
| 44 | 356846 | 3283599 | 140 | 69 | 105 | 267 | 64 | NR |
| 45 | 356846 | 3283599 | 311 | 80 | 80 | 356 | 76 | NL |
| 46 | 356846 | 3283599 | 331 | 56 | 100 | 79 | 55 | NR |
| 47 | 356846 | 3283599 | 342 | 43 | 82 | 61 | 42 | NL |
| 48 | 356846 | 3283599 | 11 | 45 | 28 | 32 | 19 | NL |
| 49 | 356846 | 3283599 | 337 | 46 | 78 | 50 | 45 | NL |
| 50 | 356846 | 3283599 | 3 | 30 | 46 | 45 | 21 | NL |
| 51 | 356772 | 3283628 | 305 | 33 | -- | -- | -- | -- |
| 52 | 369585 | 3268022 | 303 | 41 | 142 | 92 | 24 | NR |
| 53 | 376500 | 3281370 | 332 | 76 | 90 | 62 | 76 | NR |
| 54 | 376775 | 3279279 | 330 | 63 | 123 | 115 | 48 | NR |
| 55 | 369407 | 3273209 | 214 | 18 | 100 | 315 | 18 | NR |
| 56 | 369769 | 3273405 | 151 | 52 | 107 | 267 | 49 | NR |
| 57 | 369769 | 3273405 | 151 | 52 | 76 | 219 | 50 | NL |
| 58 | 369769 | 3273405 | 144 | 45 | -- | -- | -- | -- |
| 59 | 369769 | 3273405 | 153 | 46 | -- | -- | -- | -- |
| 60 | 373367 | 3264413 | 197 | 58 | 93 | 293 | 58 | NR |
| 61 | 371338 | 3269917 | 156 | 80 | 170 | 334 | 10 | NR |
| 62 | 371400 | 3269930 | 145 | 86 | 30 | 147 | 30 | TR |
| 63 | 370724 | 3270834 | 170 | 84 | 108 | 332 | 71 | NR |
| 64 | 373948 | 3271057 | 29 | 70 | 85 | 105 | 69 | NL |
| 65 | 373923 | 3272769 | 314 | 46 | 43 | 347 | 29 | NL |

* UTM coordinates from zone 12R, WGS 84 Datum

† dip direction is 90° clockwise from strike according to the right-hand rule

‡ measured in degrees from horizontal (0-180) starting in the strike direction of the fault surface

¶ Abbreviations: N - normal, T - thrust, R- right-lateral, L- left-lateral

APPENDIX B
PALEOMAGNETIC DATA

TABLE B1. FISHER AND BINGHAM STATISTICS FOR SITE-MEAN ChRM

| Drill Site/ Unit | Bedding* | | Geographic Fisher Statistics | | | | Geographic Bingham Statistics | | | | | | Tilt-Corrected Bingham Statistics | | | | | |
|---------------------|----------|-----|------------------------------|-------|---------------|----------|-------------------------------|-------|------------|---------------|------------|---------------|-----------------------------------|------|------------|---------------|------------|---------------|
| | Strike | Dip | Dec | Inc | α_{95} | κ | Dec | Inc | κ_1 | α_{95} | κ_2 | α_{95} | Dec | Inc | κ_1 | α_{95} | κ_2 | α_{95} |
| DS-17 Mtsi | 308 | 40 | 231.6 | -40.5 | 1.48 | 910.35 | 231.5 | -40.5 | -844.21 | 1.03 | -6.68 | 12.16 | 228.2 | -1.3 | -851.03 | 1.03 | -6.68 | 12.16 |
| DS-21 Mtsf | 359 | 55 | 223.7 | -39.4 | 2.61 | 182.29 | 223.6 | -39.3 | -96.36 | 2.39 | -0.15 | 2.48 | 235.6 | 5.4 | -16.82 | 5.89 | -0.27 | 6.37 |
| DS-22 Mtcc | 312 | 48 | 326.9 | 49.2 | 9.25 | 29.96 | 324.5 | 49.5 | -27.43 | 7 | -1.74 | 36.57 | 358.1 | 23.7 | -29.37 | 6.76 | -1.72 | 36.78 |
| DS-23 Mr2 | 295 | 52 | 320.1 | 58.8 | 4.54 | 228.38 | 320.1 | 58.8 | -18953 | 0.32 | -89.95 | 4.7 | 355 | 20.7 | -21312 | 0.3 | -90.33 | 4.69 |
| DS-24 Mba | 221 | 1 | 4.2 | 39.9 | 4.32 | 125.76 | 3.2 | 40.7 | -54.22 | 4.15 | -0.33 | 4.53 | 2.6 | 40.1 | -54.07 | 4.15 | -0.33 | 4.53 |

NOTE: Table 3 contains all other paleomagnetic data, including site locations

* Bedding orientation used for structural correction; dip direction is 90° clockwise from strike according to the right-hand rule

Dec - Declination in degrees; Inc - Inclination in degrees

α_{95} - cone of 95% confidence about site-mean direction; κ - precision parameter (Fisher, 1953)

REFERENCES CITED

- Agostini, A., Corti, G., Zeoli, A., and Mulugeta, G., 2009, Evolution, pattern, and partitioning of deformation during oblique continental rifting: inferences from lithospheric-scale centrifuge models: *Geochemistry Geophysics Geosystems*, v. 10, Q11015.
- Allmendinger, R.W., Marrett, R.A., and Cladouhos, T., 1994, FaultKin v. 4.3.5. A program for analyzing fault-slip data on a Macintosh computer.
- Anderson, E.M., 1951, *The dynamics of faulting and dyke formation with applications to Britain*, 2nd edition: Edinburgh, Oliver and Boyd, 206 p.
- Anderson, T.H., and Silver, L.T., 1969, Mesozoic magmatic events of the northern Sonora coastal region, Mexico: *Geological Society of America Abstracts with Programs*, v. 1, p. 3.
- Angelier, J., and Mechler, P., 1977, Sur une méthode graphique de recherche des contraintes principales également utilisable en tectonique et en séismologie: La méthode des diedres droits: *Bulletin of the Geological Society of France*, v. 7, p. 1309-1318.
- Angelier, J., Colletta, B., Chorowicz, J., Ortlieb, L., and Rangin, C., 1981, Fault tectonics of the Baja-California peninsula and the opening of the Sea of Cortez, Mexico: *Journal of Structural Geology*, v. 3, p. 347-357.
- Angelier, J., Tarantola, A., Valette, B., and Manoussis, S., 1982, Inversion of field data in fault tectonics to obtain the regional stress, 1. Single-phase fault populations - a new method of computing the stress tensor: *Geophysical Journal of the Royal Astronomical Society*, v. 69, p. 607-621.
- Aragón-Arreola, M., and Martín-Barajas, A., 2007, Westward migration of extension in the northern Gulf of California, Mexico: *Geology*, v. 35, no. 6, p. 571-574.
- Atwater, T., 1970, Implications of plate tectonics for the Cenozoic evolution of western North America: *Geological Society of America Bulletin*, v. 81, p. 3513-3536.

- Atwater, T., 1989, Plate tectonic history of the northeast Pacific and western North America, *in* Winterer, E.L., Hussong, D.M., and Decker, R.W., editors., *The Eastern Pacific Ocean and Hawaii*, Volume N: Boulder, Colorado, The Geological Society of America, p. 21-72.
- Atwater, T., and Stock, J., 1998, Pacific North America plate tectonics of the Neogene southwestern United States: An update: *International Geology Review*, v. 40, no. 5, p. 375-402.
- Beck, M.E., 1980, Paleomagnetic record of plate-margin tectonic processes along the western edge of North America: *Journal of Geophysical Research*, v. 85, p. 7115-7131.
- Bennett, S.E.K., 2009, *Transtensional Rifting in the Late Proto-Gulf of California near Bahía Kino, Sonora, México* [M.S. thesis]: Chapel Hill, University of North Carolina, 122 p.
- Bennett, S.E.K., and Oskin, M.E., 2008, A New high-precision paleomagnetic reference vector from Mesa El Burro, Mesa Cartabón, and Mesa El Pinole, Baja California for the Tuff of San Felipe, a Miocene ignimbrite marker bed exposed in Baja California and Sonora, México: American Geophysical Union Fall Meeting, San Francisco, California, abstract #T11A-1852.
- Bennett, S.E., Oskin, M., and Iriondo, A., 2007: Transition from Proto-Gulf Extension to Transtension, Coastal Sonora, Mexico, *Eos, Transactions, American Geophysical Union*, v. 88, Joint Assembly Supplement, abstract #S31A-10.
- Besse, J., and Courtillot, V., 1991, Revised and synthetic apparent polar wander paths of the African, Eurasian, North-American and Indian plates, and true polar wander since 200 Ma: *Journal of Geophysical Research*, v. 96, p. 4029-4050.
- Bott, M.H.P., 1959, The mechanics of oblique slip faulting: *Geological magazine*, v. 96, p. 109-117.
- Bryant, B.A., 1986, *Geology of the Sierra Santa Rosa Basin, Baja California, Mexico* [M.S. thesis]: San Diego, California, San Diego State University, 75 p.
- Buck, W.R., 1988, Flexural rotation of normal faults: *Tectonics*, v. 7, no. 5, p. 959-973.
- Buck, W.R., 1991, Modes of Continental Lithospheric Extension: *Journal of Geophysical Research*, v. 96, p. 20161-20178.
- Buck, W.R., 1993, Effect of lithospheric thickness on the formation of high-angle and low-angle normal faults: *Geology*, v. 21, no. 10, p. 933-936.

- Buck, W.R., and Choi, E., 2010, Constraints on the strength of faults from rider blocks on oceanic and continental core complexes: American Geophysical Union Fall Meeting, San Francisco, California, abstract #T32C-04.
- Buck, W.R., Lavier, L.L., and Poliakov, A.N.B., 1999, How to make a rift wide: *Philosophical Transactions of the Royal Society of London Series a - Mathematical Physical and Engineering Sciences*, v. 357, p. 671-690.
- Butler, R.L., 1992, *Paleomagnetism*: Cambridge, Massachusetts, Blackwell Scientific Publications, 319 p.
- Carey, E., and Brunier, B., 1974, Numerical-analysis of an elementary mechanical model applied to study of a population of faults: *Comptes Rendus Hebdomadaires Des Seances De L Academie Des Sciences Serie D*, v. 279, no. 11, p. 891-894.
- Clifton, A.E., Schlische, R.W., Withjack, M.O., and Ackermann, R.V., 2000, Influence of rift obliquity on fault-population systematics: results of experimental clay models: *Journal of Structural Geology*, v. 22, no. 10, p. 1491-1509.
- Colletta, B., Angelier, J., Chorowicz, J., Ortlieb, L., and Rangin, C., 1981, Fault patterns and neotectonic evolution of the Baja California peninsula, Mexico: *Comptes Rendus De L Academie Des Sciences Serie Ii*, v. 292, no. 14, p. 1043-1048.
- Demarest, H.H., 1983, Error analysis for the determination of tectonic rotation from paleomagnetic data: *Journal of Geophysical Research*, v. 88, no. B5, p. 4321-4328.
- DeMets, C., 1995, A reappraisal of seafloor spreading lineations in the Gulf of California: Implications for the transfer of Baja California to the Pacific plate and estimates of Pacific-North America motion: *Geophysical Research Letters*, v. 22, no. 24, p. 3545-3548.
- DeMets, C., and Dixon, T.H., 1999, New kinematic models for Pacific-North America motion from 3 Ma to present, I: Evidence for steady motion and biases in the NUVEL-1A model: *Geophysical Research Letters*, v. 26, no. 13, p. 1921-1924.
- Dokka, R.K., and Merriam, R.H., 1982, Late Cenozoic extension of northeastern Baja California, Mexico: *Geological Society of America Bulletin*, v. 93, p. 371-378.
- Dorsey, R.J., and Burns, B., 1994, Regional stratigraphy, sedimentology, and tectonic significance of Oligocene-Miocene sedimentary and volcanic rocks, northern Baja California, Mexico: *Sedimentary Geology*, v. 88, no. 3-4, p. 231-251.

- Dorsey, R.J., Housen, B.A., Janecke, S.U., Fanning, C.M., and Spears, A.L.F., 2011, Stratigraphic record of basin development within the San Andreas fault system: Late Cenozoic Fish Creek-Vallecito basin, southern California: Geological Society of America Bulletin, v. 123, no. 5-6, p. 771-793.
- Fenby, S.S., and Gastil, R.G., 1991, A seismo-tectonic map of the Gulf of California and surrounding areas, *in* Dauphin, J.P., and Simoneit, B.R., eds., The Gulf and Peninsular Provinces of the Californias: Tulsa, Oklahoma, The American Association of Petroleum Geologists Memoir 47, p. 79–83.
- Fletcher, J.M., Martin-Atienza, B., Axen, G.J., Gonzalez-Fernandez, A., Hollbrook, W.S., Kent, G., Lizarralde, D., Harding, A., and Umhoefer, P., 2003, Palinspastic reconstructions of the Gulf of California based on Airy isostatic profiles: evidence for one kinematic phase of Neogene shearing: American Geophysical Union Fall Meeting, San Francisco, California, abstract #T32D-06.
- Fletcher, J.M., Grove, M., Kimbrough, D., Lovera, O., and Gehrels, G.E., 2007, Ridge-trench interactions and the Neogene tectonic evolution of the Magdalena shelf and southern Gulf of California: Insights from detrital zircon U-Pb ages from the Magdalena fan and adjacent areas: Geological Society of America Bulletin, v. 119, no. 11-12, p. 1313-1336.
- Gans, P.B., 1997, Large-magnitude Oligo-Miocene extension in southern Sonora: Implications for the tectonic evolution of northwest Mexico: Tectonics, v. 16, no. 3, p. 388-408.
- Gastil, R.G., 1968, Fault systems in northern Baja California and their relation to the origin of the Gulf of California, *in* Dickinson, W.R. and Grantz, A., eds., Proceedings of conference on geological problems of the San Andreas Fault system: Stanford, Stanford University Publications in Geological Sciences, v. 11, p. 283-286
- Gastil, R.G., 1993, Prebatholithic history of peninsular California, *in* Gastil, R.G., and Miller, R.H., eds., The prebatholithic stratigraphy of peninsular California: Geological Society of America Special Paper 279, p. 145–156.
- Gastil, R.G., and Krummenacher, D., 1976, Reconnaissance geologic map of coastal Sonora between Puerto Lobos and Bahía Kino: Geological Society of America Map and Chart Series MC-16, scale 1:150,000, 1 sheet.
- Gastil, R.G., and Krummenacher, D., 1977, Reconnaissance geology of coastal Sonora between Puerto Lobos and Bahía Kino: Geological Society of America Bulletin, v. 88, p. 189-198.

- Gastil, R.G., Lemone, D.V., and Stewart, W.J., 1973, Permian fusulinids from near San Felipe, Baja California: American Association of Petroleum Geologists Bulletin, v. 57, no. 4, p. 746-747.
- Gastil, R.G., Krummenacher, D., Doupont, J., and Bushee, J., 1974, The batholith belt of southern California and western Mexico: Pacific Geology, v. 8, p. 73-78.
- Gastil, R.G., Phillips, R.P., Allison, E.C., 1975, Reconnaissance geology of the state of Baja California: Geological Society of America Memoir 140, 170 p.
- Gastil, R.G., Krummenacher, D., and Minch, J., 1979, Record of Cenozoic volcanism around the Gulf of California: Geological Society of America Bulletin, v. 90, no. 9, p. 839-857.
- González-Fernández, A., Dañobeitia, J.J., Delgado-Argote, L.A., Michaud, F., Córdoba, D., and Bartolomé, R., 2005, Mode of extension and rifting history of upper Tiburón and upper Delfin basins, northern Gulf of California: Journal of Geophysical Research, v. 110, no. B1, p. 1-17.
- Grove, M., Fletcher, J., Kimbrough, D., Lovera, O., Kohn, B., 2005, Neogene tectonic evolution of the Magdalena shelf: Geological Society of America Abstracts with Programs, v. 37, no. 7, p. 274.
- Hagstrum, J.T., Sawlan, M.G., Hausback, B.P., Smith, J.G., and Gromme, C.S., 1987, Miocene Paleomagnetism and tectonic setting of the Baja California peninsula, Mexico: Journal of Geophysical Research, v. 92, no. B3, p. 2627-2639.
- Hausback, B.P., 1984, Cenozoic volcanic and tectonic evolution of Baja California Sur, Mexico, in Frizzell, V.A., Jr., ed., Geology of the Baja California peninsula, v. 39: Los Angeles, California, Society of Economic Paleontologists and Mineralogists, Pacific Section, p. 219-236.
- Helenes, J., and Carreño, A.L., 1999, Neogene sedimentary evolution of Baja California in relation to regional tectonics: Journal of South American Earth Sciences, v. 12, no. 6, p. 589-605.
- Henry, C.D., 1989, Late Cenozoic basin and range structure in western Mexico adjacent to the Gulf of California: Geological Society of America Bulletin, v. 101, no. 9, p. 1147-1156.
- Herman, S.W., and Gans, P.B., 2006, A paleomagnetic investigation of large scale vertical axis rotations in coastal Sonora: Evidence for transtensional proto-Gulf deformation: Geological Society of America Abstracts with Programs, v. 38, no. 7, p. 311.

- Jones, C.H., 2002, User-driven integrated software lives: "PaleoMag" Paleomagnetism Analysis on the Macintosh: *Computers and Geosciences*, v. 28, no. 10, p. 1145-1151.
- Karig, D.E., and Jensky, W., 1972, Proto-Gulf of California: *Earth and Planetary Science Letters*, v. 17, no. 1, p. 169-174.
- Kirschvink, J.L., 1980, The least-squares line and plane and the analysis of paleomagnetic data: *Geophysical Journal of the Royal Astronomical Society*, v. 62, no. 3, p. 699-718.
- Kirschvink, J.L., Kopp, R.E., Raub, T.D., Baumgartner, C.T., and Holt, J.W., 2008, Rapid, precise, and high-sensitivity acquisition of paleomagnetic and rock-magnetic data: Development of a low-noise automatic sample changing system for superconducting rock magnetometers: *Geochemistry Geophysics Geosystems*, v. 9, no. 5, 18 p.
- Le Maitre, R.W., Bateman, P., Dudek, A., Keller, J., Lameyre, J., Le Bas, M.J., Sabine, P.A., Schmid, R., Sorensen, H., Streckeisen, A., Woolley, A.R., and Zanettin, B., 1989, A classification of igneous rocks and glossary of terms: Recommendations of the International Union of Geological Sciences Subcommittee on the Systematics of Igneous Rocks: Oxford, United Kingdom, Blackwell Scientific Publications, 193 p.
- Lee, J., Miller, M.M., Crippen, R., Hacker, B., and Vazquez, J.L., 1996, Middle Miocene extension in the Gulf extensional province, Baja California: Evidence from the southern Sierra Juarez: *Geological Society of America Bulletin*, v. 108, no. 5, p. 505-525.
- Lewis, C.J., 1994, Constraints on extension in the Gulf extensional province from the Sierra San Fermín, northeastern Baja California, Mexico [Ph.D. thesis]: Cambridge, Massachusetts, Harvard University, 361 p.
- Lewis, C.J., and Stock, J.M., 1998, Late Miocene to recent transtensional tectonics in the Sierra San Fermin, northeastern Baja California, Mexico: *Journal of Structural Geology*, v. 20, no. 8, p. 1043-1063.
- Lizarralde, D., Axen, G.J., Brown, H.E., Fletcher, J. M., Gonzalez-Fernandez, A., Harding, A. J., Holbrook, W. S., Kent, G. M., Paramo, P., Sutherland, F., and Umhoefer, P. J., 2007, Variation in styles of rifting in the Gulf of California: *Nature*, v. 448, no. 7152, p. 466-469.
- Lonsdale, P., 1989, Geology and tectonic history of the Gulf of California, *in* Winterer, E.L., Hussong, D.M., and Decker, R.W., eds., *The eastern Pacific Ocean and Hawaii*: Boulder, Colorado, Geological Society of America, *Geology of North America*, v. N, p. 499-521.

- Lonsdale, P., 1991, Structural pattern of the Pacific floor offshore peninsular California, *in* Dauphin, J.P., and Simoneit, B.R.T., eds., *The Gulf and the Peninsular Provinces of the Californias*: Tulsa, Oklahoma, The American Association of Petroleum Geologists Memoir 47, p. 87–125.
- Mammerickx, J., and Klitgord, K.D., 1982, Northern East Pacific Rise – Evolution from 25 m.y. B.P. to the present: *Journal of Geophysical Research*, v. 87, p. 6751–6759.
- Martín, A., Fletcher, J.M., López-Martínez, M., and Mendoza-Borunda, R., 2000, Waning Miocene subduction and arc volcanism in Baja California: the San Luis Gonzaga volcanic field: *Tectonophysics*, v. 318, p. 27–51.
- Merriam, R., 1965, San Jacinto fault in northwestern Sonora, Mexico: *Geological Society of America Bulletin*, v. 76, p. 1051–1054.
- Mora-Alvarez, G., and McDowell, F.W., 2000, Miocene volcanism during late subduction and early rifting in the Sierra Santa Ursula of western Sonora, Mexico, *in* Delgado-Granados, H., Aguirre-Díaz, G., and Stock, J.M., eds., *Cenozoic tectonics and volcanism of Mexico*: Boulder, Colorado, Geological Society of America Special Paper 334, p. 123–141.
- Nagy, E.A., 2000, Extensional deformation and paleomagnetism at the western margin of the Gulf Extensional Province, Puertecitos Volcanic Province, northeastern Baja California, Mexico: *Geological Society of America Bulletin*, v. 112, p. 857–870.
- Nagy, E.A., Grove, M., and Stock, J.M., 1999, Age and stratigraphic relationships of pre- and syn-rift volcanic deposits in the northern Puertecitos Volcanic Province, Baja California, Mexico: *Journal of Volcanology and Geothermal Research*, v. 93, p. 1–30.
- Nourse, J.A., Anderson, T.H., and Silver, L.T., 1994, Tertiary metamorphic core complexes in Sonora, northwestern Mexico: *Tectonics*, v. 13, p. 1161–1182.
- Nourse, J.A., Premo, W.R., Iriondo, A., and Stahl, E.R., 2005, Contrasting Proterozoic basement complexes near the truncated margin of Laurentia, northwestern Sonora-Arizona international border region: *in* Anderson, T., Nourse, J., McKee, J., and Steiner, M., eds., *The Mojave-Sonora megashear hypothesis: development, assessment, and alternatives*: Geological Society of America Special Paper 393, p. 123–182.
- Oskin, M., Stock, J., and Martín-Barajas, A., 2001, Rapid localization of Pacific-North America plate motion in the Gulf of California: *Geology*, v. 29, no. 5, p. 459–462.
- Oskin, M., and Stock, J., 2003a, Marine incursion synchronous with plate-boundary localization in the Gulf of California: *Geology*, v. 31, no. 1, p. 23–26.

- Oskin, M., and Stock, J., 2003b, Pacific-North America plate motion and opening of the Upper Delfin Basin, northern Gulf of California, Mexico: *Geological Society of America Bulletin*, v. 115, p. 1173-1190.
- Oskin, M., and Stock, J., 2003c, Cenozoic volcanism and tectonics of the continental margins of the Upper Delfin basin, northeastern Baja California and western Sonora, in Kimbrough, D.L., Johnson, S.E., Paterson, S., Martín-Barajas, A., Fletcher, J.M., and Girty, G., eds., *Tectonic evolution of northwestern Mexico and the southwestern USA: Geological Society of America Special Paper 374*., p. 421-428
- Ogg, J.G., and Smith, A.G., 2004, The geomagnetic polarity time scale, *in* Gradstein, F.M., Ogg, J.G., and Smith, A.G., eds., *A geologic time scale 2004*: Cambridge, United Kingdom, Cambridge University Press, p. 63-86.
- Pfiffner, O.A., and Burkhard, M., 1987, Determination of paleo-stress axes orientations from fault, twin and earthquake data: *Annales Tectonicae*, v. 1, p. 48-57.
- Proffett, J.M., 1977, Cenozoic geology of Yerington District, Nevada, and implications for nature and origin of basin and range faulting: *Geological Society of America Bulletin*, v. 88, no. 2, p. 247-266.
- Quidelleur, X., and Courtillot, V., 1996, On low-degree spherical harmonic models of paleosecular variation: *Physics of the Earth and Planetary Interiors*, v. 95, no. 1-2, p. 55-77.
- Ramos-Velázquez, E., Calmus, T., Valencia, V., Iriondo, A., Valencia-Moreno, M., and Bellon, H., 2008, U-Pb and (40)Ar/(39)Ar geochronology of the coastal Sonora batholith: New insights on Laramide continental arc magmatism: *Revista Mexicana De Ciencias Geológicas*, v. 25, no. 2, p. 314-333.
- Richard, P., and Krantz, R.W., 1991, Experiments on fault reactivation in strike-slip mode: *Tectonophysics*, v. 188, no. 1-2, p. 117-131.
- Sawlan, M.G., 1991, Magmatic evolution of the Gulf of California rift, *in* Dauphin, J.P., and Simoneit, B.R.T., eds., *The Gulf and the Peninsular Provinces of the Californias*: Tulsa, Oklahoma, The American Association of Petroleum Geologists Memoir 47, p. 301-370.
- Seiler, C., Fletcher, J.M., Quigley, M.C., Gleadow, A.J.W., Kohn, B.P., 2010, Neogene structural evolution of the Sierra San Felipe, Baja California: Evidence for proto-gulf transtension in the Gulf extensional province?: *Tectonophysics*, v. 488, p. 87-109.

- Seiler, C., Fletcher, J.M., Kohn, B.P., Gleadow, A.J.W., and Raza, A., 2011, Low-temperature thermochronology of northern Baja California, Mexico: Decoupled slip-exhumation gradients and delayed onset of oblique rifting across the Gulf of California: *Tectonics*, v. 30, no. 3, TC3004.
- Sibson, R.H., 1985, A note on fault reactivation: *Journal of Structural Geology*, v. 7, no. 6, p. 751-754.
- Spencer, J.E., and Normark, W.R., 1979, Tosco-Abreojos fault zone: A Neogene transform plate boundary within the Pacific margin of southern Baja California: *Geology*, v. 7, p. 554-557.
- Stewart, J.H., and Poole, F.G., 1997, Inventory of Neoproterozoic and Paleozoic strata in Sonora, Mexico: U.S. Geological Survey Open-File Report 02-97, 50 p.
- Stock, J.M., 1989, Sequence and geochronology of Miocene rocks adjacent to the Main Gulf Escarpment: Southern Valle Chico, Baja California Norte, Mexico: *Geofísica Internacional*, v. 28, p. 851-896.
- Stock, J.M., and Hodges, K.V., 1989, Pre-Pliocene extension around the Gulf of California and the transfer of Baja California to the Pacific plate: *Tectonics*, v. 8, no. 1, p. 99-115.
- Stock, J., and Molnar, P., 1988, Uncertainties and implications of the late Cretaceous and Tertiary position of North America relative to the Farallon, Kula, and Pacific plates: *Tectonics*, v. 7, no. 6, p. 1339-1384.
- Stock, J.M., Martín-Barajas, A., Suárez-Vidal, F., and Miller, M.M., 1991, Miocene to Holocene extensional tectonics and volcanic stratigraphy of northeastern Baja California, Mexico, *in* Walawender, M.J., and Hanan, B.B., eds., *Geological Excursions in Southern California and Mexico*, Guidebook for the 1991 Annual Meeting of the Geological Society of America: San Diego, California, San Diego State University, p. 44-67.
- Stock, J.M., Lewis, C.J., and Nagy, E.A., 1999, The Tuff of San Felipe: an extensive middle Miocene pyroclastic flow deposit in Baja California, Mexico: *Journal of Volcanology and Geothermal Research*, v. 93, no. 1-2, p. 53-74.
- Umhoefer, P.J., Mayer, L., and Dorsey, R.J., 2002, Evolution of the margin of the Gulf of California near Loreto, Baja California Peninsula, Mexico: *Geological Society of America Bulletin*, v. 114, no. 7, p. 849-868.
- Verosub, K.L., 1982, Geomagnetic excursions – A critical assessment of the evidence as recorded in sediments of the Brunhes epoch: *Philosophical Transactions of the Royal Society of London, Series A*, v. 306, no. 1492, p. 161-168.

Wallace, R.E., 1951, Geometry of shearing stress and relation to faulting: *Journal of Geology*, v. 59, p. 118-130.

Withjack, M.O., and Jamison, W.R., 1986, Deformation produced by oblique rifting: *Tectonophysics*, v. 126, no. 2-4, p. 99-124.

Wong, M., and Gans, P., 2003, Tectonic implications of early Miocene extensional unroofing of the Sierra Mazatán metamorphic core complex, Sonora, Mexico: *Geology*, v. 31, no. 11, p. 953-956.

Zoback, M.D., 1991, State of stress and crustal deformation along weak transform faults: *Philosophical Transactions of the Royal Society of London, Series A*, v. 337, no. 1645, p. 141-150.